FINAL REPORT

Validating the Kinematic Wave Approach for Rapid Soil Erosion Assessment and Improved BMP Site Selection to Enhance Training Land Sustainability

ESTCP Project RC-200820

FEBRUARY 2014

Stacy L. Hutchinson
J.M. Shawn Hutchinson
Kansas State University

Distribution Statement A

This document has been cleared for public release

REPORT DOCUMENTATION PAGE

Form Approved
OMB No. 0704-0188

Public reporting burden for this collection of information is estimated to average 1 hour per response, including the time for reviewing instructions, searching existing data sources, gathering and maintaining the data needed, and completing and reviewing this collection of information. Send comments regarding this burden estimate or any other aspect of this collection of information, including suggestions for reducing this burden to Department of Defense, Washington Headquarters Services, Directorate for Information Operations and Reports (0704-0188), 1215 Jefferson Davis Highway, Suite 1204, Arlington, VA 22202-4302. Respondents should be aware that notwithstanding any other provision of law, no person shall be subject to any penalty for failing to comply with a collection of information if it does not display a currently valid OMB control number. **PLEASE DO NOT RETURN YOUR FORM TO THE ABOVE ADDRESS.**

1. REPORT DATE *(DD-MM-YYYY)*
15-11-2013

2. REPORT TYPE
FINAL

3. DATES COVERED *(From - To)*
Mar 2008 – Nov 2013

4. TITLE AND SUBTITLE

Validating the Kinematic Wave Approach for Rapid Soil Erosion Assessment and Improved BMP Site Selection to Enhance Training Land Sustainability

5a. CONTRACT NUMBER
W912HQ-08-C-0010

5b. GRANT NUMBER

5c. PROGRAM ELEMENT NUMBER

6. AUTHOR(S)

Stacy L. Hutchinson and J.M. Shawn Hutchinson

5d. PROJECT NUMBER
RC-200820

5e. TASK NUMBER

5f. WORK UNIT NUMBER

7. PERFORMING ORGANIZATION NAME(S) AND ADDRESS(ES)

Stacy Hutchinson
Kansas State University
Biol and Agricultural Engg
129 Seaton Hall
Manhattan, KS 66506

J.M. Shawn Hutchinson
Kansas State University
Geography
118 Seaton Hall
Manhattan, KS 66506

8. PERFORMING ORGANIZATION REPORT NUMBER

9. SPONSORING / MONITORING AGENCY NAME(S) AND ADDRESS(ES)

10. SPONSOR/MONITOR'S ACRONYM(S)

11. SPONSOR/MONITOR'S REPORT NUMBER(S)

12. DISTRIBUTION / AVAILABILITY STATEMENT

Approved for public release; distribution is unlimited.

13. SUPPLEMENTARY NOTES

14. ABSTRACT

The rapid gully erosion prediction model, *nLS+*, was calibrated and validated at several military installations to identify areas of erosion potential and optimal locations for siting erosion-preventing best management practices. The model is operated using a geographic information system with input data from commonly available landcover datasets and digital elevation models. The computed model output is a unitless estimate of the energy of surface runoff water with the relationship between actual gully locations and accumulated energy then used to make predictions. Data acquisition and preparation times are minimal compared to existing watershed erosion models. While the *nLS+* model can be effective in identifying the location of existing gullies, it can also be operated in a forecasting mode to assess the impact of future or planned military training exercises on the formation of new gullies. Using this approach, land managers can quickly evaluate gully potential across their training areas while saving significant time normally spent on ground and air surveys.

15. SUBJECT TERMS

16. SECURITY CLASSIFICATION OF:			**17. LIMITATION OF ABSTRACT**	**18. NUMBER OF PAGES**	**19a. NAME OF RESPONSIBLE PERSON**
a. REPORT	**b. ABSTRACT**	**c. THIS PAGE**			PAUL LOWE
U	U	U	UU	135	**19b. TELEPHONE NUMBER** *(include area code)* 785-532-6804

Standard Form 298 (Rev. 8-98)
Prescribed by ANSI Std. Z39.18

TABLE OF CONTENTS

LIST OF FIGURES ..... **IV**

LIST OF TABLES ..... **VII**

LIST OF ACRONYMS ..... **IX**

EXECUTIVE SUMMARY ..... **XI**

1.0 INTRODUCTION **1**

1.1 BACKGROUND 1
1.2 OBJECTIVE OF THE DEMONSTRATION 2
1.3 REGULATORY DRIVERS 3

2.0 TECHNOLOGY/METHODOLOGY DESCRIPTION **4**

2.1 TECHNOLOGY/METHODOLOGY OVERVIEW 4
2.3 ADVANTAGES AND LIMITATIONS OF THE METHODOLOGY 7

3.0 PERFORMANCE OBJECTIVES **8**

3.1 GULLY DEFINITION 13

4.0 SITE DESCRIPTION **14**

4.1 SITE LOCATION AND HISTORY 15
4.2 SITE CHARACTERISTICS 16
4.3.1 Fort Hood, Texas *17*
4.3.2 Fort Benning, Georgia *19*
4.3.3 Fort Irwin, California *21*
4.3.4 Camp Lejeune Marine Corps Base, North Carolina *23*
4.3.5 Schofield Barracks and Kahuku Range, Island of Oahu, Hawaii *26*
4.3.6 Pohakuloa Training Area and Keamuku Parcel, Island of Hawaii, Hawaii *29*
4.3.6 Fort Riley, Kansas *32*
4.4 SITE-RELATED PERMITS AND REGULATIONS 34

5.0 TEST DESIGN **35**

5.1 CONCEPTUAL TEST DESIGN 35
5.2 BASELINE CHARACTERIZATION AND PREPARATION 36
5.3 DESIGN AND LAYOUT OF TECHNOLOGY AND METHODOLOGY COMPONENTS 36
5.4 FIELD TESTING 37
5.4.1 Model Calibration and Validation *37*
5.4.3 Equipment Calibration and Data Quality Issues: Model Sensitivity Analysis *38*
5.5 SAMPLING PROTOCOL: OPERATING THE *nLS*+ MODEL IN PREDICTIVE MODE 43

6.0 PERFORMANCE ASSESSMENT **47**

6.1 OBJECTIVE #1: IDENTIFY THE CRITICAL THRESHOLD FOR ACCUMULATED *nLS*+ VALUES FOR EACH STUDY INSTALLATION 47
6.1.1 GULLY DATA PROCESSING 47
6.1.2 MODEL CALIBRATION 55
6.1.2 MODEL VALIDATION AND ACCURACY ASSESSMENT 57
6.2 OBJECTIVE #2: DETERMINE WHETHER A SINGLE CRITICAL THRESHOLD FOR ACCUMULATED *nLS*+ VALUES IS ADEQUATE FOR ALL STUDY INSTALLATIONS 66
6.3 OBJECTIVE #3: FORECAST AREAS WHERE GULLIES ARE LIKELY TO FORM IN RESPONSE TO FUTURE MILITARY TRAINING EVENTS AT FORT RILEY AND POHAKULOA TRAINING AREA (KEAMUKU PARCEL) 71
6.3.1 COMPUTING RUT DEPTH AND IMPACT SEVERITY SCORES 71

6.3.2 GIS PROCESSING 76
6.3.3 MODELING AND RESULTS 77
6.4 OBJECTIVE #4: PROPOSE GEOGRAPHIC REGIONS WITHIN WHICH INSTALLATION-SPECIFIC CRITICAL THRESHOLDS FOR ACCUMULATED *NLS+* VALUES ARE VALID 79
6.5 OBJECTIVE #5: DEVELOP AND DISSEMINATE A DOWNLOADABLE AND EASY-TO-USE GIS-BASED MODELING TOOL WITH DOCUMENTATION 83
6.5.1 MODEL DESIGN 83
6.5.1 MODEL PERFORMANCE 86
6.5.2 MODEL GEOPROCESSING WEB APPLICATION 88

7.0 COST ASSESSMENT 89

8.0 IMPLEMENTATION ISSUES 91

8.1 MODEL PERFORMANCE, INTEGRATION, AND TECHNOLOGY TRANSFER 91
8.2 DEFINITIONS AND DATA HANDLING 93
8.3 INSTALLATION ITAM STAFFING 93

9.0 REFERENCES 95

APPENDIX A: INITIAL PROJECT POINTS OF CONTACT 99

APPENDIX B: HISTOGRAMS OF ACCUMULATED *NLS+* VALUES AFTER INITIAL PROCESSING 101

APPENDIX C: HISTOGRAMS OF ACCUMULATED *NLS+* VALUES AFTER SECONDARY PROCESSING 103

APPENDIX D: HISTOGRAMS OF FINAL LOG-TRANSFORMED ACCUMULATED *NLS+* VALUES ..105

APPENDIX E: INSTALLATION MAPS OF PREDICTED CELLS AND GULLY DENSITY SURFACE ..107

APPENDIX F: BAR CHARTS OF GULLY PREDICTION ACCURACY DISTANCES 111

APPENDIX G: SUB-MODELS OF THE ENHANCED *NLS+* GULLY MODEL 112

LIST OF FIGURES

Figure 1. Schematic illustrating the difference between sheet and concentrated flows. 4
Figure 2. Results of *nLS+* model from Fort Riley, Kansas. 6
Figure 3. Example of how the spatial precision of a predicted gully locations are evaluated with respect to the spatial resolution of the input DEM. 11
Figure 4. Map of installations initially selected for field validation of the *nLS+* model..... 15
Figure 5. Runoff potential for the soils of Fort Hood, Texas by soil hydrologic group (Source: Generalized Map of U.S. Soils, USDA NRCS)..... 18
Figure 6. Dominant landcover categories for Fort Hood, Texas (Source: 2001 National Landcover Dataset). 18
Figure 7. Climograph for Fort Hood, Texas (Source: http://www.weather.com)..... 19
Figure 8. Runoff potential for the soils of Fort Benning, Georgia by soil hydrologic group (Source: Generalized Map of U.S. Soils, USDA NRCS). 20
Figure 9. Dominant landcover categories for Fort Benning, Georgia (Source: 2001 National Landcover Dataset). 20
Figure 10. Climograph for Fort Benning, Georgia (Source: http://www.weather.com)..... 21
Figure 11. Runoff potential for the soils of Fort Irwin, California by soil hydrologic group (Source: Generalized Map of U.S. Soils, USDA NRCS). 22
Figure 12. Dominant landcover categories for Fort Irwin, California (Source: 2001 National Landcover Dataset). 22
Figure 13. Climograph for Fort Irwin, California (Source: http://www.weather.com). 23
Figure 14. Runoff potential for the soils of Camp Lejeune MCB, North Carolina by soil hydrologic group (Source: Generalized Map of U.S. Soils, USDA NRCS)..... 24
Figure 15. Dominant landcover categories for Camp Lejeune MCB, North Carolina (Source: 2001 National Landcover Dataset). 25
Figure 16. Climograph for Camp Lejeune MCB, North Carolina (Source: http://www.weather.com). 25
Figure 17. Runoff potential for the soils of Schofield Barracks, Hawaii by soil hydrologic group (Source: Generalized Map of U.S. Soils, USDA NRCS). 26
Figure 18. Runoff potential for the soils of the Kahuku Range, Schofield Barracks, Hawaii by soil hydrologic group (Source: Generalized Map of U.S. Soils, USDA NRCS)..... 27
Figure 19. Dominant landcover categories for Schofield Barracks, Hawaii (Source: 2001 National Landcover Dataset). 28
Figure 20. Dominant landcover categories for the Kahuku Range, Schofield Barracks, Hawaii (Source: 2001 National Landcover Dataset)..... 28
Figure 21. Climograph for Schofield Barracks, Hawaii (Source: http://www.weather.com)..... 29
Figure 22. Runoff potential for the soils of Pohakuloa Training Area, Hawaii by soil hydrologic group (Source: Generalized Map of U.S. Soils, USDA NRCS)..... 30
Figure 23. Runoff potential for the soils of the Keamuku Parcel, Pohakuloa Training Area, Hawaii by soil hydrologic group (Source: Generalized Map of U.S. Soils, USDA NRCS). 30
Figure 24. Dominant landcover categories for Pohakuloa Training Area, Hawaii (Source: 2001 National Landcover Dataset). 31
Figure 25. Dominant landcover categories for the Keamuku Parcel, Pohakuloa Training Area, Hawaii (Source: 2001 National Landcover Dataset). 31

Figure 26. Climograph for Pohakuloa Training Area, Hawaii (Source: http://www.weather.com). 32
Figure 27. Runoff potential for the soils of Fort Riley, Kansas by soil hydrologic group (Source: Generalized Map of U.S. Soils, USDA NRCS)..... 33
Figure 28. Dominant landcover categories for Fort Riley, Kansas (Source: 2001 National Landcover Dataset). 34
Figure 29. Climograph for Fort Riley, Kansas (Source: http://www.weather.com)..... 34
Figure 30. General schematic of the *nLS+* model for gully prediction and forecasting..... 37
Figure 31. Sensitivity of *nLS+* model output to changes in slope at the Kahuku Training Area, Schofield Barracks, Oahu. 39
Figure 32. Impact of DEM error on a flow accumulation network conducted for a portion of the Kahuku Training Area, Schofield Barracks, Oahu. 40
Figure 33. Coefficient of variation for accumulated *nLS+* values at 300 random locations, across three elevation zones, at the Kahuku Training Area, Schofield Barracks, Oahu..... 42
Figure 34. Coefficient of variation for accumulated *nLS+* values at 300 random locations, across three elevation zones, at the Kahuku Training Area, Schofield Barracks, Oahu..... 43
Figure 35. Relationship between rut depth and LAV turning radius (from Liu *et al.*, 2009)..... 44
Figure 36. Installation boxplots of flow length (upstream) extracted at each field measured gully location using 10 meter DEM as model input. 49
Figure 37. Boxplot of accumulated nLS+ values for each installation after primary and secondary processing and using 10 meter DEM as model input. 51
Figure 38. Boxplot of accumulated nLS+ values for each installation after primary and secondary processing and using LIDAR DEM as model input. 52
Figure 39. Histogram of accumulated nLS+ values for Fort Hood, Texas after primary and secondary processing. The right-skewed distribution evident here is typical of that seen for all installations. 52
Figure 40. Histogram of log-transformed accumulated nLS+ values for Fort Hood, Texas after primary and secondary processing. The improvement in normality evident here is typical of that seen across all installations and both NED and LIDAR resolutions. 53
Figure 41. Examples of boxplots of log-transformed accumulated nLS+ values, with NED DEMs as input, for Fort Benning, Georgia (left) and Fort Hood, Texas (right) showing outlying values. 54
Figure 42. Predicted gully locations (left) and gully density surface (right) representing number of predicted gullies per square kilometer for Fort Benning, Georgia based on a natural breaks classification and NED DEM model input. Gully locations used for calibration and validation are shown as blue and yellow dots, respectively, on the left image. 57
Figure 43. Predicted gully locations (left) and gully density surface (right) representing number of predicted gullies per square kilometer for Fort Hood, Texas based on a natural breaks classification and NED DEM model input. Gully locations used for calibration and validation are shown as blue and yellow dots, respectively, on the left image. 58
Figure 44. Predicted gully locations (left) and gully density surface (right) representing number of predicted gullies per square kilometer for Fort Hood, Texas based on a natural breaks classification and LIDAR DEM model input. Gully locations used for calibration and validation are shown as blue and yellow dots, respectively, on the left image. 58

Figure 45. Bar plot of distances between predicted and validation gully locations for all installations (n = 222). Predictions within a distance of 10 m or less were considered correct when using 10 m DEMs as model input. 59
Figure 46. Bar plot of distances between predicted and validation gully locations for Fort Hood, Fort Riley, and Keamuku Parcel (n = 163). Predictions within a distance of 3 m or less were considered correct when using LIDAR DEMs as model input. 62
Figure 47. Histograms showing the distribution of accumulated nLS+ values for gully locations at Kahuku Range, Hawaii before (left) and after (right) log-transformation needed to meet the normality assumption of the one-way ANOVA test. Data are based on model runs using NED DEM inputs. 67
Figure 48. Graphical results from the post-hoc Tukey HSD test based on data presented in Table 17. Intervals that do not contain a zero value (dashed vertical line) indicate a significant difference exists between installation mean accumulated nLS+ values. 70
Figure 49. Box plot of installation median log-transformed accumulated nLS+ values based on data from models runs using LIDAR DEM inputs. 71
Figure 50. Relationship between rut depth and LAV turning radius (from Liu et al., 2009). 72
Figure 51. Turning radius measurement points following the five-point method (adapted from Ayers et al., 2000). 73
Figure 52. Estimated impact severity (IS) and rut depth (RD) values for Stryker vehicle PTA19 for a portion of its off-road track during proofing maneuvers conducted at Keamuku Parcel (Pohakuloa Training Area), Hawaii. 78
Figure 53. Predicted future gully erosion sites (left) from Stryker proofing maneuvers conducted on the Keamuku Parcel (Pohakuloa Training Area), Hawaii (right). 79
Figure 54. Ecoregion assignment of installation critical nLS+ thresholds based on Euclidean allocation criteria. Majority values from the initial allocation grid (left) are used to assign each ecoregion to a unique installation (right). 82
Figure 55. Preliminary spatially distributed estimate of critical nLS+ threshold values based on the interpolation of installation results using a thin-plate spline radial basis function technique. 83
Figure 56. Screen capture image of the model toolbox and component sub-models in the ArcToolbox application of Esri's ArcGIS 10.0 GIS program. 84
Figure 57. Diagram of Sub-Model #1: Prepare Filled DEM. Model inputs are shown in blue and final outputs in green with the superscripts "P". 86
Figure 58. Cumulative model execution time based on complete model runs for all study installations. 87
Figure 59. Average sub-model execution times with standard deviation bars. 87

LIST OF TABLES

Table A. Summary of results for project quantitative performance objectives. xiv
Table 1. Manning's coefficients (*n*) used in this study for representative LULC classes contained in the National Landcover Dataset (NLCD 2006). 5
Table 2. Project performance objectives. 9
Table 3. Abbreviated comparison of biophysical and climatic characteristics for selected demonstration sites. 16
Table 4. Interpretation of USDA-NRCS soil hydrologic groups. 17
Table 5. Sensitivity of *nLS*+ model output to the distribution of LULC classes at Kahuku Training Area, Schofield Barracks, Oahu. 41
Table 6. Range of Manning's *n* coefficient values for select LULC types comprising the Kahuku Training Area, Schofield Barracks, Oahu (Chow 1959). 42
Table 7. Summary of Impact Severity (IS) scores for assessing vehicle track damage to vegetation (from Liu *et al.*, 2009) 45
Table 8. Summary of gully data acquired from installations and generated for *nLS*+ model calibration and validation. 46
Table 9. Summary statistics for installation gullies after initial data pre-processing that removed from further analysis gullies with accumulated *nLS*+ values equal to zero. 48
Table 10. Summary of outliers and outlying upstream flow length values for gullies by installation. The outlier threshold represents the first, and lowest, flow length value associated with an installation gully that was excluded from further analysis. 50
Table 11. Summary statistics for gullies at the installation level after initial and secondary data pre-processing that removed gullies with both accumulated *nLS*+ values equal to zero and outlying flow length values. 51
Table 12. Number of gullies excluded from further analysis for each installation (and total) after primary, secondary, and tertiary data pre-processing when using NED DEMs as model input... 54
Table 13. Number of gullies excluded from further analysis for each installation (and total) after primary, secondary, and tertiary data pre-processing when using LIDAR DEMs as model input. 55
Table 14. Summary statistics for calibration gullies at the installation level. 56
Table 15. Critical threshold values from calibration gully datasets for accumulated *nLS*+ values. Threshold values for gully prediction represented by the interval defined by the lower- and upper-bounds. 56
Table 16. Distance (in meters) summary statistics and prediction accuracy for *nLS*+ model results at each installation using validation gully datasets and NED DEM inputs. 60
Table 17. Comparison of predicted gully to total installation areas based on model runs using NED DEM inputs. 61
Table 18. Distance (in meters) summary statistics and prediction accuracy for *nLS*+ model results at each installation using validation gully datasets and LIDAR-derived DEMs. 62
Table 19. Comparison of predicted gully to total installation areas based on model runs using LIDAR-derived DEM inputs. 63
Table 20. Example classification error matrix used to further assess nLS+ model performance. 64
Table 21. Classification error matrix consisting of data from all installations and based on results from nLS+ model runs using NED DEM inputs. 65

Table 22. Classification error matrix consisting of data from Fort Riley, Fort Hood, and Keamuku Parcel and based on results from nLS+ model runs using LIDAR DEM inputs..... 65
Table 23. Measures of the shape of the distributions of accumulated nLS+ values at gully locations for study area military installations based on model runs using NED DEM inputs..... 66
Table 24. Results from the post-hoc Tukey HSD test based on data from NED DEM model runs. Installations in bold have significant differences in mean accumulated nLS+ values based on a 95% confidence coefficient..... 69
Table 25. Summary of impact severity scores and their corresponding meanings (Source: Li et al., 2007) 76
Table 26. Summary data from the Stryker proofing maneuver conducted at Keamuku Parcel (Pohakuloa Training Area), Hawaii (from Howard et al., 2011)..... 77
Table 27. Summary of computed data for impact severity and rut depth used to modify nLS+ model inputs and predict new gully erosion areas after the Stryker proofing maneuver conducted at Keamuku Parcel (Pohakuloa Training Area), Hawaii. 77
Table 28. Binary matrix of installation soil and landuse/landcover types used to computer the Jaccard dissimilarity index..... 80
Table 29. Values for Jaccard's distance (Jδ) for all study installations, including Fort Irwin and Camp Lejeune. Values range between 0-1, with higher values indicating more differences between sites. 81
Table 30. Summary of sub-model inputs, outputs, and overall function..... 85
Table 31. Cost model for Enhance nLS+ model..... 89

LIST OF ACRONYMS

AGNPS. .....Agricultural non-point source pollution model
ANOVA .....Analysis of variance
asl ..... above sea level
ATV ..... All-terrain vehicle
AVG ..... Average
BMP ..... Best management practice
CA ..... California
CADD. ..... Computer assisted design and drafting
CASC2D. .....Fully integrated distributed cascaded 2 dimensional hydrologic model
CD .....Compact disc
CERL .....Construction Engineering Research Laboratory
COG .....Course over Ground (heading)
CPU ..... Central Processing Unit
CRP .....Conservation Reserve Program
D8.....Eight direction flow algorithm
DoD ..... U.S. Department of Defense
DEM.....Digital elevation model
DGPS .....Differential global positioning system
DVD ..... Digital video disc
ERDC ..... Engineering Research and Development Center
ESRI ..... Environment System Research Institute
ESTCP..... Environmental Science and Technology Certification Program
FGDC .....Federal Geographic Data Committee
GHz .....Gigahertz
GIS ..... Geographic Information Systems
GPS .....Global Positioning System
GUI ..... Graphical user interface
ha.....Hectares
HSD..... Honestly Significant Difference
HMMWV ..... High mobility multi-wheeled vehicle
IS .....Impact severity
ITAM .....Integrated Training and Management
KM ..... Kilometer
L ..... Overland flow length
LAV .....Light armored vehicle
LIDAR ..... Light detection and ranging
LRAM ..... Land Rehabilitation and Maintenance
LULC .....Landuse/Landcover
MCB.....Marine Corps Base
mm ..... millimeters
MRLC ..... Multi-Resolution Land Characteristics Consortium
n..... Manning's surface roughness coefficient
NED ..... National Elevation Dataset
NEPA .....National Environmental Policy Act of 1969

NLCD ..... National Landcover Database
nLS+ ..... GIS-enabled kinematic wave model
NPS ..... Non-point source
NRCS ..... Natural Resource Conservation Service
PTA ..... Pohakuloa Training Area
R ..... Rainfall erosivity factor
RAM ..... Random Access Memory
RBF ..... Radial Basis Function
RD ..... Rut depth
RTLA ..... Range and Training Land Assessment
RUSLE ..... Revised Universal Soil Loss Equation
RUSLE2 ..... Revised Universal Soil Loss Equation 2
S ..... Slope
sec ..... Seconds
SERDP ..... Strategic Environmental Research and Development Program
SQL ..... Structured query language
SRA ..... Sustainable Range Awareness
TMDL ..... Total maximum daily load
TR ..... Turning radius
TRI ..... Training Requirements Integration
URL ..... Uniform Resource Locator
US ..... United States
USDA ..... United States Department of Agriculture
USEPA ..... U.S. Environmental Protection Agency
USPED ..... Unit stream power-based erosion deposition model
VDMTS ..... Vehicle dynamics monitoring and tracking system
VEL ..... Velocity
WWF ..... World Wildlife Fund

EXECUTIVE SUMMARY

OBJECTIVES OF THE DEMONSTRATION

Over the past decade, much effort has been expended on collecting data and modeling soil erosion resulting from military vehicle activities. Four models are often recommended for consideration and use by military land managers, including the Agricultural Non-Point Source Pollution Model (AGNPS), CASCade 2 Dimensional (CASC2D), the Revised Universal Soil Loss Equation (RUSLE), and the Unit Stream Power-based Erosion Deposition (USPED) model. While each of these has strengths, none is capable of predicting the initiation point of soil erosion and predicting the location of potential gully sites. Based on the concept of accumulating overland flow energy, an erosion potential model (*nLS+)* was calibrated and validated for five military installations (Fort Benning, Fort Hood, Fort Riley, Schofield Barracks, and Pohakuloa Training Area). By integrating data from digital elevation models (DEMs) and landuse/landcover (LULC) assessments in a geographic information system (GIS) environment, the *nLS+* model determines where surface water runoff transitions from overland sheet flow to concentrated flow and, as a result, where the potential for soil erosion and gully formation is highest.

The most common methods implemented by range managers to locate gullies on military lands are air- and ground surveys. Both are costly and labor-intensive activities that require frequent repetition as gullies tend to form dynamically as a result of interactions between the intensity and location of maneuvers, intense rainfall events, moisture content of soils, vegetation type and health, and topographic relief. Gullies not only contribute to soil erosion and water quality problems, but are a cause of injury to soldiers and damage to equipment, especially during nighttime maneuvers.

Application of the methods embodied in the *nLS+* model allows range managers to reduce the size of, and prioritize, their survey areas by focusing attention on sites most likely to develop gullies. Because of the model's flexible GIS format, additional spatial data layers such as troop movements and vehicle tracking can be added to enhance model performance and usability. The tangible dollar value is time saved in locating gullies. The unknown savings comes in reduction of injuries to soldiers and repairs to damaged equipment. The *nLS+* modeling approach can also assist with siting BMPs designed to reduce soil erosion, thereby assisting installations in meeting current, or future, sediment total maximum daily load (TMDL) requirements for streams leaving federal lands.

Three quantitative performance objectives have been identified for this project. The first is to identify the critical threshold for accumulated *nLS+* values for each study installation. For this first objective, the *nLS+* model will be calibrated and validated independently for each study installation and the threshold for accumulated *nLS+* values corresponding best to known gully locations calculated. The second quantitative performance objective determines whether a single critical threshold for accumulated *nLS+* values is adequate for each installation study site. This objective seeks to assess whether a single common critical threshold for accumulated *nLS+* values is valid for all installations or whether the individual installation threshold values are statistically different (*i.e.*, place-specific). The third, and final, quantitative performance

objective uses the *nLS+* model in a predictive mode to forecast areas where gullies are likely to form in response to future military training events. Here, the *nLS+* model can be operated after a training exercise and new areas of gully erosion predicted by using vehicle tracking data and corresponding estimates of vegetation damage and rut depth to modify the installation DEM and LULC layers. The ability to predict future erosion potential with the *nLS+* model offers several significant advantages to military installations including:

1) The ability to assess training land impacts from scheduled training exercises given current environmental conditions.
2) Providing a consistent and scientific basis to estimate LRAM costs to repair and prevent gully erosion on current, future, or rental training lands.
3) The ability to estimate and compare environmental impacts due to training events associated with installation realignment or mission change.

An additional set of qualitative performance objectives are also in place. Accomplishment of the first is dependent on the outcome of the second quantitative objective and, should installation-specific critical *nLS+* thresholds be required for satisfactory model predictive accuracy, will explore appropriate geographic regions where critical *nLS+* thresholds might be valid. The second qualitative and final overall performance objective is the development and deployment of a downloadable GIS tool that ITAM personnel can use to run the *nLS+* model themselves.

TECHNOLOGY DESCRIPTION

Determining the overland flowpath of surface water runoff is a key process in erosion modeling because concentration of overland flow is a primary cause of soil erosion. The efficiency of best management practices (BMPs) for preventing or minimizing NPS pollution, such as vegetated buffer systems, is significantly affected by overland flow conditions. However, the ability to classify varying flow regimes, from sheet flow to concentrated flow, is problematic because it is difficult to quantify the energy content of runoff water.

The kinematic wave theory has proven to be a useful tool for assessing the process of overland flow at varying flow regimes and, based on this theory, the relationship $nL/S^{0.5}$ has been used to categorize hydrological flow regimes into sheet flow or concentrated flow, where n is Manning's surface roughness coefficient for overland flow, L is the length of overland flow (feet), and S is the slope.

Here, this relationship is inverted and the flow length variable omitted ($S^{0.5}/n$). Flow length is replaced with profile curvature, a measure of topographic shape parallel with the direction of flow, to incorporate the influence of flow acceleration and deceleration on soil erosion and deposition ($(S^{0.5}/n) * C_{PROF}$). This "enhanced *nLS* equation" is operationalized in a GIS as a multilayer raster calculation using classified LULC and DEM data, with calculated values summed in a weighted accumulation as simulated runoff travels along a flow path, thereby indirectly incorporating flow length back into the computation. The relationship between actual gully locations and accumulated *nLS+* values are then compared to develop a predictive model and prediction map.

The *nLS+* model can also be used to predict the impact of future training events on overland flow and the formation of new gully incision points. Relationships established in past research between vehicle turning radius, vegetation damage, and rut depth can be integrated within the *nLS+* modeling framework using standard GIS data processing and manipulation techniques. The key input for this forecasting *nLS+* model is vehicle tracking data from global positioning systems (GPS), collected during field exercises, which can be used to modify existing installation DEMs and LULC maps. After modifications to these input datasets are made, the model is re-run and the results assessed by installation land managers to forecast the expected impact of recent, or planned, military training exercises on gully formation. This new capability benefits installations by helping make training areas safer for soldiers and can assist range managers in estimating costs associated with post-exercise training area repairs.

The model, itself, is designed as a series of four sub-models for users who wish to predict the current location of gullies or forecast the formation of new gullies in response to a training event. Data sets required for gully prediction include LULC and DEM inputs. From these data layers, the Manning's *n*, slope, profile curvature, and other required intermediate data products are computed. In forecast mode, input data include a filled DEM and Manning's *n* grid (output from the model in prediction mode) and a form of vehicle tracking data from GPS devices that includes, at minimum, vehicle coordinates and velocity. Model LULC and DEM inputs can be obtained from nationally available geographic datasets such as the National Landcover Database (NLCD) and National Elevation Dataset (NED) to minimize data acquisition and preparation times.

DEMONSTRATION RESULTS

Gully data for selected installations were obtained from ITAM staff and collected by project personnel during site visits. To meet assumptions of normality required by statistical procedures, these data were evaluated at each of three stages to remove gully observations with outlying values of flow length and flow accumulation using extracted descriptive values from outputs of the *nLS+* model runs . After pre-processing using NED DEM inputs, 71 of 389 (18%) of the original gullies sampled from all installations were excluded from further analysis. The remaining gullies for each installation (n = 318) were divided into calibration and validation datasets with 30% of the total number of gullies (or a minimum of 10) used for model calibration (n = 96) and the remainder for validation (n = 222). Following pre-processing with DEMs acquired by light detection and ranging (LIDAR) methods, 41 of 277 (15%) of the original gullies sampled from all installations were excluded, with 74 and 163 observations used model calibration and validation, respectively. Project results for the set of quantitative objectives are summarized in Table A and described below.

Table A. Summary of results for project quantitative performance objectives.

Performance Objective	Success Criteria	Summary of Results
1. Identify the critical threshold for accumulated *nLS+* values for each study installation.	• > 80% of gully locations correctly identified for each installation using the installation specific critical threshold. • The valid precision of the prediction is dependent on the spatial resolution of the DEM with predictions considered correct if located within a one cell resolution buffer distance of actual gully sites.	• Distances at which 80% correct criterion was reached using NED DEM inputs: Fort Benning: 20 m Fort Hood: 30 m Fort Riley: 30 m Kahuku Range: 20 m Keamuku: 10 m • Distances at which 80% criterion was reached using LIDAR DEM inputs: Fort Hood: 9 m Fort Riley: 6 m Keamuku: >12 m
2. Determine whether a single critical threshold for accumulated *nLS+* values is adequate for all study installations.	• Between installation variation of critical threshold values and gully locations is less than the within installation variation.	• ANOVA indicated significantly different *nLS+* values among installations when using NED DEM inputs. • Kruskal-Wallis Chi-squared analysis indicated significantly different *nLS+* values among installations when using LIDAR DEM inputs.
3. Forecast areas where gullies are likely to form in response to future military training events at Pohakuloa Training Area.	• Success criteria from quantitative objective #1.	• Using actual vehicle tracking data from maneuvers at Keamuku Parcel, and modified NED DEM and LULC inputs, the *nLS+* model forecasted 3 additional hectares of erosion activity.

At the NED DEM resolution, and considering all installations, 131 of 222 total validation gullies (59%) were predicted to within 10 m of their actual location. This percentage increases to 79% and 89% for distances within 20 and 30 m, respectively. Mean distance to the correct location ranged from a low of 4.93 m (Keamuku Parcel) to a high of 14.73 m (Fort Hood). Percentage correct predictions (<= 10 m) for individual installations ranged from a high of 85% (Keamuku Parcel) and a low of 50% (Fort Benning), with the total range in distances varying from 20 m (Keamuku Parcel) to nearly 96 m (Fort Hood). Only the predictions for Keamuku Parcel met the success criteria of having more than 80% of gully locations correctly identified using installation-specific accumulated *nLS+* thresholds within the required distance precision. If the precision condition is loosened to a distance window of 2 times DEM cell resolution, model success was also achieved at Fort Benning and Kahuku Range. All installations reached the minimum 80% prediction accuracy level at 3 times the NED DEM cell resolution. Overall model accuracy was 86%, though commission error for the predicted gully class was nearly 100%. Though the model suffered from extreme overprediction of gully locations, the total land area identified as likely erosion sites ranged from a low of 496 ha (Kahuku Range) to a high of 16,862 ha (Fort Hood), with the total installation area susceptible to predicted gully erosion falling between 12% (Fort Riley) and 21% (Keamuku Parcel).

For the three installations for which LIDAR DEMs were available – Fort Riley, Fort Hood, and Keamuku Parcel Priority 1 Area – 98 of 162 validation gullies were predicted to within 3 meters of their correct location. Correct predictions increased to 76% and 82% for distances within 6 and 9 m, respectively. Mean distance to the correct location ranged from a low of 1.64 m (Fort Riley) to a high of 100.32 (Keamuku Parcel). Percentage correct predictions (<= 3 m) for individual installations ranged from a high of 75% (Fort Riley) to a low of 5% (Keamuku Parcel), with the total range in distances varying from approximately 11 m at Fort Riley to over 303 m at Keamuku Parcel. No installation met the established success criteria at the LIDAR DEM resolution, however the 80% criterion was reached at 6 m at Fort Riley and 9 m at Fort Hood. Overall model accuracy was very high 98% though, again, the error of commission for the predicted gully class was large. Again, despite the tendency to greatly overpredict the number of gully sites, the total land area predicted to have high erosion potential ranged from a low of 12 ha (Keamuku Parcel) to a high of 1,241 ha (Fort Hood), with the total estimated installation area susceptible to predicted gully erosion ranging between 1-2% for all sites.

A one-way analysis of variance (ANOVA) test was used to compare mean differences in accumulated *nLS+* values from gully locations across each installation based on data calculated from NED DEM inputs. The resulting F test statistic equaled 11.931 (numerator df = 4, denominator df = 104.086, p-value << 0.001) which allowed rejection of the null hypothesis that installation mean accumulated *nLS+* values were equal. A Tukey's Honestly Significant Difference (HSD) test was performed to examine all possible pairwise differences between installation means to help identify which installation(s) contributed most to the ANOVA result. Values calculated for two installations – Fort Benning and Fort Hood – contribute most to the difference. While Forts Benning and Hood are similar to each other, they were significantly different in all pairwise comparisons except for Kahuku Range-Fort Benning. Fort Riley, Kahuku Range, and Keamuku Parcel had comparable mean accumulated *nLS+* values.

A non-parametric Kruskal-Wallis one-way ANOVA test was used to test the equality of median accumulated *nLS+* values of gullies at three installations using data from LIDAR DEM model runs. The calculated Kruskal-Wallis chi-squared test statistic of 89.67 (df = 2, p-value << 0.01) allowed rejection of the null hypthosis indicating that installation accumulated *nLS+* values were significantly different. As was the result with NED-derived *nLS+ values, d*efining a single critical threshold for log-transformed accumulated *nLS+* values is not appropriate for the installations studied and using LIDAR DEM inputs.

Three Stryker vehicles from a reconnaissance platoon of the 2nd Brigade of the 25th Infantry Division were tracked during an off-road proofing mission on Keamuku Parcel using GPS-based tracking systems to determine vehicle movement patterns and estimate soil loss. Track data were recorded by GPS and received as a text file with geographic coordinate information acquired at approximately one second intervals. Each GPS record also included measures of vehicle velocity (VEL) and course over ground (COG) along with a detailed date/time stamp identifying when the position record was acquired. Rut depth (RD) was calculated as a function of vehicle turning radius based on a known relationship between the inside and outside tracks for a Light Armored Vehicle (LAV). Impact severity (IS) scores were also calculated based on turning radius and vehicle velocity estimates to estimate the percentage of soil and vegetation damaged during off-road maneuvers. The IS and RD estimates based on the GPS tracking data were used modify the original Manning's *n* and NED DEM input layers used in an earlier *nLS+* model run for Keamuku Parcel to better reflect post-maneuver landscape conditions. The model was re-run using these modified DEM and Manning's *n* grids using the previously calibrated and validated installation-specific accumulated *nLS+* threshold values. This "re-analysis" of model results showed an additional 326 cells that were candidate sites for gully erosion. Given the 10 m spatial resolution of the NED DEM used, this translates into an additional 3.26 ha of new land area that may be subject to active erosion or approximately 0.12 ha per off-road kilometer travelled by the maneuvering vehicles.

Because earlier results showed that a single critical threshold for accumulated *nLS+* values was not valid for all study installations, using either NED or LIDAR DEM inputs, methods were explored for regionalizing the installation-specific thresholds to make model results more applicable at new locations. It was initially thought that ecoregion boundaries might serve as a useful framework for extending model results. However, results from a Jaccard dissimilarity index and installation characteristics such as soil hydrologic group, landcover type, and slope indicated that using common biogeophysical properties (*e.g.*, ecoregions) as the means to make installation critical *nLS+* values, as computed here, more spatially explicit would not be successful. Since ecoregionalization of critical *nLS+* threshold values does not hold promise at this time, two different techniques were applied to help visualize how these thresholds might be applied in a more spatially continuous manner. First, ecoregions were linked to each installation based on a Euclidean distance allocation and assigned that installation's threshold values. The second approach used a thin-plate spline radial basis function (RBF) interpolation method to create a spatially continuous threshold estimate.

The *nLS+* model was developed with the ArcGIS 10.0 (Esri, Redlands, CA) suite of GIS software applications routinely utilized across Department of Defense (DoD) agencies and installations. The model is packaged as "toolbox" with multiple sequenced tools than can be

downloaded and used on a local computer workstation running ArcGIS version 10.0. The toolbox and associated modeling tools also includes an integrated help system to explain the underlying processes, data requirements, and recommendations for default settings or values as they apply to execution of the model. Feedback from installation ITAM GIS technicians helped shape the final form of the modeling tool as a sequence of smaller and quicker performing sub-models rather than one large model. Comments and questions generated during site visits were very useful during creation of the integrated help system to guide users through the geoprocessing procedures.

The final model – Rapid Soil Erosion Assessment Toolbox – is comprised of six total sub-models labeled within the toolbox by number and title. Users run the model and arrive at final results by executing each sub-model in numeric sequence from #1 (Prepare Filled DEM) to #4 (Predict Gully Locations). Sub-models #5-6 can be used to forecast future gully locations by modifying the installation DEM and Manning's *n* grid with GPS-derived vehicle tracks. Average run time for the model, including all sub-models and assuming a non-LIDAR DEM and satellite resolution landuse/landcover grid for the installation is already on hand, ranged between 1.1 and 8.3 minutes on a typical desktop computer workstation. When working with spatial data at the spatial resolution of installation LIDAR datasets (3 m), processing time was 3-4 times longer in duration.

IMPLEMENTATION ISSUES

Project results were largely positive, despite not meeting the success criteria established for all performance objectives. One issue that remains with interpreting model results is the large rate of false positive gully predictions (*i.e.*, errors of commission). Despite this issue, when used as a guide to identify areas with the most potential for gully erosion, the model results support time and cost savings by significantly reducing the total area of land being considered for more frequent and/or intensive field monitoring. Also, vehicle tracking data is not routinely collected by installations and made available to ITAM staff to support model use in "forecast" mode. However, the *nLS+* model represents a tool available now to military land managers that promotes training land sustainability by demonstrating the data types, analytical methods, visualization tools, and information delivery mechanisms that could become routine across installations for assessing training land condition and trends. One installation – Fort Riley – already incorporates the model in assessments of soil erosion potential and as a tool for planning gully surveys in the field. For maximum benefit, this single method needs to be complemented with others that together form a coordinated suite of environmental/sustainability indicators for key monitoring themes that can be collected, assessed, and synthesized to help identify when, and where, sustainable use of training lands is, and is not, being achieved.

During the course of this project, it was clear that no consensus definition for the term "gully" exists among installation natural resource managers. Contributing to this inconsistency might be the varying definitions for, and meanings behind, the terms "gully" and "gap" presented in military literature, along with the different disciplinary perspectives held by the land managers themselves. In addition to this definitional concern, tremendous variability exists in how installation land managers and GIS technicians measure and record gully information. The by-product of this inconsistent definition and lack of best practices for recording gullies are datasets

that differ considerably in spatial, temporal, and attribute quality. Much of the variation in model results reported in this study is attributed to this lack of a common definition, as well as differences in how gullies are recorded in the field and then represented in digital form. The gully definition presented in this report, informed both the agricultural sciences and military mobility restrictions, should be considered for official adoption. Further, a geodatabase structure should be proposed and shared with installations to enforce more uniform documentation of gullies with a minimum set of geometries and attributes.

If the *nLS+* model finds widespread use across installations, it is important that an organization be identified to maintain the model and make any updates and/or revisions necessitated by future GIS software versions. As with any GIS-based model for which installation use is expected, the *nLS+* model is an ideal candidate to be delivered to end-users as a Web-based geoprocessing service made available, and maintained, by a central environmental organization. Uniform data and information products could then be delivered on a scheduled basis to installations for action. All data products required by the *nLS+* model, and other environmental/sustainability indicators, could be stored in a geospatially-enabled relational databases to facilitate access to current data. Storing data in the geospatially enabled relational database supports distributed viewing and editing by land managers and their staffs, as well as distribution via mapping and geoprocessing web services similar to the "Integrated Training Area Management (ITAM) Map Viewer" Web application used by Fort Riley (http://services.geog.ksu.edu/frk_rtla).

Most of this project was conducted during an extremely volatile period for installation ITAM staffs. Frequent changes in ITAM personnel, including directors, and significant reductions in the number of GIS staff members was a near universal issue at each installation participating in this effort. While certainly a factor in the execution of this project, continued staffing issues for any installation office interested in better understanding the spatial and temporal dynamics of gully formation will discourage widespread adoption and use of model-based natural resource management tools. Prerequisites for successful implementation include technical staffs with training in GIS as well as administrative leaders who both see value in the approach and can effectively use model output to improve land rehabilitation planning and budgeting efforts.

1.0 INTRODUCTION

This section is intended to provide a general overview of the project. Specific subsections, including project background, demonstration objectives, and regulatory drivers are described.

1.1 BACKGROUND

The 2000 National Water Quality Inventory reported that 40% of the nation's water bodies do not meet water quality standards and identified non-point source pollution (NPS) as the leading cause of surface water degradation (USEPA 2000). Over 290,000 miles of river, almost 7,900,000 acres of lake, and 12,500 square miles of estuary failed to meet water quality standards. Military training maneuvers have the potential to significantly alter land surfaces, reduce quality and promote NPS pollution, resulting in a reduction of training land quality and the inability of military installations to meet water quality standards as defined by current, and future, TMDLs mandated in Section 303(d) of the 1972 Clean Water Act.

Military readiness depends upon high quality training. A prerequisite of effective maneuver training is repetition and a large land base, which creates intense stress on military lands. Environmental protection requirements place additional restrictions on land use and availability. Because military training schedules are set well in advance to make the best use of installation training facilities and National Training Centers, there is little flexibility to modify training events while maintaining readiness. Management practices are required that allow for high military training tempos while protecting surface water quality and reducing NPS pollution generation.

In order to meet this need, the military initiated the Integrated Training and Management (ITAM) program with the overall goal to achieve optimum sustainable use of military lands. The ITAM program provides Army range officers with the capability to manage and maintain training lands while supporting mission readiness. ITAM integrates mission requirements with environmental requirements and environmental management practices, and establishes the policies and procedures to achieve optimum, sustainable use of training and testing lands. There are multiple components of ITAM including Training Requirements Integration (TRI), Range and Training Land Assessment (RTLA), Land Rehabilitation and Maintenance (LRAM), Sustainable Range Awareness (SRA), and Geographic Information Systems (GIS).

TRI is the component of the ITAM Program that provides a decision support procedure for integrating training requirements with land management, training management, and natural and cultural resources management processes and data derived from RTLA and Army Conservation Program components. TRI supports the Army's requirements for environmentally sustainable training lands. The goals for TRI are twofold: (1) to ensure sustained accessibility to adequate training lands to support training to standards under realistic natural conditions, and (2) to provide military trainers and land managers with the necessary technical and analytical

information to integrate doctrinally based training and testing with land constraints and quantify training land carrying capacity.

RTLA programs are focused on training support and training land management, and may be used to support National Environmental Policy Act (NEPA) and other compliance and planning efforts related to Army transformation, restationing, and realignment. Current policies allow installation-level land managers and range operations staffs to determine how they can best collect and use resource data to support foundational, long-term, and site-specific land management decisions such as training area allocation, training area use, and land rehabilitation effectiveness. Analyzing the impact of military training on soil erosion is part of the RTLA program. Over the past decade a great deal of effort has been given to collecting data and modeling soil erosion from track vehicle activity. A Tri-Service CADD/GIS Technology Center recently technical report (Doe *et al.*, 1999) that evaluated the applicability of several soil erosion models for use on military lands. The report recommends four models for consideration by military land managers: AGNPS, CASC2D, RUSLE, and USPED. Each of these models has strengths to consider. However, none of the models is capable of predicting the initiation point of soil erosion and locating potential gully sites. More recent information concerning erosion modeling and gully location tools on military lands was not found.

Currently, range managers send personnel to the field to survey training lands and locate gullies. This is a constant and labor intensive process as gully development is a dynamic process influenced by a variety of factors including maneuver locations and intensities, rainfall, soil moisture content, vegetation type and health, and topographic relief. Gullies not only contribute to soil erosion and water quality problems, but are a cause of injury to soldiers and damage to equipment when a gully of sufficient depth is encountered during maneuvers, especially at night.

1.2 OBJECTIVE OF THE DEMONSTRATION

Based on the concept of accumulating overland flow energy, an erosion potential model was developed for Fort Riley, Kansas as part of a research project funded by the Strategic Environmental Research and Development Program (SERDP, SI 1339 – Assessing the Impact of Maneuver Training on NPS Pollution and Water Quality). By integrating data from DEMs and LULC assessments in a GIS environment, the model determined where surface water runoff transitioned from overland sheet flow to concentrated flow (*i.e.*, transitional flow) and, as a result, where the potential for soil erosion and gully formation was highest.

This model was calibrated and validated with field data from two watersheds near Fort Riley and was shown to be successful in identifying the location of gullies (Steichen *et al.* 2009). However, additional assessment of model performance is necessary to ensure results are valid outside of the Flint Hills ecoregion (Omernik 1987) in which Fort Riley is located. The first objective of this project is to run the erosion potential model for additional military installations selected from regions with different precipitation regimes, landcover conditions, topographic characteristics, and soil types.

A second objective is to operate the erosion potential model in a predictive mode to better assess the impact of military training activities on future gully formation. To accomplish this, vehicle tracking data from Stryker vehicle proofing maneuvers conducted at Pohakuloa Training Area in

Hawaii were obtained and used to modify current installation DEMs and LULC maps. Anticipated changes to the land surface as a result of the wheeled vehicle maneuvers is derived from both past research and concurrent work (ESTCP Proposal #08 E-S13-030, Vehicle Dynamics Monitoring and Tracking System (VDMTS): Monitoring Mission Impacts in Support of Land Management).

1.3 REGULATORY DRIVERS

Since the passage of the National Environmental Policy Act (NEPA) in 1969 and the publication of US Army Regulation 200-2 (Department of Army 1988), the military has been required to minimize or avoid both short and long-term environmental impacts caused by military training. Because there is a limited amount of available land for military training, it is in the Army's best interest to protect these areas to fulfill their mission requirements for realistic training and testing. Additionally, the Clean Water Act (1972) and the Clean Water Act Amendments of 1987 require control of non-point source pollution (NPS).

2.0 TECHNOLOGY/METHODOLOGY DESCRIPTION

Demonstration technology and methodology is described in the following section.

2.1 TECHNOLOGY/METHODOLOGY OVERVIEW

Determining the flow path of surface water runoff is a key process in erosion modeling because the concentration of overland flow is a primary cause of soil erosion (Abrahams and Atkinson 1993, Bennett *et al.*, 2000). The efficiency of best management practices (BMPs) such as vegetated buffer systems for minimizing, or preventing, NPS pollution is significantly affected by overland flow conditions (Abrahams and Atkinson 1993, Abraham *et al.*, 1999). However, the ability to classify varying flow regimes, from sheet flow to concentrated flow, is problematic due to the difficulty of quantifying the energy content of runoff water (Meyer *et al.* 1999).

Many researchers have shown that the kinematic wave theory is a useful tool for assessing the process of overland flow at varying flow regimes (Laguna and Giraldez 1993, Wong and Chen 1999, Singh 2001). Based on this theory, McCuen and Spiess (1995) showed that the relationship of $nL/S^{0.5}$ effectively categorized hydrological flow regimes into sheet flow or concentrated flow (Figure 1), where n is Manning's coefficient for overland flow, L is the length of overland flow (feet), and S is the slope.

Figure 1. Schematic illustrating the difference between sheet and concentrated flows.

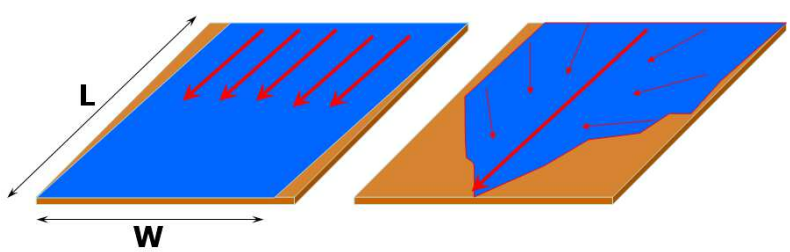

In this project, the equation presented by McCuen and Spiess (1995) is inverted and the flow length variable omitted ($S^{0.5}/n$). Inversion allows the smoother surfaces with lower Manning's n coefficients (*i.e.*, potential for more soil erosion) to yield higher computed values than rougher surfaces (higher Manning's n coefficients) and is important for determining 'maximum value' thresholds for potential gully erosion. Flow length is eliminated from the equation and replaced with profile curvature, a measure of topographic shape parallel with the direction of flow, to incorporate the influence of flow acceleration and deceleration on soil erosion and deposition (Moore *et al.*, 1991). The values from this final modified form of the equation, $(S^{0.5}/n) * C_{PROF}$, are then summed in a weighted accumulation as simulated runoff travels along a flow path, thereby indirectly incorporating flow length back into the computation:

$$\sum_{i}^{n} (S^{0.5} / n) * C_{PROF}$$

where:
S = slope grade
n = Manning's n surface roughness coefficient
C_{PROF} = profile curvature

This enhanced *nLS* equation (abbreviated from here on as *nLS+*) is operationalized in a GIS as a multilayer raster calculation using classified LULC data and DEMs. Slope is calculated from a DEM using a 3 x 3 cell neighborhood and the average maximum technique (Burrough and McDonnell 1988). Classified LULC dataset provide the relevant Level I or Level II landcover types (Anderson *et al.*, 1976) on a cell-by-cell basis for an entire study area. This nominal data is reclassified into quantitative estimates of Manning's *n* by using a look-up table of coefficient values (Table 1) (Arcement and Schneider 1984, Engman 1986, Foster *et al.* 1985, McCuen and Spiess 1995). Profile curvature is also calculated on a cell-by-cell basis based on a fourth-order polynomial derived from a 3 x 3 window of DEM elevation values (Zeverbergen and Thorne 1987).

Table 1. Manning's coefficients (*n*) used in this study for representative LULC classes contained in the National Landcover Dataset (NLCD 2006).

Landuse/Landcover Class	***n***	***Landuse/Landcover Class***	***n***
Open Water	0.0001	Shrub/Scrub	0.13
Developed High Intensity	0.015	Hay/Pasture	0.13
Developed Medium Intensity	0.015	Herbaceous	0.24
Developed Low Intensity	0.05	Woody Wetlands	0.4
Developed Open Space	0.05	Emergent Herbaceous Wetlands	0.4
Barren Land	0.05	Evergreen Forest	0.4
Cultivated Crops	0.06	Deciduous Forest	0.5
Mixed Forest	0.12		

The computed *nLS+* output grid represents a unitless estimate of surface runoff water energy as it flows downslope. These individual cell-based energy estimates, linked by the direction of overland flow, can then be summed in the fashion of a weighted flow accumulation grid. To accomplish this, the D8 algorithm (O'Callaghan and Mark 1984) is used to create a flow direction grid that estimates the direction of water flow from cell-to-cell (*i.e.*, "upstream" to "downstream") using slope and aspect information from a DEM input. Individual cell values computed from slope, Manning's *n* coefficients, and profile curvature are then summed to generate a weighted flow accumulation grid where each output cell is populated with a value equal to the summed energy of cells flowing into it from the "upstream" direction. The

relationship between actual gully locations and accumulated energy are then compared to develop a predictive model (Figure 2).

Figure 2. Results of *nLS+* model from Fort Riley, Kansas.

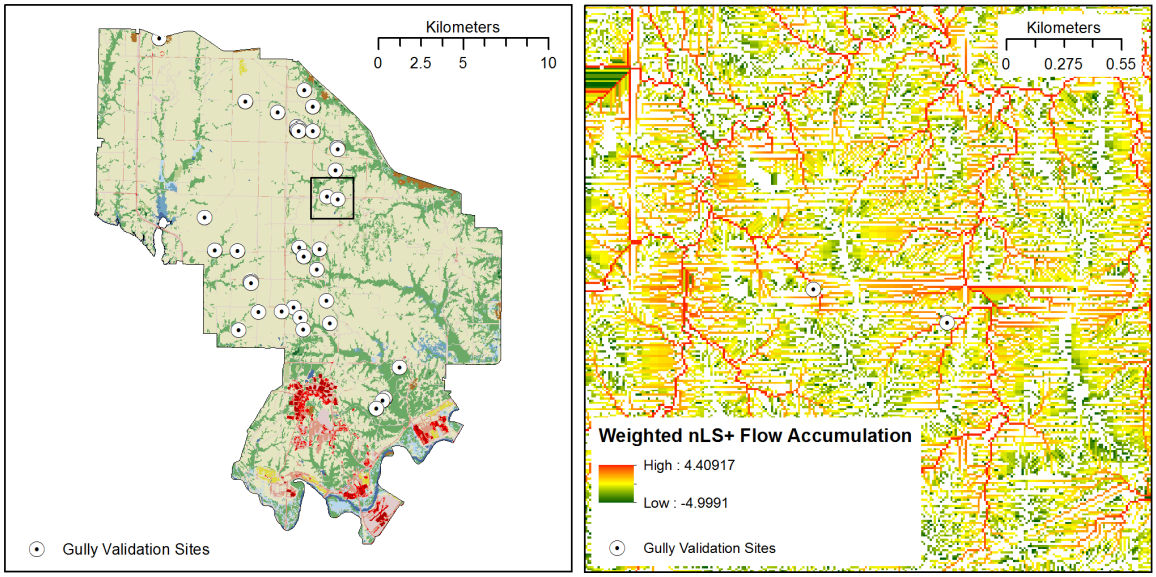

This modeling approach is designed to use common geographic datasets (*e.g.*, NLCD, NED) based upon 10-30 meter grid cell resolution source data. Because the *nLS+* model has few input requirements, for which easily accessed datasets are available nationwide, data acquisition and preparation times can be minimized compared to other existing erosion modeling approaches.

The *nLS+* model can also be used to predict the impact of future training events on overland flow and the formation of new gully incision points. The ecological impact of military vehicle maneuvers has been well studied (Ayers *et al.*, 2005a, Ayers *et al.*, 2005b, Rice and Ayers 2005, Rice *et al.*, 2006, Liu *et al.*, 2009). The relationships quantified by these studies between vehicle turning radius and both vegetation damage and rut depth can be seamlessly integrated with the *nLS+* modeling framework using standard GIS data processing and manipulation techniques. Inputs for the predictive *nLS+* model can include GPS-derived vehicle tracking data, obtained from field exercises or comparable computer simulations, which can be mapped and used to modify existing installation DEMs and LULC maps. The basis for these modifications comes from previous research that evaluated land surface alterations by vehicle type, operating characteristics, and soil conditions.

After modifications to these input datasets are made, the *nLS+* model is re-run and the results assessed by installation land managers to forecast the expected impact of recent, or planned, military training exercises on future gully formation. Such information benefits installations by helping make training areas safer for people and equipment, and can assist land managers with estimating the costs associated with post-exercise training area repairs.

2.3 ADVANTAGES AND LIMITATIONS OF THE METHODOLOGY

Currently, locating gullies is a time-consuming and potentially dangerous task if conducted on the ground and very expensive if completed via air survey. Application of the user-friendly tools demonstrated in this project allows land managers to reduce the size of, and prioritize, search area by focusing attention on sites most likely to develop gullies in accordance with the biophysical characteristics of the training area. Because of the model's flexible GIS format, additional spatial data layers such as troop movements/vehicle tracks can be easily added to enhance the model performance and usability. The tangible dollar value is time saved in locating gullies. The unknown savings comes in reduction of injuries to soldiers and repairs to damaged equipment. The *nLS+* modeling approach can also assist with siting BMPs designed to reduce soil erosion, helping installations meet current, and future, sediment TMDLs for streams leaving federal lands.

The ability to predict future erosion potential with the *nLS+* model offers several significant advantages to military installations including:

4) The ability to assess training land impacts from scheduled training exercises given current environmental conditions.
5) Providing a consistent and scientific basis to estimate LRAM costs to repair and prevent gully erosion on current, future, or rental training lands.
6) The ability to estimate and compare environmental impacts due to training events associated with installation realignment or mission change.

Financial considerations can be expanded from analyzing the expected expense of only one exercise to predicting annual and/or re-occurring costs by simulating multiple training exercises. Other federal and state environmental and natural resource agencies may find the *nLS+* model useful for assessing impacts caused by specific land management decisions such as identifying lands for the Conservation Reserve Program (CRP) and gully erosion risks associated with forest clear cut, road building, and off-road all-terrain vehicle (ATV) operations.

The *nLS+* model was developed using, and for, the ArcGIS 10.0 (Esri, Redlands, CA) suite of GIS software applications that are routinely utilized across U.S. Department of Defense (DoD) agencies and installations. Because of this, the model itself can be delivered in a variety of forms, including as an ArcToolbox "tool", a Python script, or as an ArcGIS ModelBuilder graphic model.

An interesting part of this demonstration includes development of an ArcGIS Server application to deliver *nLS+* modeling capability to a large number of users over networks through a single shared system. This prototype delivery method facilitates the technology transfer process by centralizing model development and maintenance, simplifying model use, facilitating access to required input datasets, and eliminating the need to physically distribute executable files and updates.

3.0 PERFORMANCE OBJECTIVES

The performance objectives outlined in Table 2 represent the means and metrics by which the successful demonstration of this project will be made. A total of five performance objectives are described, including the objective, the metric(s) associated with each objective, a list of the basic data required to realize the metric(s), and the specific criteria by which the successful completion of each objective may be evaluated. More detailed explanations of the data analyses supporting assessments of the performance objectives are presented in Section 6.0 (Performance Assessment).

Three quantitative performance objectives have been identified for this project. The first is to identify the critical threshold for accumulated *nLS+* values for each study installation. For this first objective, the *nLS+* model will be calibrated and validated independently for each study installation and the threshold for accumulated *nLS+* values corresponding best to known gully locations calculated. The installation-level data required to accomplish this objective includes:

- Digital elevation data, in the form of a DEM, that can be obtained from the USGS National Elevation Dataset (NED) (http://ned.usgs.gov) or local products of higher spatial resolution or currentness.
- Digital LULC maps, in the form of the 2006 NLCD, that can be obtained from the Multi-Resolution Land Characteristics Consortium (MRLC) (http://www.mrlc.gov) or local products of higher spatial resolution or currentness.
- Manning's surface roughness coefficients (*n*), obtained from the literature that correspond to each NLCD LULC type present across all study installations.
- Global Positioning System (GPS) derived coordinates for known gully locations collected by installation ITAM personnel. If such data does not exist for an installation, project personnel will obtain sufficient data for model calibration and validation during scheduled site visits.

This objective will be successfully accomplished when a critical threshold for accumulated *nLS+* values is both identified and able to correctly predict the location of 80% of known gullies at each installation. Model prediction accuracy assessments will be determined by using a GIS to measure the distance between an actual gully and its nearest predicted location. The spatial precision of the predicted location of a gully is dependent on the spatial resolution, or grain, of the DEM used during model operation. Gully predictions will be considered to be correct if located within a one cell resolution buffer distance of an actual gully site in a "Queen's Case" scenario. For example, if a DEM with a 10 meter spatial resolution is used as input into the *nLS+* model calculations, then a prediction within 10 meters in vertical or horizontal direction, or 1.4 times the cell resolution (*e.g.,* 10.4 meters) diagonally, would be a correct identification (Figure 3).

Table 2. Project performance objectives.

Performance Objective	Metric	Data Requirements	Success Criteria	Results
Quantitative Objectives				
1. Identify the critical threshold for accumulated *nLS+* values for each study installation.	Correspondence between the installation specific critical threshold value and gully locations	• Installation digital elevation models. • Installation landcover maps. • Manning's surface roughness coefficients (*n*) for installation landcover types. • Ground truth dataset of actual gully locations.	• > 80% of gully locations correctly identified for each installation using the installation specific critical threshold. • The valid precision of the prediction is dependent on the spatial resolution of the DEM with predictions considered correct if located within a one cell resolution buffer distance of actual gully sites.	• Distances at which 80% correct criterion was reached using NED DEM inputs: Fort Benning: 20 m Fort Hood: 30 m Fort Riley: 30 m Kahuku Range: 20 m Keamuku: 10 m • Distances at which 80% criterion was reached using LIDAR DEM inputs: Fort Hood: 9 m Fort Riley: 6 m Keamuku: >12 m
2. Determine whether a single critical threshold for accumulated *nLS+* values is adequate for all study installations.	Correspondence between a single critical threshold value and gully locations	• Computed accumulated *nLS* values for each known gully location for all study installations.	• Between installation variation of critical threshold values and gully locations is less than the within installation variation.	• ANOVA indicated significantly different *nLS+* values among installations when using NED DEM inputs. • Kruskal-Wallis Chi-squared analysis indicated significantly different *nLS+* values among installations when using LIDAR DEM inputs.

3. Forecast areas where gullies are likely to form in response to future military training events at Pohakuloa Training Area.	Correspondence between actual or suspected gullies and the most appropriate critical threshold value identified for the installation.	• All data from quantitative objective #1. • Vehicle paths (from tracking data or training simulations). • Vehicle-specific estimates of soil and vegetation damage. • Evidence of post-maneuver gully activity.	• Success criteria from quantitative objective #1.	• Using actual vehicle tracking data from maneuvers at Keamuku Parcel, and modified NED DEM and LULC inputs, the *nLS+* model forecasted 3 additional hectares of erosion activity.
Qualitative Objectives				
4. Propose geographic regions within which installation specific critical thresholds for accumulated *nLS+* values are valid.	Between installation variation of critical threshold values and gully locations is greater than the within installation variation.	• Results from ANOVA • Peer-reviewed ecoregion system (*e.g.*, EPA Level II/III ecoregions).	Place installations into regions of similar critical thresholds for accumulated *nLS* values according to the logic and methods used to develop generally accepted ecological regions.	Ecoregion framework showed to be inappropriate for assigning threshold values; potential use of Euclidean distance allocation and interpolation for assigning values illustrated.
5. Develop and disseminate a downloadable and easy-to-use GIS-based modeling tool with documentation.	Ability of an ITAM GIS technician to obtain and operate the model.	Feedback from ITAM GIS technicians on ability to find model on the SRP website, its usability, and the value of documentation.	An ITAM GIS technician can download the model, acquire necessary data, and generate results within four hours.	GIS model developed with significant feedback from ITAM personnel; results can be generated within four hours.

Figure 3. Example of how the spatial precision of a predicted gully locations are evaluated with respect to the spatial resolution of the input DEM.

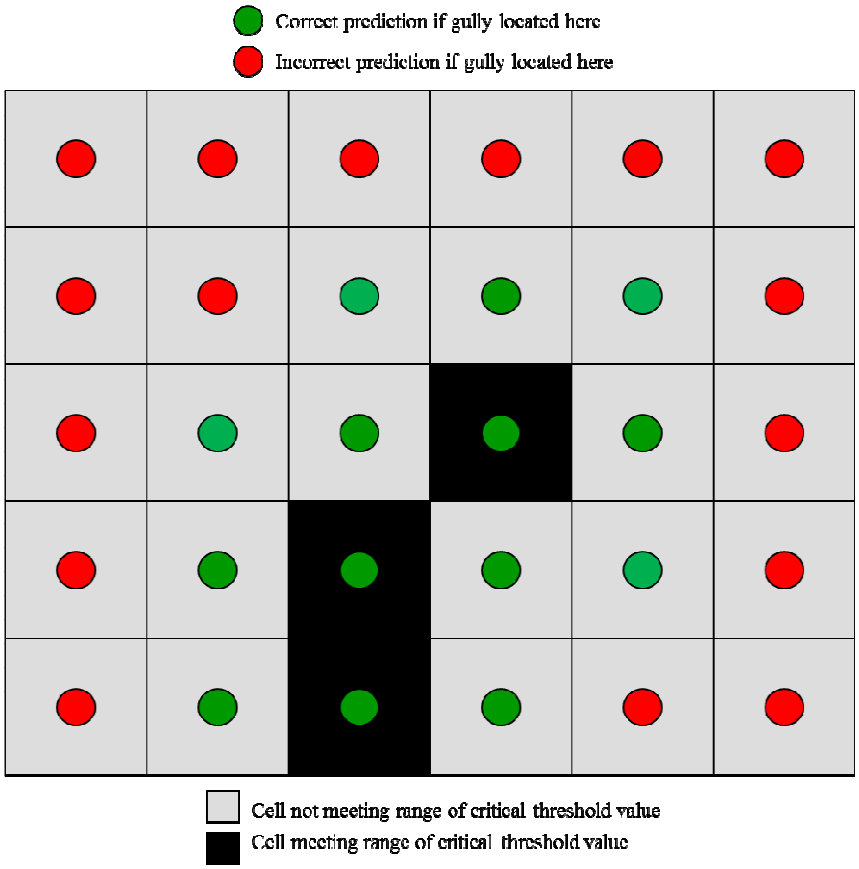

The second quantitative performance objective is to determine whether a single critical threshold for accumulated *nLS+* values is adequate for each installation study site. This objective seeks to assess whether a single common critical threshold for accumulated *nLS+* values is valid for all installations or whether the individual installation threshold values are statistically different and place-specific. After critical thresholds for accumulated *nLS+* values have been identified for each installation study area (see Performance Objective #1), they will be compared statistically to determine whether "between installation" variation of *nLS+* threshold values are less than the "within installation" variation. The requirement to identify and use only a single threshold value for any installation will be indicated if "within installation" variation is greater than "between installation" variation. If "between installation" variation is greatest, then evidence exists that each study installation requires a place-specific threshold in order to meet model prediction accuracy criteria.

The third, and final, quantitative objective involves using the *nLS+* model in a predictive mode to forecast areas where gullies are likely to form in response to future military training events at Pohakuloa Training Area. This objective requires operation of the *nLS+* model after a training exercise. In this case, vehicle tracking data will be used to modify the input DEM and LULC layers (and associated Manning's *n* coefficient) using information on the type of vehicle that

made the track, the radius of track curves, vehicle speed, and empirical data that relates vehicle turning radius and speed into estimates of vegetation damage and rut depth. Past research by investigators from the University of Tennessee and the Engineering Research and Development Laboratory – Construction Engineering Research Laboratory (ERDC-CERL) quantifying vehicle track impacts in terms of rut depth and vegetation damage will inform how the original DEM and LULC datasets will be altered. Coupled with known vehicle track locations, it is possible to estimate for every location along the tracks the maximum depth of the associated rut and how much vegetation was likely removed during maneuvers.

Though actual vehicle track widths will almost always be less than the spatial resolution of the DEM and LULC datasets used as input in the *nLS+* model, vehicle-induced changes to the landscape will be applied to any pixel through which a track passes, regardless of that pixel's dimension. Because the model, and its resulting gully predictions, are based on a raster, or grid, format it is not necessary to account for sub-pixel impacts or processes. All that is necessary to know is (1) that a vehicle passed through a cell and (2) the estimated reduction in elevation (*i.e.*, rut depth) and change in surface roughness (*i.e.*, vegetation removal) caused by vehicle passage.

The installation-level data required to accomplish this objective includes:

- Digital elevation data, in the form of a DEM, that can be obtained from the USGS National Elevation Dataset (NED) (http://ned.usgs.gov) or local products of higher spatial resolution or currentness.
- Digital LULC maps, in the form of the 2006 NLCD, that can be obtained from the Multi-Resolution Land Characteristics Consortium (MRLC) (http://www.mrlc.gov) or local products of higher spatial resolution or currentness.
- Manning's surface roughness coefficients (*n*), obtained from the literature that correspond to each NLCD LULC type present across all study installations.
- The location of new vehicle tracks after the completion of a training exercise, to be provided by GPS-based vehicle tracking data acquired at Pohakuloa Training Area..
- Vehicle-specific estimates of soil and vegetation damage obtained from the literature.
- Ground truth dataset of any post-maneuver gully activity.

As with Performance Objective #1, this objective will be successfully accomplished when a critical threshold for accumulated *nLS+* values is both identified and able to correctly identify 80% of areas showing evidence of new gully activity within a distance dictated by spatial resolution of the DEM source.

In addition to the three quantitative performance objectives described above, two qualitative objectives (Performance Objective #4 and #5) have also been identified. Performance Objective #4 is related to, and dependent upon, the outcome of Performance Objective #2. If it is determined that installation-specific critical thresholds are required to realize satisfactory model predictive accuracy, then geographic regions where these critical *nLS+* thresholds might be valid will be explored.

The final objective, Performance Objective #5, is development and deployment of a downloadable GIS tool that natural resources and training land management personnel can use to

run the *nLS+* model themselves. Throughout the duration of the project, feedback was sought from ITAM GIS technicians at each installation with regard to *nLS+* model usability, quality of model documentation, and best means of model dissemination. Success for this objective is defined by the ability of a typical installation GIS technician to download the model, acquire necessary data for model operation (either local or nationally-available datasets, and generate model results within a time duration of four hours.

3.1 GULLY DEFINITION

For this demonstration, a gully is defined as a small channel with steep sides caused by erosion and cut in unconsolidated materials by concentrated, but intermittent, flow of water usually during and immediately following heavy rains or ice and snow melt. A gully generally is an obstacle to wheeled vehicles and too deep (*e.g.,* > 0.5 m) to be obliterated by ordinary tillage (USDA 2009). Because identifying gullies from aerial photography or satellite imagery depends heavily on spatial resolution, only gullies at least 1 m wide will be considered in this work (Frazier *et al.,* 1983). Because gully depth cannot be determined using non-stereo digital orthophotography, we have not listed depth as a defining criterion for gullies. However, it is highly unlikely to have a gully that is 1 m wide (or greater) that does not have significant depth (*e.g.,* > 0.5 m).

The proposed use of the USDA gully definition, as well as the term "gully" itself, is valid given the natural resource emphasis of the project, usage within CERL natural resource working groups, and current geospatial data standards applied across the DoD. A comparable and competing term found military mobility literature is "gap", which is defined as any battlefield terrain feature too wide to be crossed using a vehicle's self-bridging capability (Department of Defense 1985). The 1-meter "rule of thumb" width associated with the USDA gully definition is also a good match with mobility restrictions for single-axle wheeled military vehicles that lack a self-bridging capability. Expected gully depths, given the 1-meter width criterion, exceed the minimum step value for light armored vehicles such as the M113 and most, if not all, single-axle tactical wheeled vehicles such as the High-Mobility Multipurpose Wheeled Vehicle (HMMWV) (Overholt 2001).

4.0 SITE DESCRIPTION

Several criteria were used to identify military installations that would make ideal study sites for calibrating and validating the *nLS+* model. First consideration was given to the location of the installation, and its associated biological and physical characteristics. Because *nLS+* model was developed and tested at Fort Riley, Kansas, preferred candidate sites for calibration and validation included those of different soils, topography, landcover, and climate which would require the model to successfully predict gully locations using inputs with a wide range of values. In addition to selecting installations that were different from Fort Riley, the inclusion of at least one site that was similar was also considered important to provide data confirming the validity of model results at Fort Riley.

Also important to site selection was the anticipated level of support that this project would receive by installation environmental managers. Assistance by installation personnel was essential to project success by providing the research team training land access, sharing environmental and geospatial data, and ensuring that base-specific safety procedures were followed. Related to this was a third criterion, which considered whether a candidate site was already home to related research projects and/or environmental certification programs. Installations with a history of supporting research conducted by scientists in the federal government and/or academia were likely to make superior collaborators.

From the perspective of military operations, three additional selection criteria were employed. First, candidate sites that were important, or "mission critical", installations supporting high levels of training activities, especially vehicle-based training, were preferred. Second, candidate sites looking at a potential future changes in alignment or mission would stand to benefit most from the anticipated advantages of the validated *nLS+* model. Finally, the opportunity to involve multiple military service branches was emphasized.

After a preliminary survey of military installations, and in consultation with our designated DoD service liaison (A. Anderson, ERDC-CERL), six installations were selected to serve as study sites for the validation of the erosion potential model: (1) Fort Hood, (2) Fort Benning, (3) Fort Irwin, (4) Camp Lejeune Marine Corps Base, (5) Schofield Barracks, and (6) Pohakuloa Training Area. In addition to these six sites, concurrent work was continued at Fort Riley for the duration of the study.

Though seven total sites were identified for this demonstration site, and are described in the following section, only five sites opted to participate after the project was approved and funded: Schofield Barracks, Pohakuloa Training Area, Fort Hood, Fort Benning, and Fort Riley. Despite initial interest, Fort Irwin and Camp Lejeune cited several reasons for lack of participation, including limited (and frequently changing) personnel, limited time available to facilitate work given other demands, and lack of long-term benefit.

4.1 SITE LOCATION AND HISTORY

The initial group of study sites selected (Figure 4) included critical military training installations within the U.S. Department of Defense (*e.g.*, Fort Hood, Fort Irwin) which were home to military land managers with confirmed interest in this project, those with a history of working with researchers (*e.g.*, Pohakuloa Training Area, Fort Benning), as well as installations experiencing new management challenges due to mission changes and the fielding of new equipment which placed increased pressure on training lands (*e.g.*, Pohakuloa Training Area, Schofield Barracks). In addition, Camp Lejeune Marine Corps Base was selected to complement the six Army reservations.

Figure 4. Map of installations initially selected for field validation of the *nLS+* model.

The selected sites included a diverse set of landscapes and biophysical characteristics. For example, landcover spans the range from hot desert to tropical rainforest, soils from lava flows to sand, and landforms from mountains to coastal wetlands. Table 3 summarizes a general set of descriptive features and phenomena that are then discussed in more detail in Section 4.3. The dominant landcover listed for each installation allows one to deduce approximate surface roughness conditions, the rainfall-runoff erosivity factor (or R factor) to better appreciate the erosive power of rainfall that occurs locally (*i.e.*, high values indicate more potential for water-based soil erosion), and runoff potential, as determined by the U.S. Department of Agriculture (USDA) Natural Resource Conservation Service (NRCS) soil hydrologic group which characterizes soil water infiltration capabilities. Note that the listed runoff potential for Fort Irwin of "low" or "high" reflects the frequency of sandy soils and impermeable rock surfaces throughout the installation.

Table 3. Abbreviated comparison of biophysical and climatic characteristics for selected demonstration sites.

Installation	***Ecoregion*** [(1)]	***Dominant Landcover*** [(2)]	***Annual Avg Precip (mm)*** [(3)]	***R Factor*** [(4)]	***Runoff Potential*** [(5)]
Camp Lejeune	Middle Atlantic Coastal Plain	Evergreen Forest	1373.4	389	Low
Fort Benning	Southeastern Plains	Deciduous Forest	1233.6	377	Low to Intermediate
Fort Riley (Original Validation Site)	Flint Hills	Grassland	826.5	188	High
Fort Hood	Edwards Plateau	Grassland	825.1	243	High
Fort Irwin	Mojave Basin and Range	Bare Land, Shrub/Scrub	110.1	14.5	Low or High
Pohakuloa Training Area	Tropical High Shrublands/Dry Forest	Bare Land, Shrub/Scrub	539.3	65.2	High
Schofield Barracks	Tropical Moist Forest	Shrub/Scrub, Evergreen Forest	1263.7	288	High

(1) Identification based upon USEPA Level 3 Ecoregions or World Wildlife Fund (WWF) Terrestrial Ecoregion designations.
(2) Calculated from data from the National Landcover Dataset 2001 (NLCD 2001).
(3) Data obtained from weather.com (http://www.weather.com).
(4) Rainfall-Runoff Erosivity Factor (R) determined using data from the USDA RUSLE2 Climate Database (Version 1.26.6.4).
(5) Assessment based upon the Soil Hydrologic Group of the dominant soil or soils as described in the USDA NRCS Generalized Soil Map of the United States.

It is important to note that while Schofield Barracks and Pohakuloa Training Area are two of the selected study sites, validation activities were conducted only on subsets of the installations. At Schofield Barracks, installation ITAM staff were primarily concerned with soil erosion within the Kahuku Range. At Pohakuloa Training Area, the newly acquired Keamuku Parcel (formerly privately owned cattle grazing land) was studied in preparation for the first of many future Stryker training exercises.

4.2 SITE CHARACTERISTICS

Brief descriptions of each original selection of study sites follow. These overview descriptions are intended to highlight some of the key biophysical differences between installations that (1) contributed to their selection as a study site and (2) will test model performance given high variation in *nLS+* model inputs. Biophysical characteristics in the descriptions include the identification of major installation soils (*e.g.*, order, great group, series), soil water infiltration capacities and runoff potential (see Table 4 for a description of soil hydrologic groups), general

topographic conditions, dominate landuse/landcover categories, and climate. When combined together, an understanding of each of these conditions or surface properties contribute to a better qualitative understanding of the potential for soil erosion and its primary environmental drivers without requiring application of a watershed-based hydrologic model to quantitatively estimate surface water runoff.

Table 4. Interpretation of USDA-NRCS soil hydrologic groups.

Soil Hydrologic Group	***Typical Soil Textures***	***Infiltration Capacity***	***Runoff Potential***
A	Sandy, Sandy Loam, Loam	> 2 in/hr	Lowest
B	Sandy Clay Loam, Silt Loam	0.6-2.0 in/hr	Intermediate Low
C	Clay Loam, Silty Clay Loam	0.2-0.6 in/hr	Intermediate High
D	Silty Clay, Clay	< 0.2 in/hr	Highest

4.3.1 Fort Hood, Texas

Located in central Texas next to the city of Killeen, Fort Hood soils are comprised by six series (Slidell 42%, Eckrant 29%, Doss 16%, Cho 3%, Brackett 5%, and Bosque 5%). The two dominant soils series are Slidell and Eckrant. Slidell soils are moderately well-drained vertisols with fine particle size. Eckrant soils are well-drained mollisols typified by clayey-skeletal soil particle size. Eckrant soils are typical of upland sites, while Slidell soils can be found midslope prior to giving way to the Doss and Bosque soils located along drainages. The remaining soil series are generally well-drained mollisols, though Brackett is an inceptisol, with loamy to fine-loamy particle size. Slidell and Eckrant soils are classified as soil hydrologic group D (71%), Doss-Cho-Brackett as group C (24%) and Bosque as group B (5%). Slidell soils are found in areas of 0-5° slope and Eckrant from 0-8° slope.

Fort Hood is located in the Cross Timber ecological region. Landcover is primarily grassland (33%) with significant amounts of evergreen forest (24%) and shrub/scrub cover (18%). Most of the evergreen forest is located on upland Eckrant soils and with lesser densities found locally along drainages. Elevations range from 180 to 378 meters (m) above sea level (asl), with an average slope of 5.8% (maximum slope = 168%). Areas of higher slope include the transition zones between Slidell and Eckrant soils, as well areas along drainage ways.

Fort Hood's climate is Humid Subtropical (Koppen-Geiger climate classification = Cfa) based on long-term weather data recorded at nearby Killeen. The maximum monthly temperature occurs in August (36° C) and the annual average maximum temperature is nearly 26° C. The minimum average monthly temperature of 1° C occurs in January and can be as warm as 22° C in July and August. Average annual precipitation totals 835.1 millimeters (mm) per year, but 25% of that total falls in May and June alone. Though summers are relatively dry, no month averages less than 34 mm of precipitation per month.

Figure 5. Runoff potential for the soils of Fort Hood, Texas by soil hydrologic group (Source: Generalized Map of U.S. Soils, USDA NRCS).

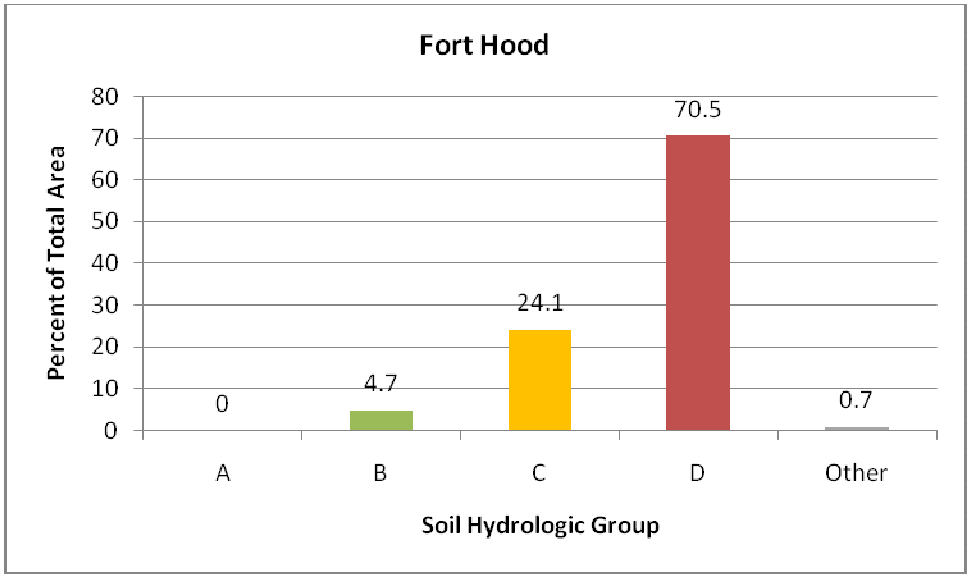

Figure 6. Dominant landcover categories for Fort Hood, Texas (Source: 2001 National Landcover Dataset).

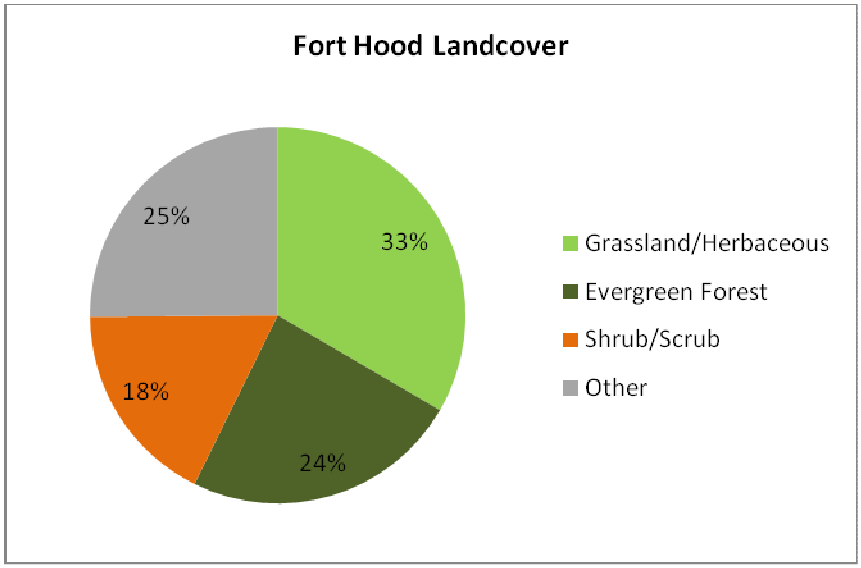

Figure 7. Climograph for Fort Hood, Texas (Source: http://www.weather.com).

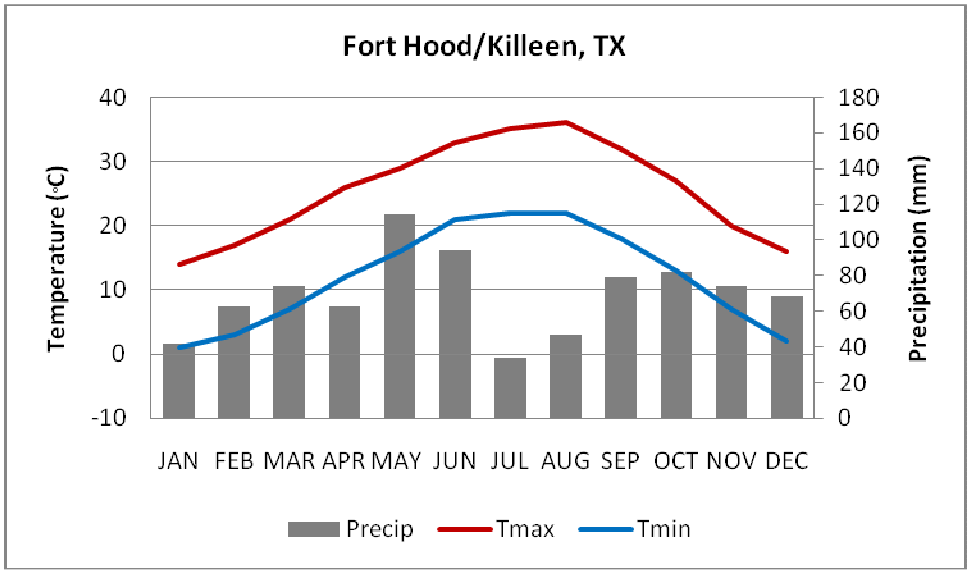

4.3.2 Fort Benning, Georgia

Within the Fort Benning installation, eight soils series have been identified: Vaucluse (45%), Wagram (41%), Mantachie (4%), Chewacla (1.5%), Lakeland (1.3%), Norfolk (1%), Troup (1%), and Luverne (0.7%). Two soil series (Vaucluse and Wagram) account for 86% of all soil types, with Vaucluse dominating in the north and Wagram in the south. In general, Vaucluse soils are found in steeper areas (2-8 ^{o} slope) while Wagram soils coincide with areas of less slope (0-5°). The Mantachie, Troup, and Luverne series are found exclusively across the Chattahoochee River in the Alabama portion of the installation. Both dominant soil series are Ultisols with Vaucluse soils being fine loamy and Wagram soils loamy in texture. The remaining soil series are Ultisols, Inceptisols, or Entisols of fine or fine-loamy texture. Water infiltration rates are either good or poor, with 46% of Fort Benning soils rated at soil hydrologic group A and 51% in group C. The important group A soil is the Wagram series, while Vaucluse is group C.

Elevations at Fort Benning range from 51 to 226 m asl, with an average slope of 7.8% (maximum slope = 86.1%). The installation is located in the Southeastern Plains ecological region. Three landcover types comprise 70% of the installation area: Deciduous Forest (34%), Evergreen Forest (23%), and Mixed Forest (13%). Deciduous forests are found extensively throughout the northern portions of the installation while the largest concentration of the evergreen forest type is in the south. Mixed forest can be found across the entire installation, but the largest concentration is located in the northeast.

Figure 8. Runoff potential for the soils of Fort Benning, Georgia by soil hydrologic group (Source: Generalized Map of U.S. Soils, USDA NRCS).

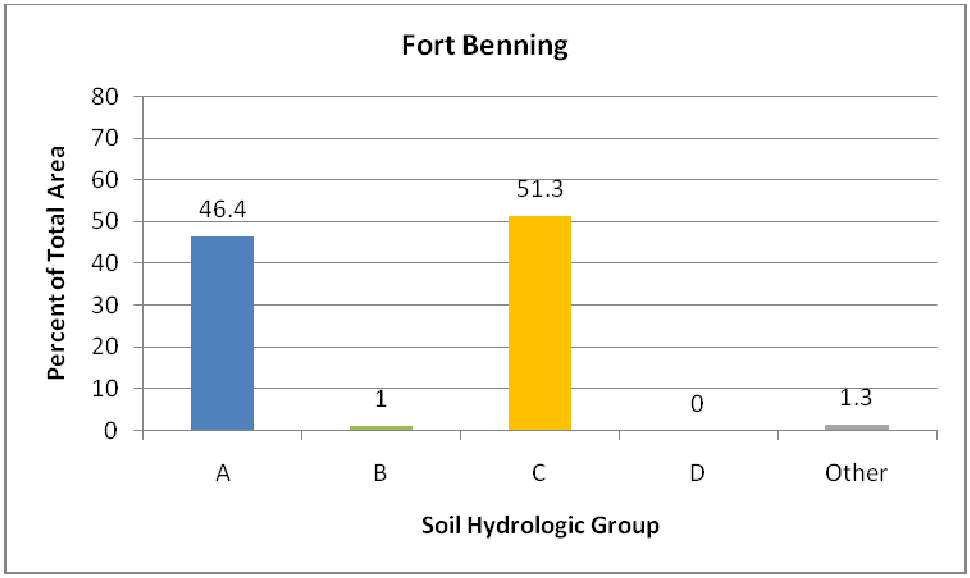

Figure 9. Dominant landcover categories for Fort Benning, Georgia (Source: 2001 National Landcover Dataset).

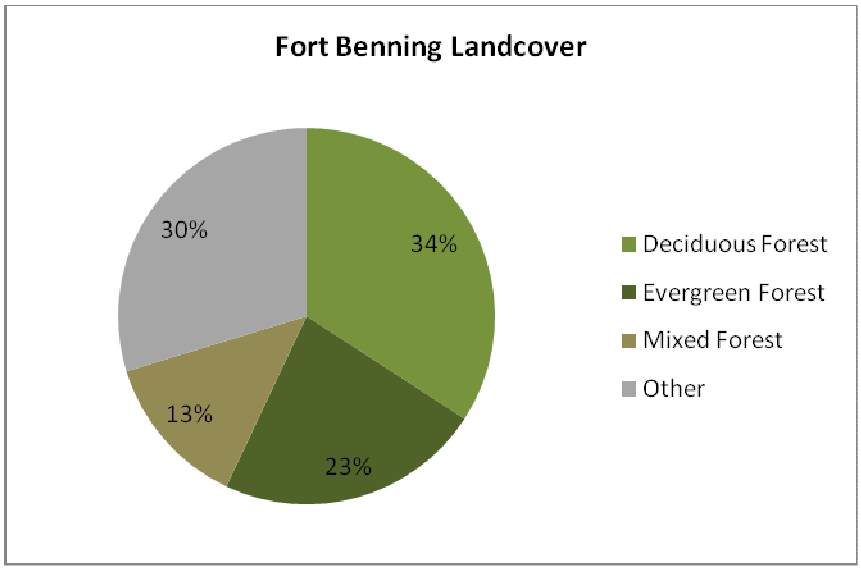

Climate is characterized as Humid Subtropical (Koppen-Geiger climate classification = Cfa). The maximum monthly temperature occurs in July and August (33° C). The annual average maximum temperature just exceeds 24° C. The minimum average monthly temperature of 3° C occurs in January and monthly average low temperatures can be as warm as 22° C in July and August. Average annual precipitation totals 1233.6 mm per year. Precipitation amounts are

evenly distributed throughout the year and range from an average low of 59.2 mm in October and an average high of 128 mm in July.

Figure 10. Climograph for Fort Benning, Georgia (Source: http://www.weather.com).

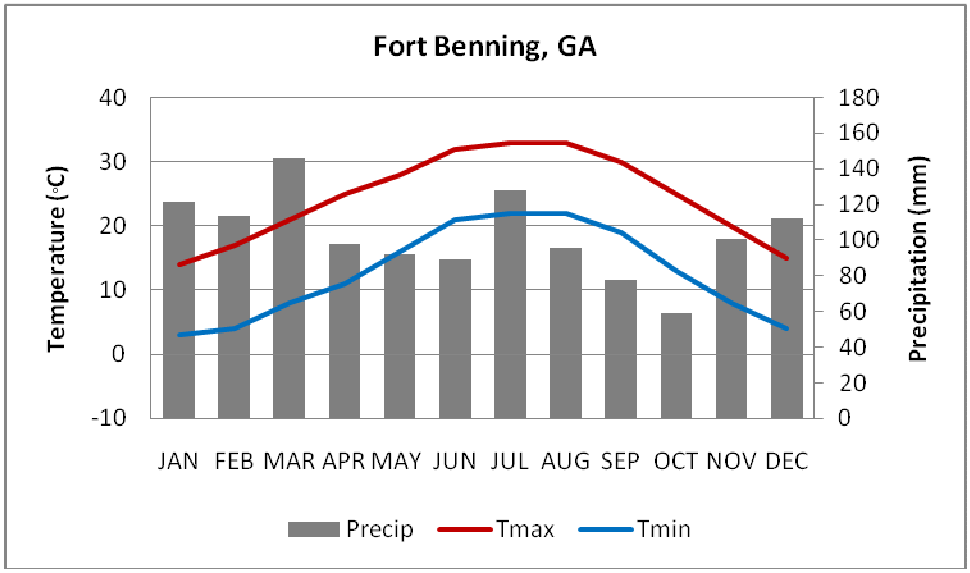

4.3.3 Fort Irwin, California

The soils of Fort Irwin consists of ten series (Cajon 45%, Lithic Torriorthents 12%, Nickel 12%, Calvista 11%, Badland 8%, Tecopa 6%, Upspring 5%, Playas 2%, and less than 1% each of Gunsight and St. Thomas). High-slope mountain soils are primarily Lithic Torriorthents, Tecopa, Upspring, and Calvista. Lowland soils with low slope, the primary maneuver areas of the installation, are dominated by Cajon, Nickel, Badland, and Playas. By percent area, soils of the Entisol order are most common (69% of total area) and include Upspring, Tecopa, St. Thomas, Lithic Torriorthents, and Cajon series. The Cajon series are of the Typic Torripsamments subgroup, with the remaining Entisols being Lithic Torriorthents. The remaining series are in the Aridisol order, with Calvista being a Lithic Haplocalcids and Nickel and Gunsight Typic Haplocalcids. When developed soil structure is present, textures are typically described as loamy or loamy-skeletal. By soil hydrologic group, 46% of Fort Irwin soils are group A, 44% group D, and 12% group B. Only three soils series are not in the group D category and include Cajon (group A), Nickel (group B), and Gunsight (Group B). All other soil series are group D.

Figure 11. Runoff potential for the soils of Fort Irwin, California by soil hydrologic group (Source: Generalized Map of U.S. Soils, USDA NRCS).

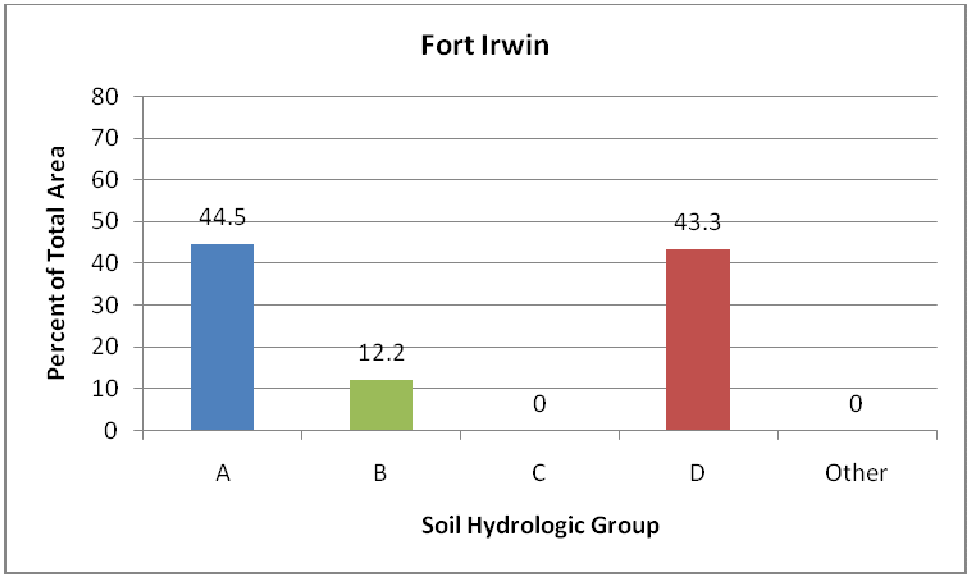

Fort Irwin is located in the Mojave Basin and Range ecological region. Landcover is primarily shrub/scrub (85%) with significant areas of barren land (15%). Elevations range from 310 to 1875 m asl, with an average slope of 13.8% (maximum slope = 496%).

Figure 12. Dominant landcover categories for Fort Irwin, California (Source: 2001 National Landcover Dataset).

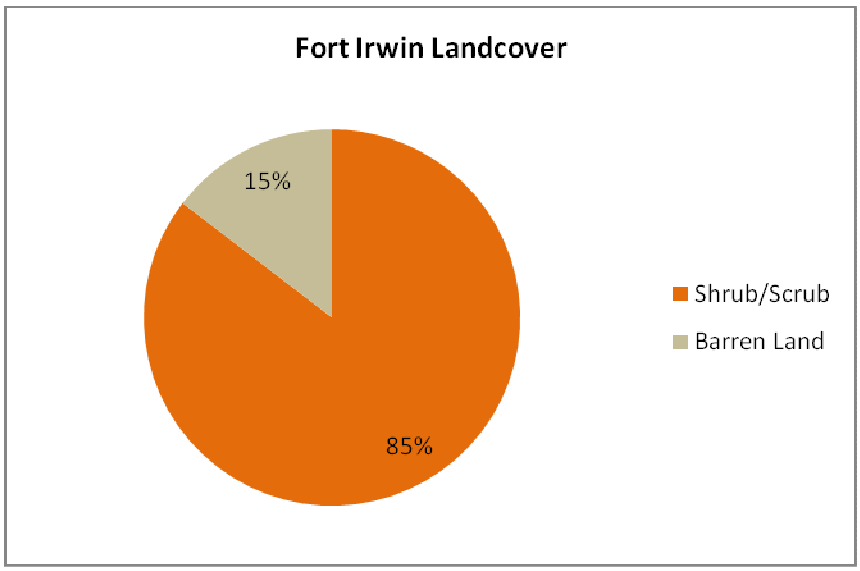

Climate at Fort Irwin is Warm Desert (Koppen-Geiger climate classification = Bwh) based on climate data recorded south of the installation at Barstow. Maximum average monthly temperatures range from a low of 17 ^{o}C in January and December to a high of 39 ^{o}C in July. The annual average maximum temperature is nearly 28 ^{o} C. The minimum average monthly temperature of 1° C occurs in January and December. Summertime average monthly low temperatures range between 16-20 ^{o}C. The average annual precipitation totals 110.1 mm per year, most of which falls during winter and early spring (December – March). Average monthly precipitation is less than 10 mm for each of the remaining eight months.

Figure 13. Climograph for Fort Irwin, California (Source: http://www.weather.com).

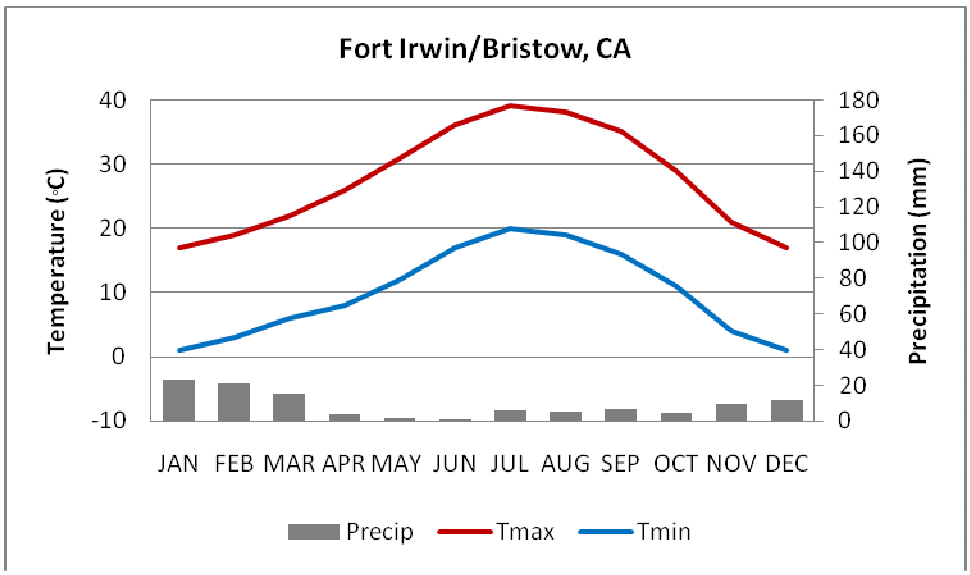

4.3.4 Camp Lejeune Marine Corps Base, North Carolina

Camp Lejeune Marine Corps Base (MCB) features seven soils series (Woodington 34%, Baymeade 28%, Leon 16%, Kureb 12%, Norfolk 4.5%, Bohicket 3.4%, and Meggett 2.9%). Two soil series (Woodington and Baymeade) account for 62% of the soils within the base. Baymeade soils are found exclusively in the east and north in areas characterized by slope values from 1-6°, while Woodington soils occur in topography with less relief (0-2° slope). In the east, Meggett and Leon soils interrupt large contiguous zones of the Baymeade along streams and in upland sites, respectively. Woodington soils cover the majority of the inland portions of the installation on the west side and transition to Leon, Kureb, then Bohicket before reaching the Atlantic Ocean in the east. Both dominant soil series are Ultisols with the Woodington series being of coarse-loamy texture and Baymeade of loamy texture. Vaucluse soils are fine loamy and Wagram soils are loamy in texture. The other series of the order Ultisol is the fine-loamy Norfolk series. The remaining soil series include fine Alfisols (Meggett), sandy Spodols (Leon), Entisols (Kureb and Bohicket). Series in soil hydrologic group A include Baymeade and Kureb, Norfolk in group B, Leon and Woodington in group B/D, and Bohickett and Meggett in Group D. The B/D group are dominant (49% of installation) followed by group A (40%).

Figure 14. Runoff potential for the soils of Camp Lejeune MCB, North Carolina by soil hydrologic group (Source: Generalized Map of U.S. Soils, USDA NRCS).

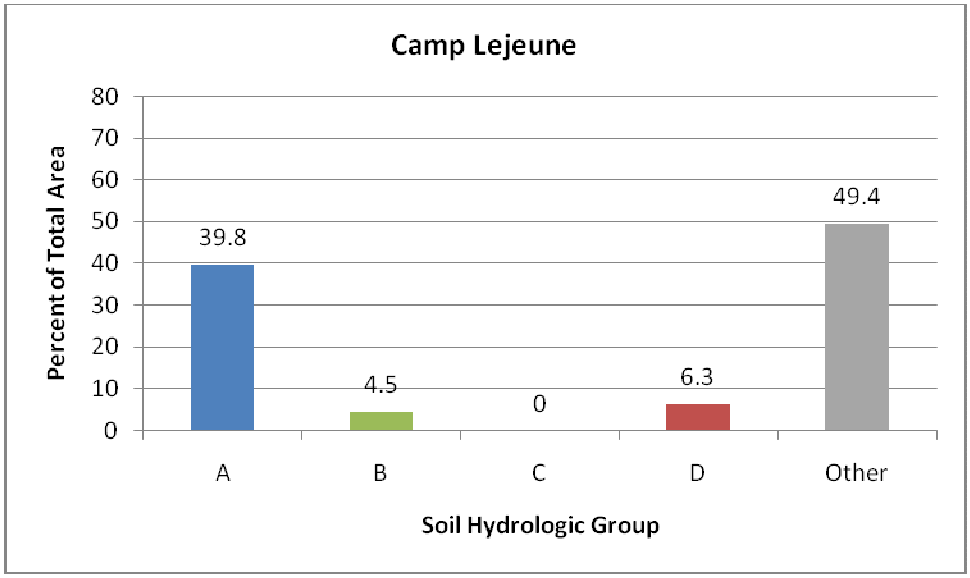

Elevations at Camp Lejeune range from -1 to 24 m asl, with an average slope of 2.6% (maximum slope = 65.3%). The installation is located in the Middle Atlantic Coastal Plain ecological region and three landcover types comprise 63% of the installation area: Evergreen Forest (25%), Woody Wetlands (24%), and Grassland/Herbaceous (13%). Evergreen forests are scattered throughout the installation, while woody wetlands and grassland sites are more concentrated inland of the southeastern coastline.

Climate is characterized as Humid Subtropical (Koppen-Geiger climate classification = Cfa). The maximum monthly temperature of 32° C occurs in July. The annual average maximum temperature is 23° C. The minimum average monthly temperature of 1° C occurs in January and monthly average low temperatures can be as warm as 22° C in July. Average annual precipitation totals 1,373.4 mm per year with a monthly high of 179.8 mm in July and a monthly low of 77.7 mm in April.

Figure 15. Dominant landcover categories for Camp Lejeune MCB, North Carolina (Source: 2001 National Landcover Dataset).

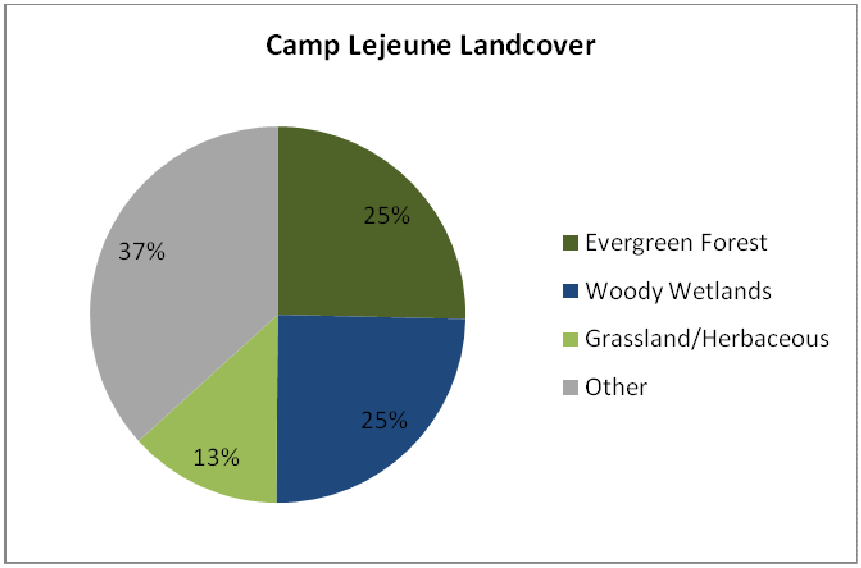

Figure 16. Climograph for Camp Lejeune MCB, North Carolina (Source: http://www.weather.com).

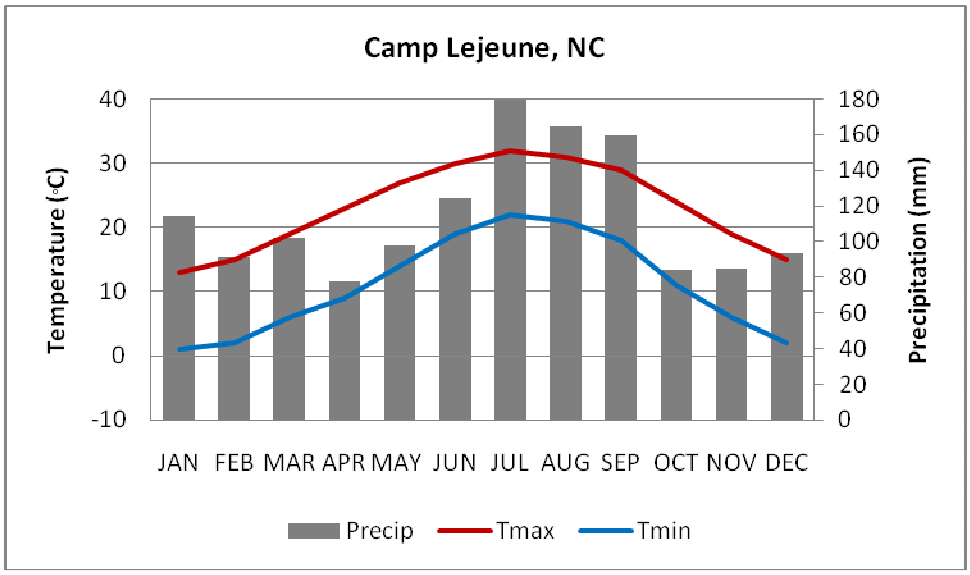

4.3.5 Schofield Barracks and Kahuku Range, Island of Oahu, Hawaii

For purposes of this summary, Schofield Barracks includes the following reservations and ranges: Dillingham, East Range, Helemano, Kawailoa, Kahuku, Kunia, Makua, Schofield Barracks, and Wheeler. Defined as such, Schofield Barracks consists of nine soils series or great groups (Udorthents 62%, Lithic Ustorthents 12%, Wahiawa 9%, Waikane 8%, Manana 8%, and less than 0.5% each of Haplustolls, Lualualei, Kawaihapai, and Hanalei). The Udorthent great group is the dominant soil of Schofield Barracks and is most common in the Ko'olau mountain range where the Kahuku Range, Kawailoa Reservation, and the eastern half of East Range are located. Udorthent soils are also found along the Waianae Range and compose a portion of the soils for Schofield Barracks and the Makua Reservation. In general, soils transition from Udorthents to Lithic Ustorthents then Manana and Wahiawa soils as elevation and slope decreases. Only three soils comprise over 99% of the important Kahuku Range on the northern tip of the island of Oahu: the mountain Udorthents (48%), mid-slope to beach Waikane (48%), and Manana along drainages. Given the diversity of environments at Schofield Barracks, it is not surprising that the military reservation, in its entirety, includes soils from six different orders. The most important of these orders are Entisols (Udorthents and Lithic Ustorthents), Oxisols (Wahiawa), and Ultisols (Manana and Waikane). Excluding rock, soil textures are generally fine to very-fine. Water infiltration capability of most Schofield Barracks soils is poor, with 75% of the area classified into soil hydrologic group D (Udorthents, Lithic Ustorthents, and Lualualei) and 8% in group C (Manana, Haplustolls, Hanalei). Locally important soils in lowland section of Schofield Barracks, Kahuku, and western East Range such as Wahiawa and Waikane are group B soils.

Figure 17. Runoff potential for the soils of Schofield Barracks, Hawaii by soil hydrologic group (Source: Generalized Map of U.S. Soils, USDA NRCS).

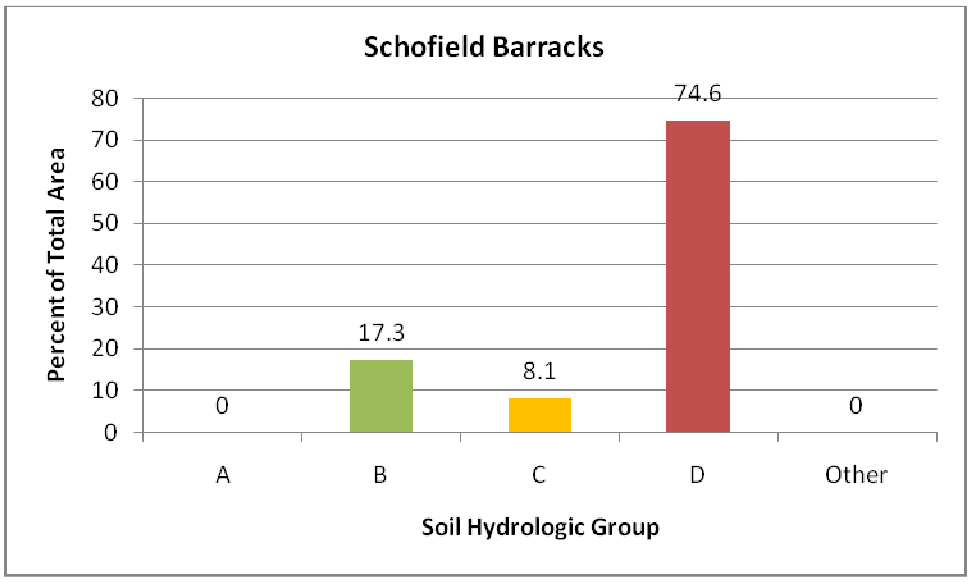

Figure 18. Runoff potential for the soils of the Kahuku Range, Schofield Barracks, Hawaii by soil hydrologic group (Source: Generalized Map of U.S. Soils, USDA NRCS).

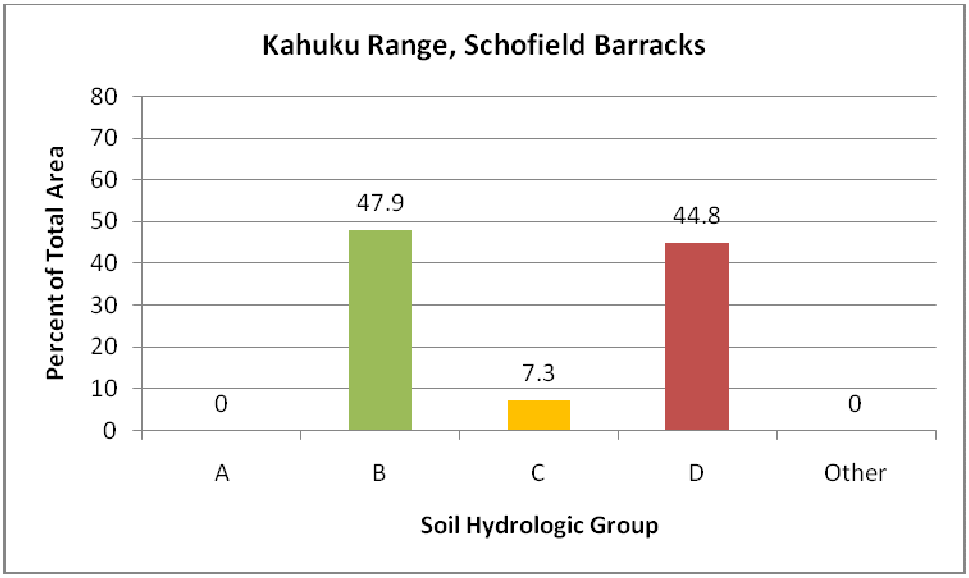

Elevations at Schofield Barracks range from sea level to 1,233 m asl, with an average slope of 42% (maximum slope = 448%). The component lands of Schofield Barracks span three different WWF ecoregions whose boundaries coincide closely to elevation differences. Military lands located in the higher interior of Oahu are in the Hawaii Tropical Moist Forest (Schofield Barracks, East Range, Wheeler, Kunia, Helemano, southern half of Kahuku). Moving downslope and towards the northern and western coasts, moist forest transitions to the Hawaii Tropical Dry Forest (northern half of Kahuku, Makua, and Dillingham). Approximately 90% of Schofield Barracks landcover types fall into one of three categories: Evergreen Forest (73%), Shrub/Scrub (10%), and Developed/Open Space (6%). In the Kahuku Range, elevations run from a low 15 to a high of 648 m asl with an average slope of 38%. Landcover types here are similar to that of the installation as a whole, but with slightly higher percentages for Evergreen Forest (78%) and Shrub/Scrub (15%).

The climate of Oahu is classified as Tropical Wet and Dry (Koppen-Geiger climate classification = Aw). Average monthly maximum and minimum temperatures vary little during the year, with maximum monthly temperatures fluctuating from a winter low of 25° C to a summer high of 28° C. Minimum monthly temperatures range from a low of 16° C to a high of 19° C. Average annual precipitation totals nearly 1,264 mm per year. Precipitation is heaviest during winter with summers being relatively dry. However, no month receives an average monthly total of less than 53 mm (August).

Figure 19. Dominant landcover categories for Schofield Barracks, Hawaii (Source: 2001 National Landcover Dataset).

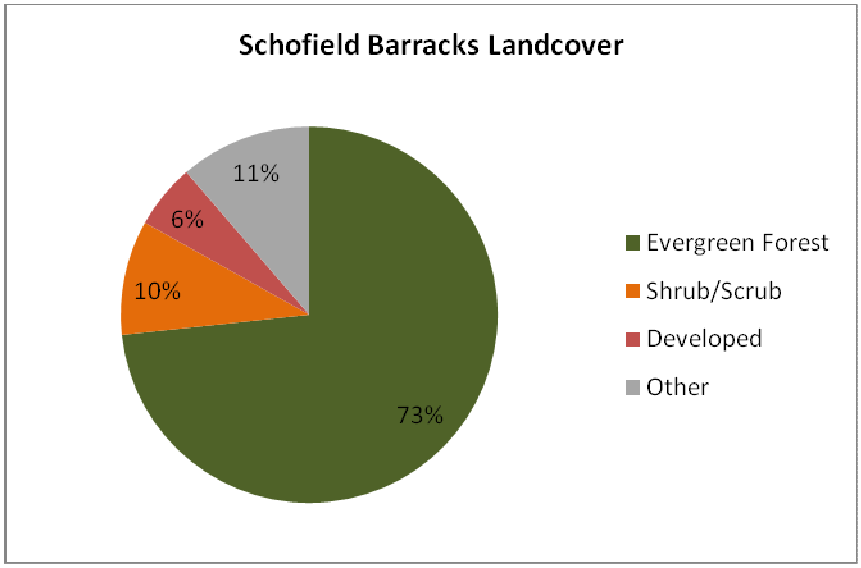

Figure 20. Dominant landcover categories for the Kahuku Range, Schofield Barracks, Hawaii (Source: 2001 National Landcover Dataset).

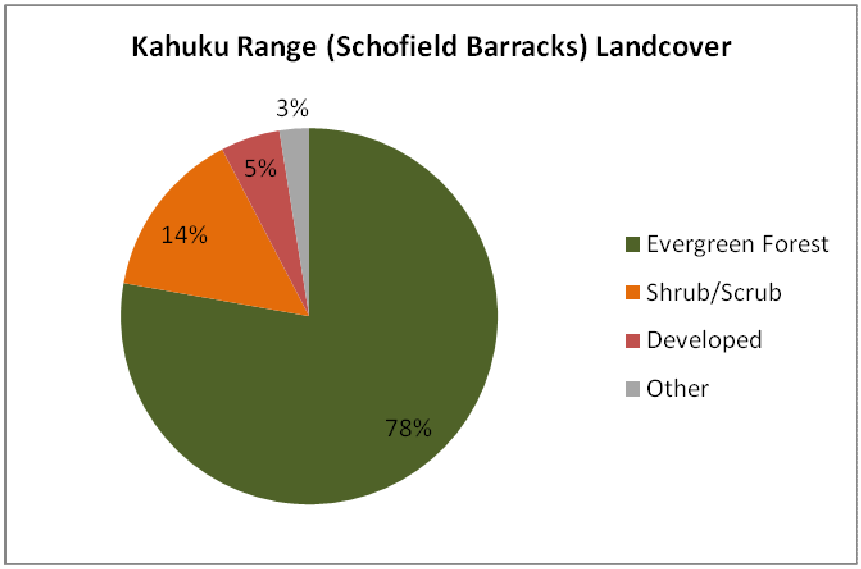

Figure 21. Climograph for Schofield Barracks, Hawaii (Source: http://www.weather.com).

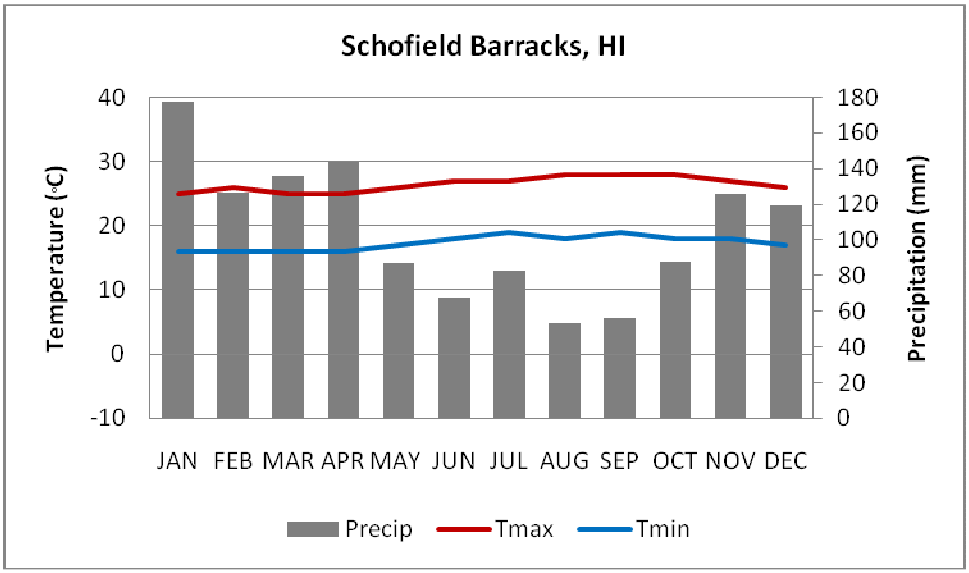

4.3.6 Pohakuloa Training Area and Keamuku Parcel, Island of Hawaii, Hawaii

Soils of Pohakuloa Training Area (PTA) include lava flows (78%) and six soil series (Apakuie 8%, Waikaloa 6%, Puu Pa 4%, Kiloa 2%, Waimea 1%, and Malama 0.1%). Over three-quarters of installation, and nearly all of the original southern portion situated in the topographic saddle between Mauna Kea to the north and Mauna Loa to the south, consists of lava flows of soil hydrologic group D. The remaining soil series are found primarily in the northern Keamuku Range and, in addition to lava flows (3%), include: Waikaloa 35%, Puu Pa 24%, Apakuie 19%, Kiloa 11%, Waimea 8%). These series are in the Andisol (Apakuie, Puu Pa, Waikaloa, and Waimea) and Histosol (Kiloa) orders and have medial to medial-skeletal textures. The Keamuku Range is located on the gently sloping western flank of Mauna Kea and, in general, soils transition from Apakuie and Waimea at higher elevations to Waikaloa then Puu Pa and Kiloa at lower elevations. As opposed to the southern portion of PTA, soil water infiltration rates tend to be good to very good in Keamuku Range. Nearly 54% of soils are in soil hydrologic group A and 43% are in group B. The remaining 3% of land area is former lava flow with very poor (group D) infiltration rates.

Elevations at PTA range from 749 to 2,727 m asl, with an average slope of 7.3% (maximum slope = 196.3%). In the Keamuku Range, elevations range from the installation low of 749 meters to a high of 1,735 m asl. Given that its position on the side of the Mauna Kea volcano, average slope in Keamuku is higher (10.6%), though a bit less extreme (maximum = 115.0%).

PTA spans two different ecological regions. The southeastern half of the original installation, and southeastern third when including the new Keamuku parcel, is in the Hawaii Tropical High Shrublands. The remainder of the installation, including all of Keamuku, is in the Hawaii Tropical Dry Forest. Considering the entire PTA installation, landcover is predominately of two types, Shrub/Scrub (47%) and Barren Land (36%), with an additional 14% of the land area in the

Grassland/Herbaceous category. In the Keamuku Range, however, 57% of the area is Grassland/Herbaceous, 40% Shrub/Scrub, and 2% Barren Land.

Figure 22. Runoff potential for the soils of Pohakuloa Training Area, Hawaii by soil hydrologic group (Source: Generalized Map of U.S. Soils, USDA NRCS).

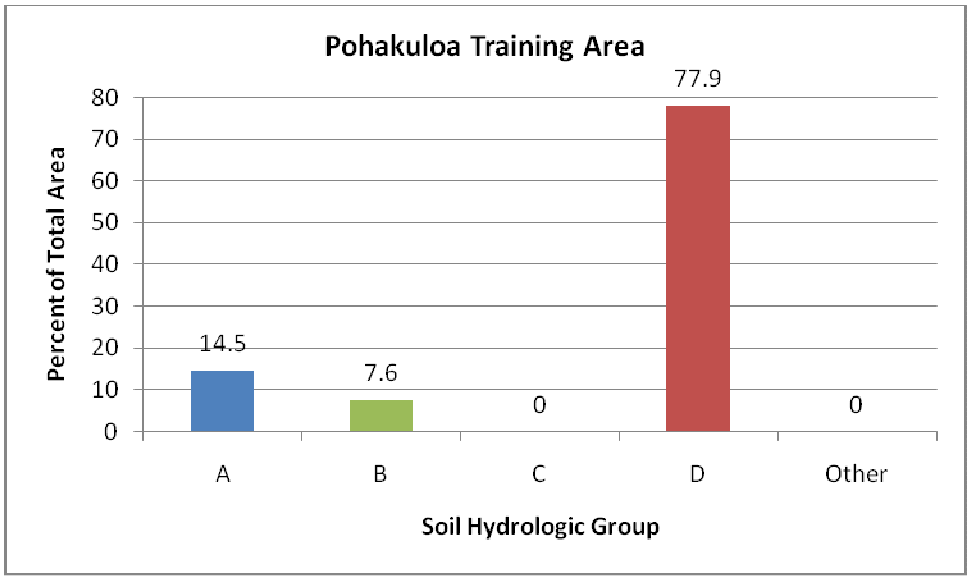

Figure 23. Runoff potential for the soils of the Keamuku Parcel, Pohakuloa Training Area, Hawaii by soil hydrologic group (Source: Generalized Map of U.S. Soils, USDA NRCS).

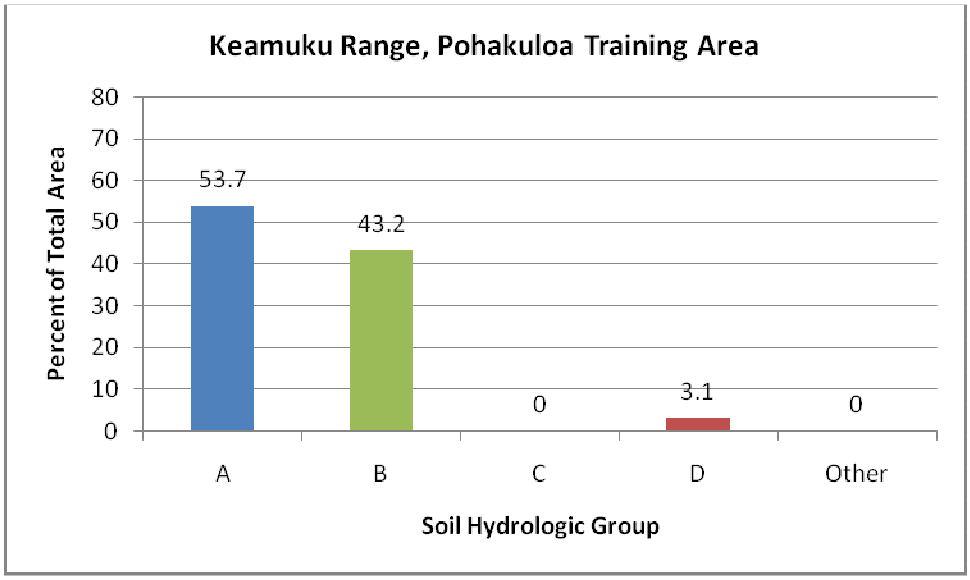

Figure 24. Dominant landcover categories for Pohakuloa Training Area, Hawaii (Source: 2001 National Landcover Dataset).

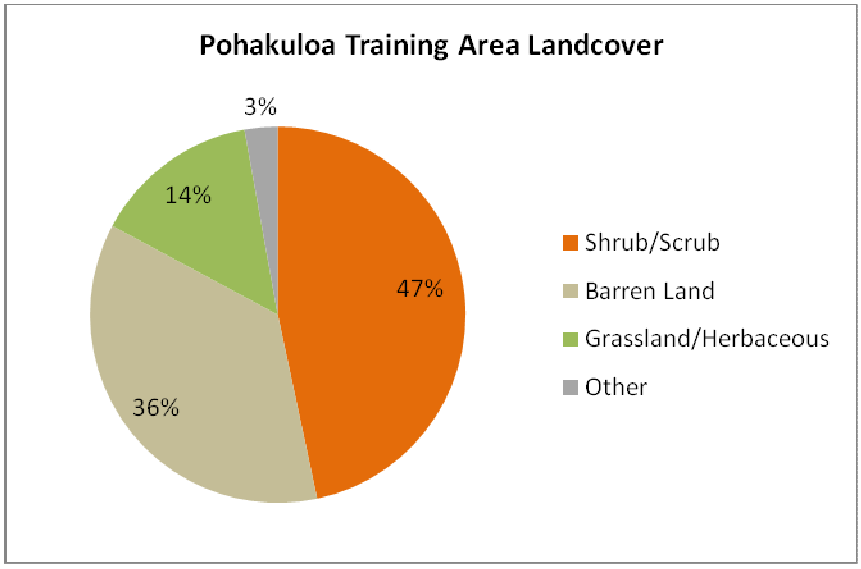

Figure 25. Dominant landcover categories for the Keamuku Parcel, Pohakuloa Training Area, Hawaii (Source: 2001 National Landcover Dataset).

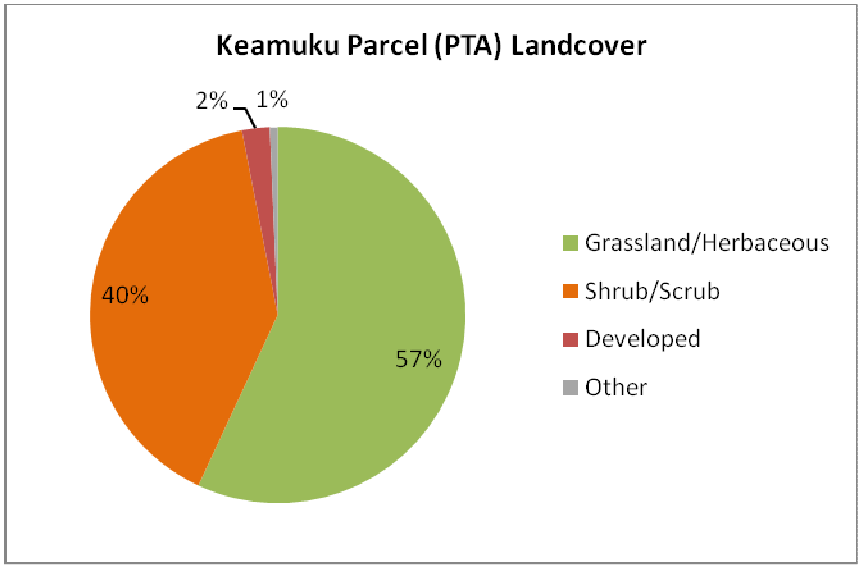

Like its neighboring installation on Oahu, climate at PTA (as measured at the nearby town of Waimea) is Tropical Wet and Dry (Koppen-Geiger climate classification = Aw) with average monthly maximum and minimum temperatures varying little during the year. Maximum monthly temperatures range from a winter low of 27° C to a summer high of 31 ^{o} C. Minimum monthly temperatures range from a low of 17° C to a high of 22° C. Though the pattern of monthly average temperatures is quite similar between Schofield Barracks and PTA, significant

differences exist with regard to precipitation amount and timing. Average annual precipitation at PTA totals only 539.3 mm per year with distinct winter wet and summer dry periods. Average monthly precipitation is highest in December with 93.7 mm and lowest in August with 12.4 mm. This precipitation pattern, along with spring and summer winds, contributes to the occasionally significant wind-based soil erosion events during the dry season.

Figure 26. Climograph for Pohakuloa Training Area, Hawaii (Source: http://www.weather.com).

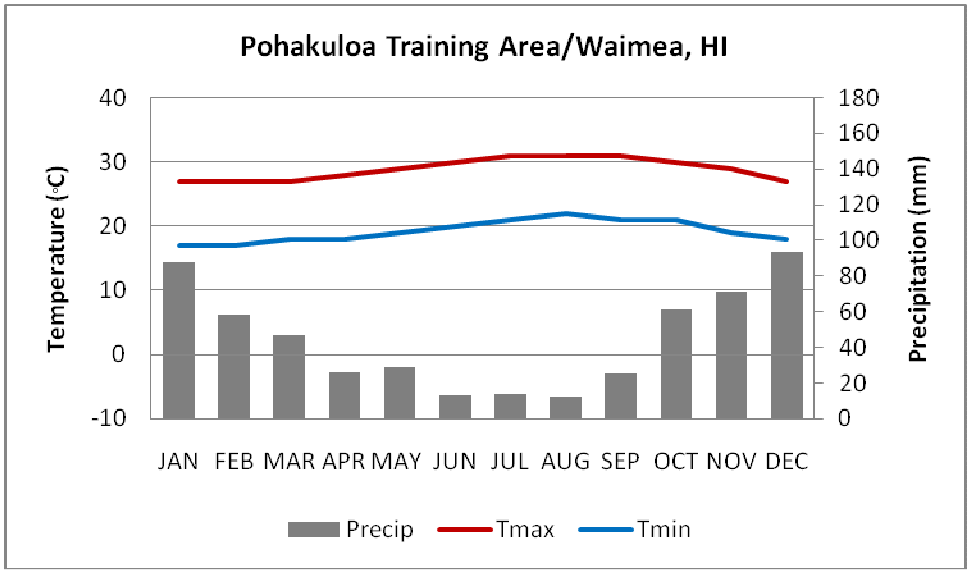

4.3.6 Fort Riley, Kansas

The soils of Fort Riley consist of six series: Wymore (60%), Clime (16%), Smolan (9%), Kipson (7%), Eudora (7%), and Labette (1%). Over two-thirds of the installation is of the Wymore and Clime type, including nearly all of the primary maneuver area in the uplands of the north and northwest. All Fort Riley soils are Mollisols. With the exception of the Eudora and Kipson series, which have coarse-silty and fine texture, respectively, installation soils are also characterized as having fine textures. Soils generally transition from Wymore to Clime, then Kipson, Smolan, Eudora, and Labette as elevation decreases from the uplands to the Kansas River and Wildcat Creek drainages to the south and east. The Wymore and Kipson series' are of the soil hydrologic group D. Clime, Smolan, and Labette soils are of group C, and Eudora soils are group B. Most soils are found in areas of relatively flat terrain, with specific series determined by upland versus lowland position. The exception to this is the Clime series, which are typically located in higher slope areas (5-20°).

Figure 27. Runoff potential for the soils of Fort Riley, Kansas by soil hydrologic group (Source: Generalized Map of U.S. Soils, USDA NRCS).

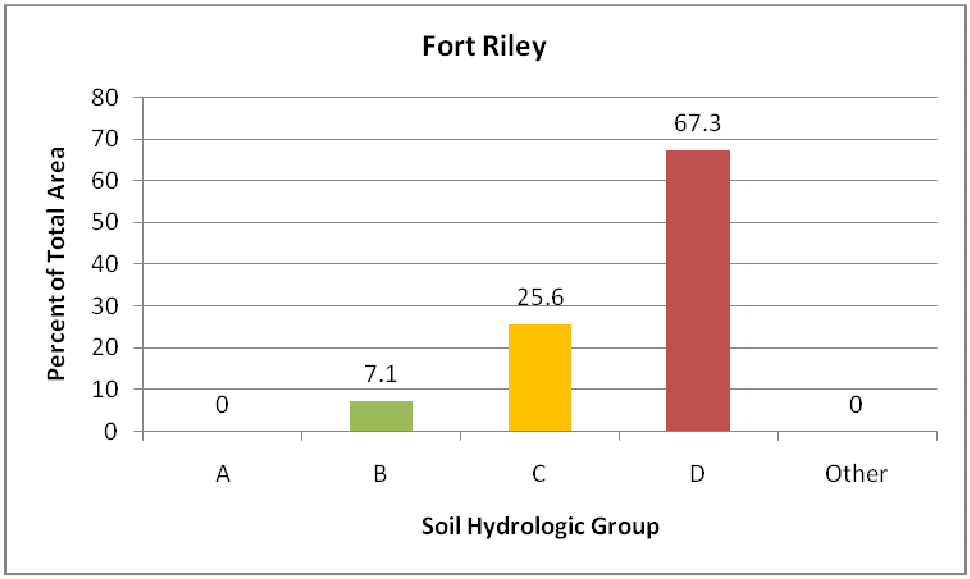

Elevations are Fort Riley range from 379 to 419 m asl, with average slope of 6.7% (maximum slope = 111%). Areas in the higher slope range include the transition zones represented by the Clime soil series. Slopes can also be locally significant along the larger perennial streams. Fort Riley is located in the Flint Hills ecological region. Landcover is primarily grassland (67%), with lesser amounts of deciduous forest (17%) and developed/open space (6%). Most of the installation's deciduous is located along draws, intermittent streams, and perennial streams.

Fort Riley's climate is Hot Summer Continental (Koppen-Geiger climate classification = Dfa). Maximum average monthly temperatures range from a low of 3° C in January to a high of 32° C in July. The annual average maximum temperature is just over 18° C. The minimum average monthly temperature of -9° C occurs in January, but average monthly low temperatures can be as high as 19° C in July. The average annual precipitation totals 826.5 mm per year, most of which falls during the March-July time period. However, only three months (January, February, and December) average less than 28 mm of precipitation.

Figure 28. Dominant landcover categories for Fort Riley, Kansas (Source: 2001 National Landcover Dataset).

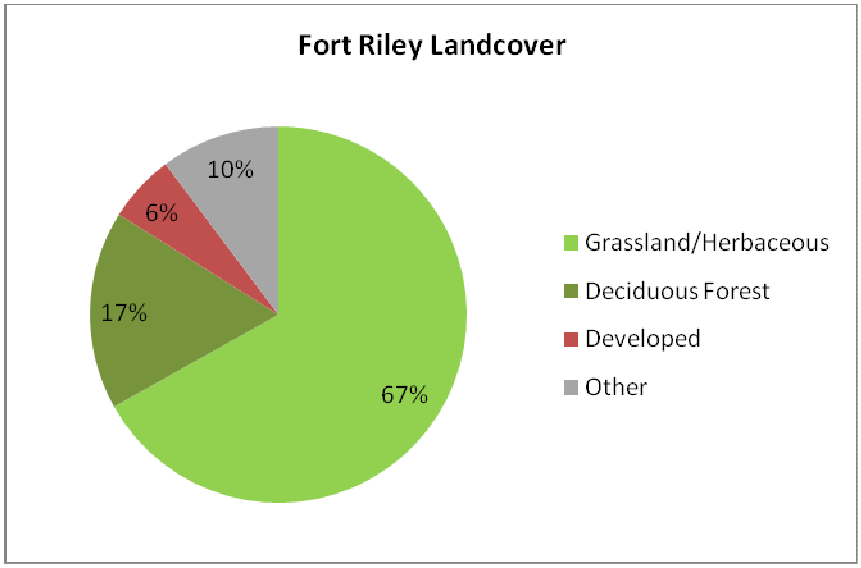

Figure 29. Climograph for Fort Riley, Kansas (Source: http://www.weather.com).

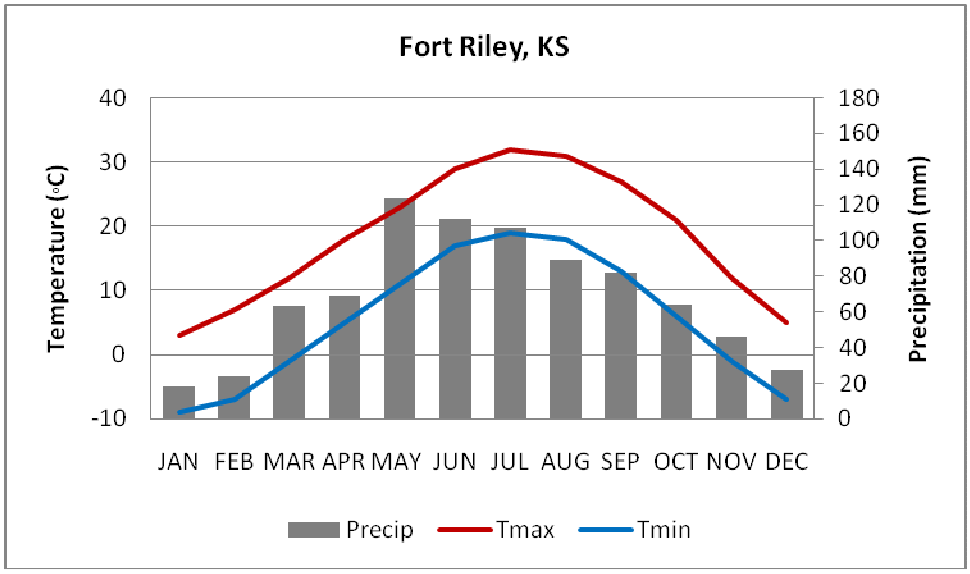

4.4 SITE-RELATED PERMITS AND REGULATIONS

No permits or regulations apply to this demonstration project.

5.0 TEST DESIGN

A detailed description of the test design from conception through execution is documented below.

5.1 CONCEPTUAL TEST DESIGN

The data collection, model development, data analysis, accuracy assessment, and technology transfer activities associated with this project took place during three primary project phases:

- Phase 1: Calibration
- Phase 2: Validation
- Phase 3: Training and Technology Transfer

During Phase 1 (Calibration), field visits to each installation site were conducted during the first and second year of funding. During these visits, installation spatial data was inventoried and any unique datasets acquired from local ITAM offices. If not already collected by installation personnel, gully locations on training lands were collected using GPS and/or "heads-up" digitizing of digital orthophotographs to serve as a model calibration and validation dataset. Also during Phase 1, the need to purchase satellite imagery to classify current LULC type and condition information was assessed. For all installations, it was determined that 2006 NLCD data sufficiently described current LULC types and spatial distributions. After returning from installation visits, the *nLS+* model was calibrated for each installation and critical *nLS+* threshold values (including measures of central tendency and dispersion) identified. Upon calibration, an erosion potential map for each site was created and shared with installation ITAM staff.

A second series of visits to each installation study site were conducted during Phase 2 (Validation) activities, which were completed during the third and fourth year of funding. Field work focused primarily on acquiring additional gully locations (where and when necessary). Poor initial model validation results were believed to be a result of gullies being defined and mapped in different ways – both among staff at a given installation as well as between installations. For example, gullies at some installations included "mini-canyons" while others met the gully definitional requirements outlined in our report. Research team personnel began familiarizing installation ITAM personnel with the *nLS+* model background and operation and conducted GIS training with the model. Subsequent to each site visit, the installation *nLS+* model was refined by re-calibration when additional gully observations were recorded and then validated by assessing the calibrated model accuracy. Phase 2 activities also included initial efforts to operate the *nLS+* model in predictive mode at Pohakuloa Training Area.

During the final year of funding (Phase 3: Training and Transfer), final maps of gully locations, model results, and gully density estimates were shared with installation ITAM staff, along with CD/DVD copies of completed GIS models, installation data, and results. Final work related to operating the *nLS+* model in predictive mode was also completed.

5.2 BASELINE CHARACTERIZATION AND PREPARATION

For each installation, *nLS+* models were developed using nationally available datasets. Initial gully data layers were constructed using high resolution photography when available. During the initial installation visits, any relevant locally available data, such as improved LIDAR derived DEM products and local gully information was obtained. If gully information was not available, project personnel worked with the installation land management office to gain access the training areas and conduct limited field surveys of gully locations.

Gullies were characterized based on their topographic position, width, depth, and length at the current gully head location. Gully location was determined using a GPS unit and each site was documented with digital photography. Where possible, gullies were characterized by width, depth, and length. This descriptive information was helpful when used during the model validation stage to document local differences in the meaning of the term "gully". Wherever possible, gully data collection in the field conformed with the gully definition presented in in Section 3.

5.3 DESIGN AND LAYOUT OF TECHNOLOGY AND METHODOLOGY COMPONENTS

Figure 30 shows the general framework of the *nLS+* model, which is designed as a series of four sub-models for users who wish to predict the current location of gullies or forecast the formation of new gullies in response to a training event. Data sets required for gully prediction include LULC and DEM inputs. From these data layers, the Manning's *n*, slope, profile curvature and other required intermediate data products are computed. In forecast mode, input data include a filled DEM and Manning's *n* grid (output from the model in prediction mode) and a form of vehicle tracking data from GPS devices that includes, at minimum, vehicle coordinates and velocity.

Figure 30. General schematic of the *nLS+* model for gully prediction and forecasting.

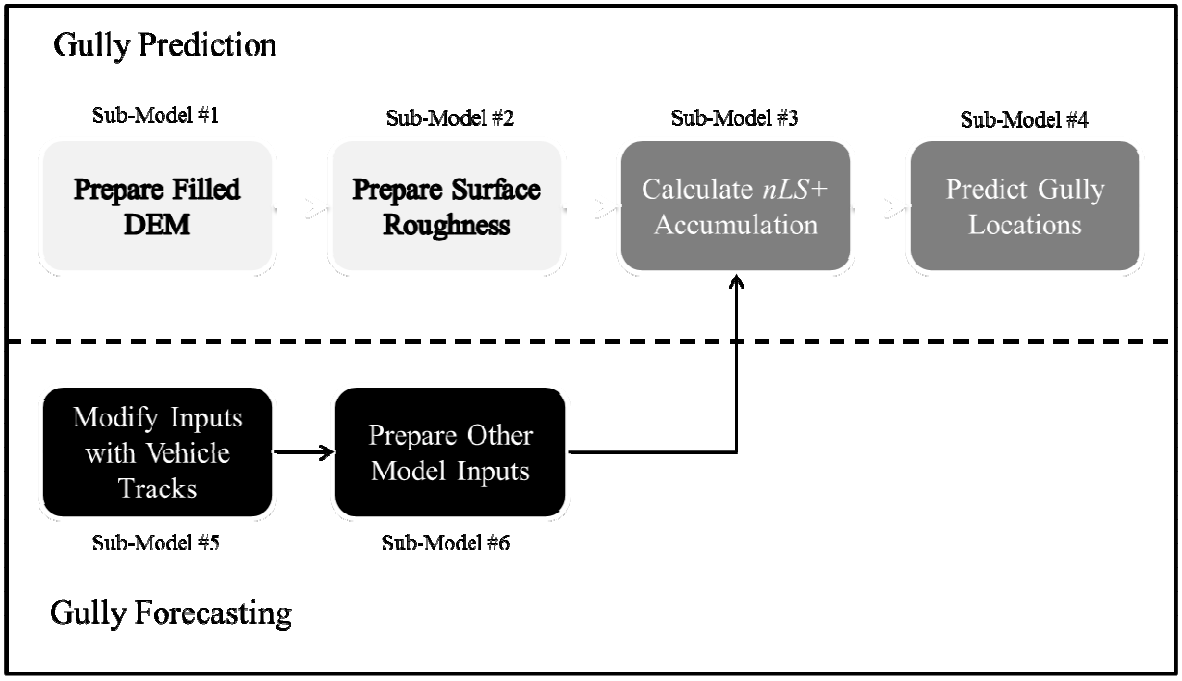

5.4 FIELD TESTING

A detailed description of each phase of the demonstration including model calibration and validation to include a model sensitivity analysis is detailed in the next sections.

5.4.1 Model Calibration and Validation

After the initial *nLS+* model was run, a point file of gully head locations, acquired in the field or digitized from digital orthophotography, was overlaid with model results to extract the accumulated *nLS+* value at each gully location. The model was calibrated using approximately 30% of the known gully locations and validated with the remaining data points. During calibration, actual gully locations were relocated ("snapped") to the highest flow accumulation grid value within a 1 cell distance from the recorded GPS location to account for error in the DEM. A series of descriptive statistics were then generated from the accumulated *nLS+* values to best characterize the critical threshold where overland sheet flow is expected to transition to concentrated flow.

Once the model was calibrated and the critical threshold range for the installation determined, the model was validated using the remaining 70% of actual gully locations. The prediction of where sheet flow transitions to concentrated flow and, therefore where gullies are most likely to be found, was developed via a Structured Query Language (SQL) query for the calibration

threshold value range within the accumulated *nLS+* value layer generated by the *nLS+* model. Actual gully locations that fall within a one cell buffer distance of those meeting the SQL query conditions were assessed as an accurate prediction.

5.4.3 Equipment Calibration and Data Quality Issues: Model Sensitivity Analysis

A series of sensitivity analyses were conducted to better understand the relative importance of two model inputs (slope and Manning's *n* coefficient), and any associated data error/uncertainty, on model output and the resulting correlation with accumulated *nLS+* values and gully locations.

The key factors affecting computed *nLS+* values are Manning's surface roughness coefficient (*n*) and slope (*S*). The first sensitivity test evaluated the relative importance of slope in shaping accumulated *nLS+* values. In this analysis, a DEM for Schofield Barracks' Kahuku Range was modified by flattening and exaggerating the elevation values at 10% increments for a total range of elevation model inputs between 10% and 200% of actual elevation. The modified DEMs were used to calculate slope and, in turn, these modified slopes were used as the inputs for 10 total *nLS+* model runs. The accumulated *nLS+* values from each model run were recorded and compared at 100 fixed locations. Graphical results (Figure 31) indicated that slope was the dominant control on model output, and that the *nLS+* model is very sensitive to slope especially at low values.

Figure 31. Sensitivity of *nLS+* model output to changes in slope at the Kahuku Training Area, Schofield Barracks, Oahu.

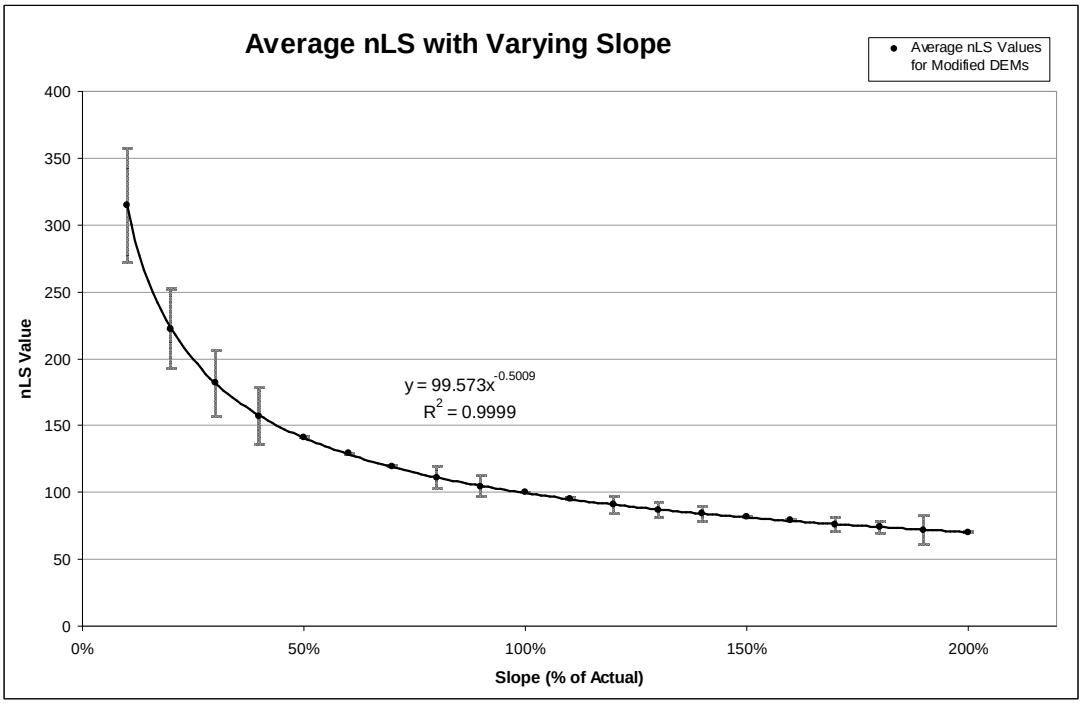

The variation in model output at low slopes, shown by the long error bars in the portion of the Figure 31 at 40% and less of actual slope, suggests that Manning's *n* (*i.e.*, vegetation) may be a more important factor at lower slopes. However, some of this variation can also be attributed to DEM error, which impacts *nLS+* value accumulation most in upland areas. Figure 32 illustrates the flow accumulation paths resulting from 20 different DEM inputs, where each cell in each DEM input was randomly modified +/- 7 meters (which corresponds closely to the general accuracy standard published for the NED). By overlaying the flow accumulation from each modified DEM, it is shown that the impact of DEM error is most important in the lower slope upland areas, because small changes in elevation can mean significant changes in the route of overland flow as it moves downhill (the areas in yellow and light orange). In areas of steeper slopes, and after overland flow has left the upland areas, the flow paths begin to converge and become consistent (the areas in dark orange, red, and blue), despite the modified elevations. Understanding the model's sensitivity to slope is important, and points to potential large gains in model accuracy if high spatial resolution DEMs, such as those generated by LIDAR, are used as input to the *nLS+* model.

Figure 32. Impact of DEM error on a flow accumulation network conducted for a portion of the Kahuku Training Area, Schofield Barracks, Oahu.

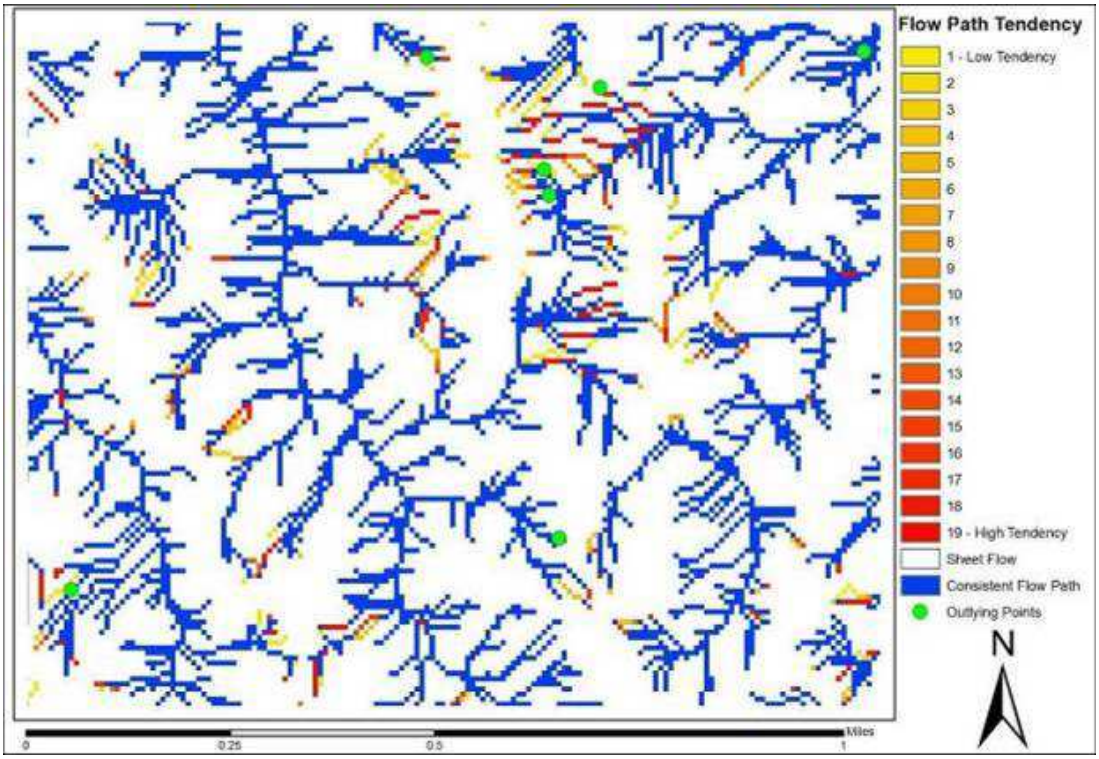

The Manning's *n* factor, derived from remotely-sensed LULC data products, describes the land surface's ability to provide resistance to flow. For example, bare ground has a low roughness factor while permanent vegetation has a higher roughness factor. This variable indirectly accounts for climate and soils using vegetation as a proxy. A number of factors can affect the accuracy of Manning's *n*, including the classification accuracy of the LULC product, the phenological development of vegetation, land management activities, and site disturbance.

Two different sensitivity analyses were performed to better understand the importance of Manning's *n* specification on *nLS*+ model performance. The first tested *nLS*+ model sensitivity to the geographic distribution of LULC types, and the corresponding "normal" Manning's *n* values. Again the Kahuku Training Area at Schofield Barracks served as the test site and single peer-accepted values for Manning's *n* were substituted for known vegetation classes. A total of 10 random LULC layers, based on actual Schofield Barracks vegetation, were generated in a manner that resulted in the total area of each LULC class being similar. Essentially, this became an evaluation of how important it is to accurately classify each pixel of LULC layer, or whether it is sufficient to know the correct percentages of each LULC type within an area of interest. The *nLS*+ model was run 10 times, once for each modified LULC input and using the same DEM for each iteration. The accumulated *nLS*+ value at the watershed outlet varied only 0.3% over all model runs indicating little sensitivity to the spatial distribution of LULC types (Table 5).

Table 5. Sensitivity of *nLS+* model output to the distribution of LULC classes at Kahuku Training Area, Schofield Barracks, Oahu.

Landcover Distribution No.	Percent of Total Area for each Landcover Class														Ouput nLS Value (X 10^{-3})
	Mixed Cliff Communities	*Mixed Grassland*	*Bare Soil*	*Guinea grass*	*Java plum Forest*	*Mixed Alien Grassland*	*Diverse Native Forest*	*Eucalyptus Mixed Forest*	*Ironwood Mixed Forest*	*Christmas berry Forest*	*Strawberry guava Shrubland*	*Disturbed Alien Grasslands*	*Cropland and pasture*	*Roads*	
1	0.01	0.12	0.71	2.90	8.09	15.89	22.38	22.14	15.62	8.17	3.06	0.75	0.13	0.02	217.3
2	0.02	0.17	0.81	3.01	8.06	15.80	22.16	22.25	15.90	7.89	2.98	0.77	0.16	0.02	216.4
3	0.02	0.14	0.74	2.83	8.38	15.81	21.87	22.42	15.91	8.04	2.88	0.79	0.14	0.02	216.7
4	0.03	0.15	0.74	2.87	7.89	15.82	22.10	22.56	15.82	8.22	2.81	0.83	0.13	0.01	217.5
5	0.03	0.11	0.77	2.94	8.04	15.86	21.90	22.19	16.11	8.04	3.05	0.80	0.13	0.01	217.1
6	0.01	0.12	0.78	2.92	8.10	15.71	22.40	22.08	16.00	8.06	2.96	0.75	0.11	0.01	217.0
7	0.02	0.15	0.76	2.90	7.88	15.82	22.32	22.05	16.26	8.15	2.76	0.76	0.18	0.01	217.1
8	0.02	0.12	0.82	2.90	8.15	15.77	22.40	22.27	15.61	8.15	2.89	0.75	0.12	0.02	217.3
9	0.02	0.13	0.75	2.88	8.00	15.62	22.30	22.19	15.82	8.20	3.10	0.85	0.13	0.01	217.5
10	0.02	0.11	0.81	2.85	8.06	15.88	22.30	21.85	16.14	8.11	2.95	0.76	0.14	0.02	216.8

The final analysis evaluated model sensitivity to actual Manning's *n* coefficients. Portions of the 2006 NLCD and NED for the Kahuku Training Area were used as *nLS+* model input. However, instead of replacing each LULC type with a single Manning's *n* value, one in a range of accepted values for each LULC type were selected at random for each cell (Table 6). In order to better assess model sensitivity to variations in Manning's *n*, highly detailed information specific to the unique Hawaiian vegetation was used. Figure 33 highlights an area of cropland/pasture where individual cells were randomly coded with the Manning's *n* values of 0.02 (yellow), 0.03 (light green), or 0.04 (dark green).

The *nLS+* model was executed a total of 100 times and the resulting accumulated *nLS+* values recorded at 300 fixed locations. Random selection of a range of accepted Manning's *n* values resulted in output *nLS+* values that varied less than 25% for most locations (Figure 34). Those sites that varied by more than 25% were located at higher elevations within the watershed – the same low slope locations where the *nLS+* model was shown to be both highly sensitive to, and suffer most from, DEM error.

Table 6. Range of Manning's *n* coefficient values for select LULC types comprising the Kahuku Training Area, Schofield Barracks, Oahu (Chow 1959).

Landcover Description	Manning's n Values		
	Minimum	Normal	Maximum
Bare Soil	0.02	0.03	0.04
Kukui Forest	0.11	0.15	0.2
Ironwood Mixed Forest	0.08	0.1	0.12
Cropland and pasture	0.02	0.03	0.04
Disturbed Alien Grasslands	0.025	0.03	0.035
Eucalyptus Mixed Forest	0.11	0.15	0.2
Evergreen forest land	0.11	0.15	0.2
Haole koa / Guinea grass Mixed Grassland	0.03	0.035	0.05
Paper bark eucalyptus Forest	0.11	0.15	0.2
Ohi'a / Acacia koa / Uluhe Diverse Native Forest	0.1	0.12	0.16
Mixed Cliff Communities	0.03	0.04	0.05
Mixed Rangeland*	0.04	0.06	0.08

Figure 33. Coefficient of variation for accumulated *nLS+* values at 300 random locations, across three elevation zones, at the Kahuku Training Area, Schofield Barracks, Oahu.

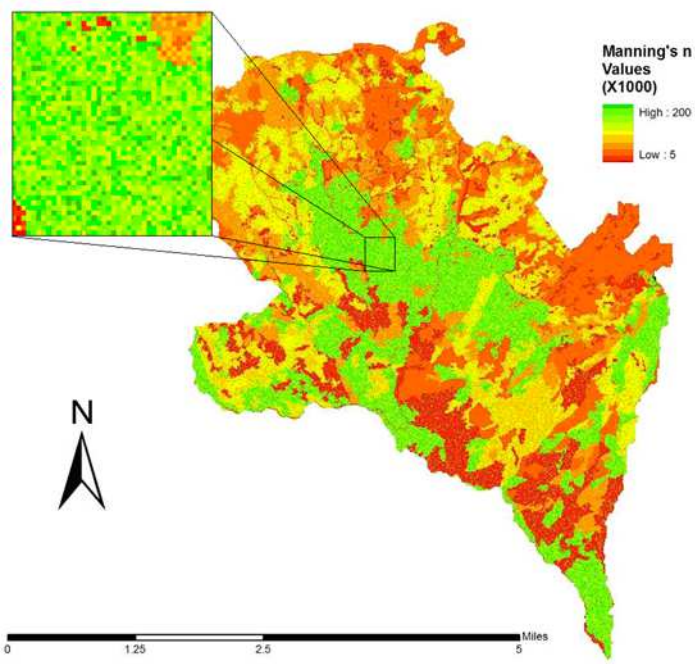

Figure 34. Coefficient of variation for accumulated *nLS+* values at 300 random locations, across three elevation zones, at the Kahuku Training Area, Schofield Barracks, Oahu.

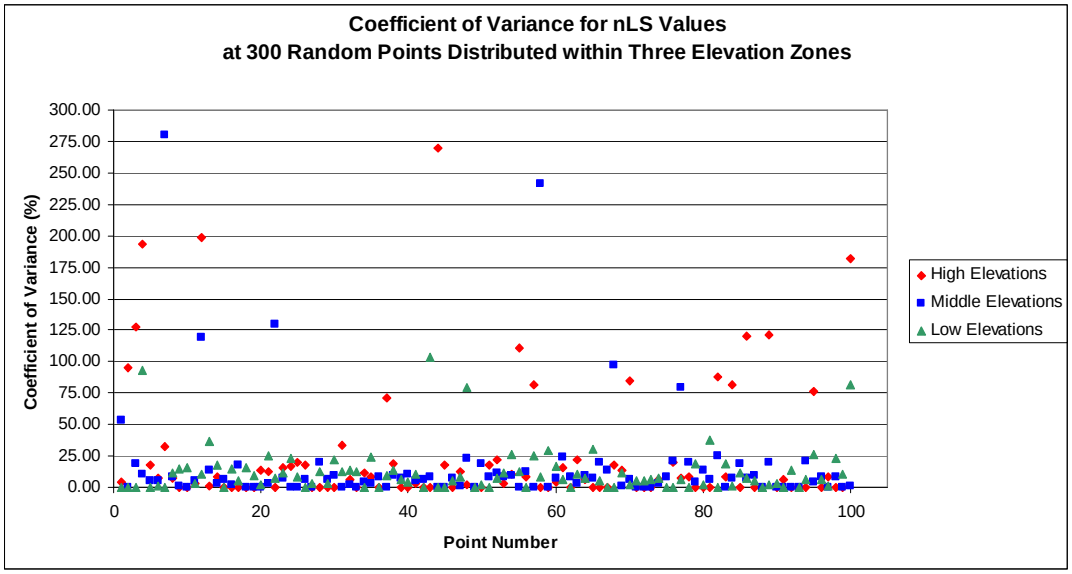

After this preliminary analysis of training lands at Schofield Barracks, Hawaii, it was anticipated that erosion features of interest across our selected study sites would likely be correlated with more than one critical threshold for accumulated *nLS+* values, but that these multiple threshold values would exhibit regional similarities (*e.g.*, Fort Riley ≅ Fort Hood ≅ US Great Plains states). Analysis of the sensitivity of *nLS+* output to spatially (and temporally) variable inputs indicates that regional similarities would likely be governed by average slope conditions, with gully locations most likely to be present on severely sloped training lands typified by lower higher accumulated *nLS+* values. Additionally, regardless of average slope, gullies will be related to higher threshold values in areas undergoing accelerated rates of erosion due to changes in natural landcover resulting in "smoother" surfaces (*e.g.*, former forest now in grassland, native grassland replaced with annual invasive species, *etc*.).

5.5 SAMPLING PROTOCOL: OPERATING THE *nLS+* MODEL IN PREDICTIVE MODE

Key to operating the *nLS+* model in predictive mode at Pohakuloa Training Area (PTA) (Performance Objective #4) was the ability to obtain vehicle track data (via GPS tracking data or training simulations) and use the track location and characteristics to modify existing installation DEMs and LULC maps. After making appropriate modifications to these input datasets, the *nLS+* model was re-run after a training event and field data collected to determine whether the model successfully forecasted new areas of actual (or suspected) gully activity.

The basis for the modification of the DEM and LULC inputs come from previous research that evaluated land surface alterations by vehicle type, operating characteristics, and soil conditions (Ayers et al., 2000, Ayers *et al.*, 2005a, Ayers *et al.*, 2005b, Rice and Ayers 2005, Rice *et al.*, 2006). Much of this work culminated in the quantification of non-linear relationships between

vehicle turning radii and velocities on resulting vegetation damage and rutting depth for different soil types and soil moisture conditions.

Three Stryker vehicles from a reconnaissance platoon of the 2nd Brigade of the 25th Infantry Division were tracked during an off-road proofing mission on the Keamuku Parcel at PTA using GPS-based tracking systems to determine vehicle movement patterns and estimate soil loss impacts (Howard *et al.*, 2011). Track data recorded by GPS units onboard the three vehicles were obtain from Dr. Paul Ayers (pers. comm.). The data was received as a text file with geographic coordinate information acquired at approximately one second intervals. Each GPS record also included key attributes such as vehicle velocity (VEL) and course over ground (COG) along with a detailed date/time stamp identifying when the position record was acquired.

Rut depth was calculated as a function of vehicle turning radius. To do so required first the calculation of vehicle turning radii from the original GPS track file. Estimates of vehicle turning radii for each recorded location were based on five consecutive position fixes and using the five-point method outlined in ERDC/CERL Technical Report 00-43 (Ayers *et al.*, 2000).

Liu *et al.*, (2009) described the relationship between the inside and outside tracks for a Light Armored Vehicle (LAV) operating in a spiral test pattern at two speeds (4 and 8 m/sec) during experimental maneuvers at Fort Lewis, Washington in 2002 (Figure 35).

Figure 35. Relationship between rut depth and LAV turning radius (from Liu *et al.*, 2009).

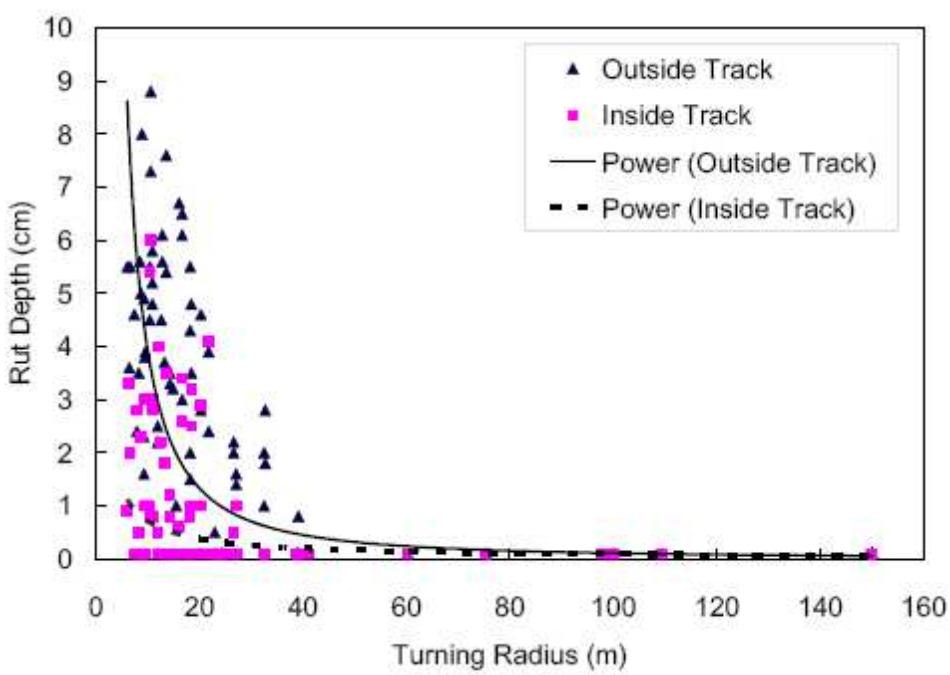

Based on these findings, a generic power function was defined to estimate vehicle rut depth using the curve for the outside track that generates the deeper rut:

$$RD = 67.571 * TR^{-1.278}$$

where:
RD = rutting depth (cm) for wet soil conditions
TR = vehicle turning radius (m)

A qualitative measure of vehicle damage to the land surface, including amount of vegetation removed or dislodged during vehicle operation is provided by the Impact Severity (IS) score, which ranges from 0-100% (Table 7). To account for possible vegetation removal after the passage of a military vehicle, an IS score was calculated to reflect the percentage of soil and vegetation damaged at each vehicle location (ERDC 2000):

$$IS = 261(TR^{-0.75}) * VEL^{0.62}$$

where:
IS = impact severity (%)
TR = vehicle turning radius
VEL = vehicle velocity (m/s)

Table 7. Summary of Impact Severity (IS) scores for assessing vehicle track damage to vegetation (from Liu *et al.*, 2009)

Impact Severity (%)	***Description***
0	No visible disturbance as compared to surrounding vegetation/area
10	Laying down of vegetation; few, if any, broken stems; no evidence of vegetation shearing
20	Some broken stalks/plants; visible soil disturbance, possibly exposing bare soil
40	Obvious depressed soil and vegetation with significant vegetative damage and slight removal; piling on track edge evident; movement of plants/soils towards the edge of vehicle track without completely shearing plant at roots; some bare soil exposed
60	About 1/3 of vegetation still present and intact on the track; significant amount of bare soil exposed; larger piling of vegetation on edge of track due to shearing motion of the vehicle, fully removing species from the track; some of the pile has overturned, exposing roots
80	Few vegetative species still intact on vehicle path; piling of vegetation and soil on the edge of the path; pile is completely overturned, exposing roots
100	Complete removal of vegetation and soil; shearing action of vehicle has left vehicle track bare; sheared vegetation and soil is piled on edge of track

Following the turning radius, impact severity, and rut depth calculations, vehicle track files were imported into a GIS and combined into a single file of all GPS position records. These points, and their corresponding attributes, were then converted into two gridded track files representing the calculated values for impact severity (IS) and rut depth (RD), respectively, at the same spatial resolution of the DEM used to describe installation terrain. During this point to raster conversion, the maximum value for IS and RD were retained if more than one GPS point would be located within the same grid cell. The IS grid was used to scale the original Manning's *n* surface roughness coefficients downward to reflect changes in vegetation condition. The resulting scaled Manning's *n* and RD grids were then re-incorporated back into the original Manning's *n* grid and DEM for the Keamuku Parcel to serve as new inputs for the *nLS+* model that more accurately reflected post-maneuver landscape conditions.

5.6 SAMPLING RESULTS

A total of 389 gully locations were used in *nLS+* model calibration and validation (Table 8). Most gully locations were provided by installation ITAM staff; however a significant proportion (17-100%) were generated by project personnel during field visits and through heads-up digitizing of high-resolution aerial photographs. Digital files of gully locations are available in GIS format (*i.e.*, shapefiles) and are packaged with the *nLS+* model tools.

Table 8. Summary of gully data acquired from installations and generated for *nLS+* model calibration and validation.

Installation	Total Gully Locations	Installation Provided (%)	Project Generated (%)
Fort Benning	65	53 (82%)	12 (18%)
Fort Hood	192	159 (83%)	33 (17%)
Fort Riley	49	18 (37%)	31 (63%)
Kahuku Range	47	36 (77%)	11 (23%)
Keamuku Parcel	36	0 (0%)	36 (100%)

6.0 PERFORMANCE ASSESSMENT

The following section provides a summary of all data analysis conducted in the assessment of the performance objectives.

6.1 OBJECTIVE #1: IDENTIFY THE CRITICAL THRESHOLD FOR ACCUMULATED *nLS+* VALUES FOR EACH STUDY INSTALLATION

Data analysis in support of the first performance objective is broken down into information concerning gully data processing, model calibration, and model validation and accuracy.

6.1.1 Gully Data Processing

Data on the location of gullies at selected installations were obtained from ITAM staff and/or collected during site visits. Excluding Fort Riley and Keamuku Parcel, gully data obtain from ITAM personnel were typically collected using global positioning systems (GPS) and input into a geographic information system (GIS) as line features. At Fort Riley and Keamuku Parcel, gully data were recorded as point features. Descriptive attributes for gullies were often, but not always, included in the GIS files, though the types of data collected (*e.g.*, name, location description, cause, width, depth, length) varied significantly. In this analysis, all mapped gullies for each installation were converted in a GIS into point features prior to further processing and model execution.

The *nLS+* model was run for each installation, which resulted in the production of several key continuous value gridded outputs, including flow length (upstream), flow accumulation (unweighted), and accumulated *nLS+* values (weighted). Gully points were moved (*i.e.*, "snapped") to the highest flow accumulated value within one digital elevation model (DEM) pixel distance of their mapped locations to minimize later model error due to elevation inaccuracies in the base elevation datasets. The *nLS+* model was run for each installation using 10 meter resolution DEMs from the NED as the elevation source. In addition, higher resolution and LIDAR-derived DEMs were available for three installations: Fort Riley, Fort Hood, and the "priority 1" area of Keamuku Parcel. For these installations, their associated gully data was processed twice given the differences in the gridded model outputs caused by using a different elevation source.

Gullies for each installation were assessed and "cleaned" in two separate procedures using extracted descriptive values from outputs of the *nLS+* model runs. The first procedure eliminated any snapped gullies positioned on a pixel for which the accumulated *nLS+* values equaled zero. For all installations, and based on model output at a 10 meter resolution, this removed from further analysis a total of 25 gullies, leaving 364 of 389 (94%) of the original gully dataset. For the three LIDAR installations, 12 total gullies were removed, with 265 of 277 (96%) of the original gullies remaining (Table 9).

Table 9. Summary statistics for installation gullies after initial data pre-processing that removed from further analysis gullies with accumulated *nLS+* values equal to zero.

Installation	**No. of Gullies**		**Accumulated *nLS+* Values**				
	After	*Before*	*Mean*	*SD*	*1st Quartile*	*Median*	*3rd Quartile*
Fort Benning	55	65	9.63	20.37	0.79	2.43	10.94
Fort Hood	190	192	26.74	112.15	0.34	1.66	8.710
Fort Riley	46	49	491.80	2824.10	1.81	7.59	49.28
Kahuku Range	37	47	42.21	149.82	1.81	7.91	18.95
Keamuku	36	36	662.29	2414.01	2.72	13.77	79.63
*Fort Riley – L	42	49	2,515.41	7,617.68	3.60	14.31	602.40
*Fort Hood – L	192	192	8,199.22	35,315.39	85.49	697.50	3,698.00
*Keamuku – L	31	36	29,069.48	56,327.36	6,073.06	10,188.80	22,539.90
* The L designation indicates LIDAR data were used during the *nLS+* model runs.							

After initial processing to remove spurious accumulated *nLS+* values from the combined gully dataset, box and whisker plots for each installation based on flow length (m) were used to assess the presence of outlying values (Figure 36 and 37). The "boxes" in each plot represent the interquartile range, or the distance between the first and third quartile values, and contain the median (dark horizontal line) flow length value representative of installation gullies. The "whiskers" extend below and above the first and third quartiles, respectively, a distance of 1.5 times the interquartile range or below to zero if that value is reached first.

Figure 36. Installation boxplots of flow length (upstream) extracted at each field measured gully location using 10 meter DEM as model input.

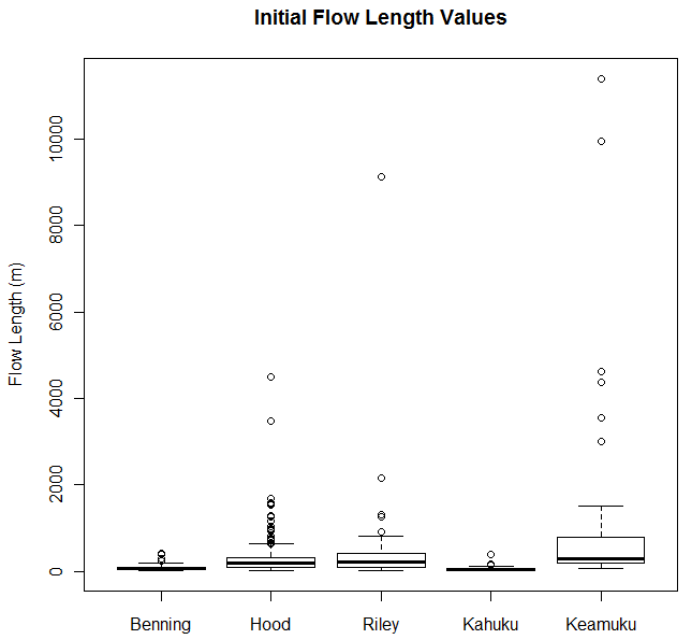

Figure 37. Installation boxplots of flow length (upstream) extracted at each field measured gully location using 3 meter LIDAR DEMs as model input.

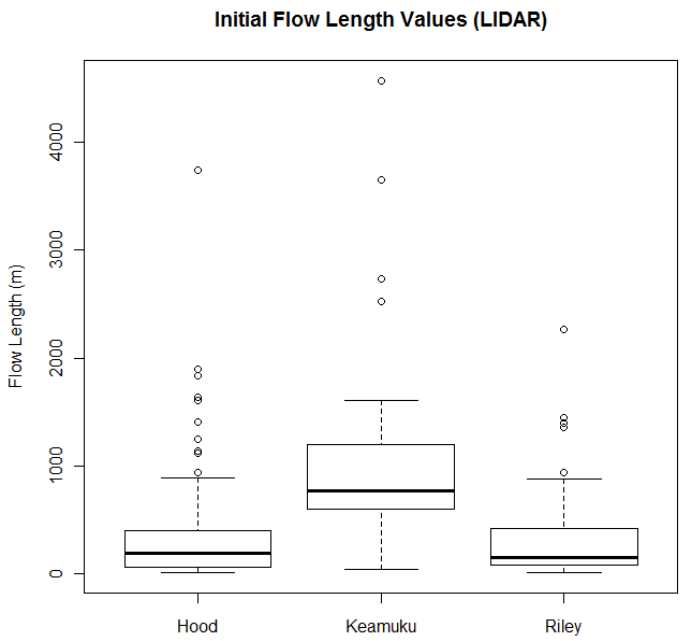

As a second pre-processing step, any gully characterized by an upstream flow length value beyond the lower or upper whisker was removed from the dataset and excluded from further analysis. These "excess" flow length values typically characterized gullies that greatly exceeded the group targeted for this model analysis in terms of width and depth, as well as the associated type of overland flow (*e.g.*, sheet versus concentrated flow). For all installation gullies, at both NED and LIDAR resolutions, only high outlying values of flow length were present. A very conservative total of 43 and 23 additional gullies at NED and LIDAR resolutions, respectively, were removed from analysis during this step (Table 10). The value defining an outlying flow length value for each installation greatly exceeded the typical values associated with sheet flow for all natural landcover types (USDA 1986, McCuen and Spiess 1995).

Table 10. Summary of outliers and outlying upstream flow length values for gullies by installation. The outlier threshold represents the first, and lowest, flow length value associated with an installation gully that was excluded from further analysis.

Installation	No. of Outliers	Outlier Threshold (m)
Fort Benning	5	241.4
Fort Hood	23	651.1
Fort Riley	5	925.3
Kahuku Range	4	140.7
Keamuku Parcel	6	3014.2
Fort Riley – L	7	771.4
Fort Hood – L	12	1,900.0
Keamuku – L	4	2,527.1

After secondary processing, 321 of the original 389 gullies (83%) remained (Table 11) when considering flow lengths computed from NED data. When using the higher spatial resolution LIDAR as model input, 243 of the original 277 gullies (88%) were retained. A comparison of Tables 9 and 11 shows how the removal of gullies characterized by excessive flow length resulted in dramatic reductions in mean accumulated *nLS+* values for each installation, as well as the associated standard deviations. For example, the mean accumulated *nLS+* value for Fort Hood after initial processing with the NED DEM was 26.74 which declined to 4.88 after the secondary cleaning procedure. Similarly, the dispersion of accumulated *nLS+* values declined from 112.15 to 8.28.

After primary and secondary pre-processing, another pair of boxplots was generated for accumulated *nLS+* values (Figures 37 and 38) at each analysis resolution. The distribution of values for each installation was very skewed and included a number of high outliers. This general assessment was confirmed after examining histograms of accumulated *nLS+* values for each installation. The histogram of accumulated *nLS+* values for Fort Hood clearly illustrates the "right-skewed" distribution characteristic of that for all installations (Figure 39).

Table 11. Summary statistics for gullies at the installation level after initial and secondary data pre-processing that removed gullies with both accumulated *nLS+* values equal to zero and outlying flow length values.

Installation	No. of Gullies		Accumulated *nLS+* Values				
	After	*Before*	*Mean*	*SD*	*1st Quartile*	*Median*	*3rd Quartile*
Fort Benning	50	55	4.37	5.01	0.71	2.06	6.43
Fort Hood	167	190	4.88	8.28	0.26	4.88	5.84
Fort Riley	41	46	37.97	74.83	1.10	3.00	24.69
Kahuku Range	33	37	1.43	0.79	0.81	1.53	1.96
Keamuku Parcel	30	36	108.16	255.16	2.44	8.72	33.91
Fort Riley – L	36	42	468.68	1,545.26	3.45	46.87	48.85
Fort Hood – L	180	192	2,916.66	6,727.01	65.53	48.29	2,560.00
Keamuku – L	27	31	12,531.2	12,996.05	5,454.46	7,575.60	14,583.65

Figure 37. Boxplot of accumulated nLS+ values for each installation after primary and secondary processing and using 10 meter DEM as model input.

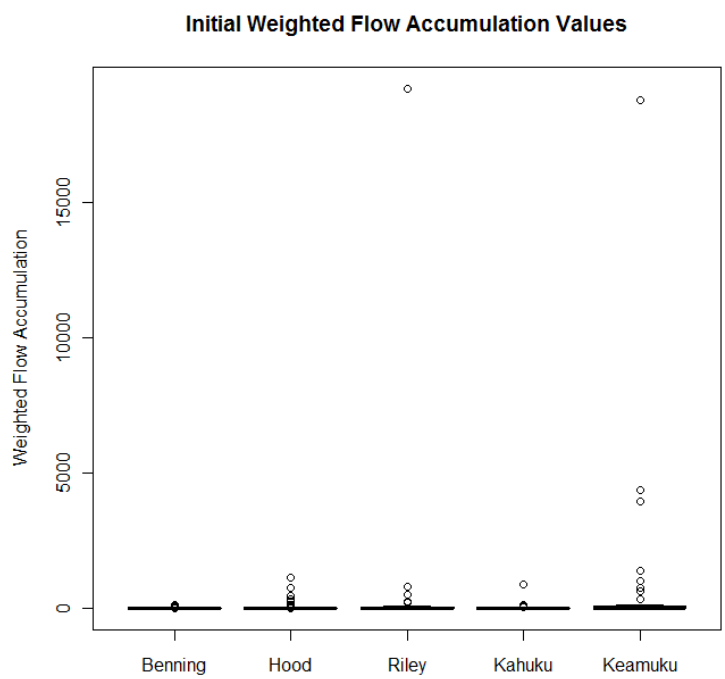

Figure 38. Boxplot of accumulated nLS+ values for each installation after primary and secondary processing and using LIDAR DEM as model input.

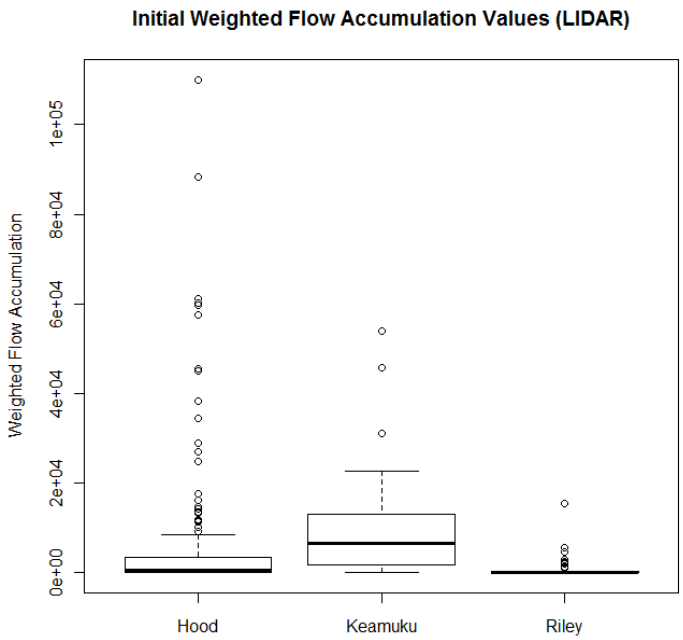

Figure 39. Histogram of accumulated nLS+ values for Fort Hood, Texas after primary and secondary processing. The right-skewed distribution evident here is typical of that seen for all installations.

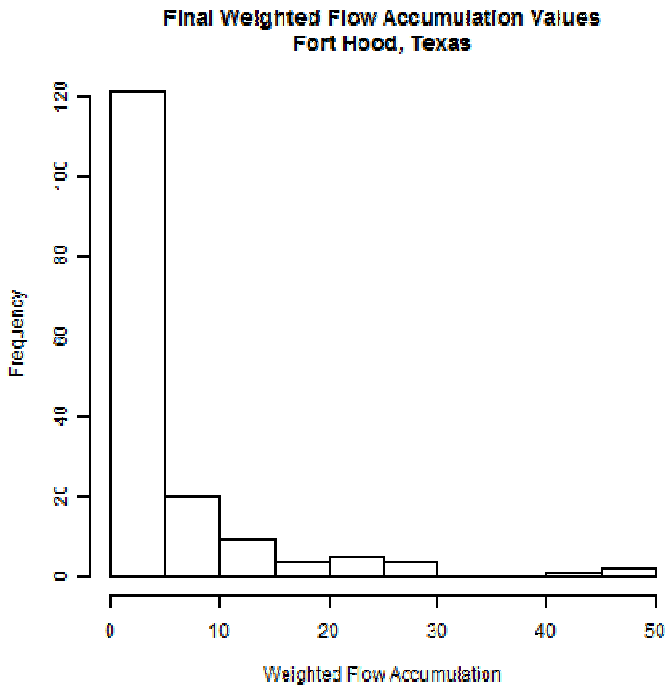

The extremely skewed (*i.e.*, non-normal) distribution of accumulated *nLS+* values for gullies prevents using the installation mean and standard deviation to compute the critical thresholds required to predict locations of gully formation. For example, the standard deviations of installation accumulated *nLS+* values exceed the mean for 4 of the 5 installations studied, even after secondary processing (Table 11). To facilitate better selection of appropriate accumulated *nLS+* thresholds, and to help meet the assumptions associated with later statistical tests associated with Performance Objective #2, a log transformation was applied to the original accumulated *nLS+* values extracted for each installation gully. After transformation, the range of values more closely approximated normal distributions, as typified by the resulting histogram for Fort Hood (Figure 40).

Figure 40. Histogram of log-transformed accumulated nLS+ values for Fort Hood, Texas after primary and secondary processing. The improvement in normality evident here is typical of that seen across all installations and both NED and LIDAR resolutions.

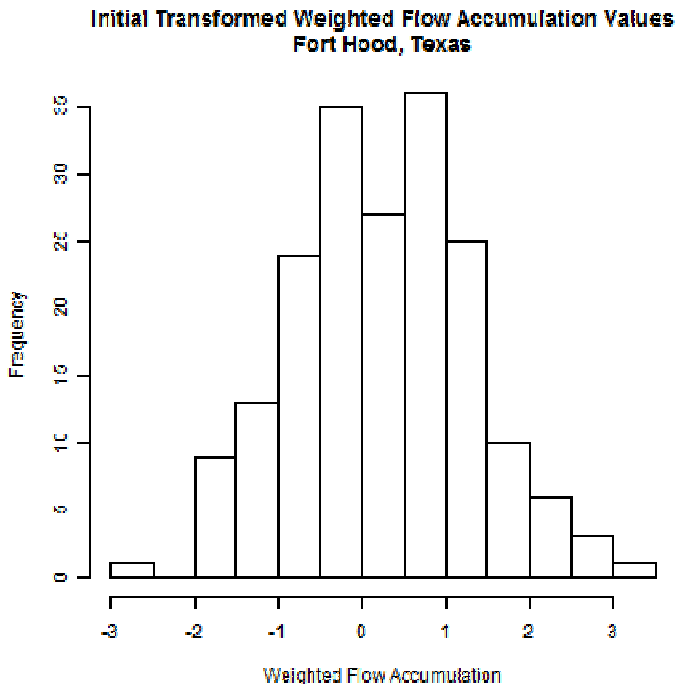

After log-transformation, a final series of boxplots were generated of the transformed accumulated *nLS+* values for gullies at each installation. Outlying low values were detected for two installations at NED resolution: Fort Benning (n = 2) and Fort Hood (n = 1) (Figure 41). An additional five outliers were identified at LIDAR resolution, including 3 at Keamuku Parcel and 1 each at Forts Riley and Hood. As a tertiary and final data pre-processing step, these outliers were also removed from further analysis. After all pre-processing was complete, 71 of 389 (18%) of the original gullies sampled from all installations were excluded from analysis (Tables

12 and 13). Considering only those installations with available LIDAR data, 41 of 277 (15%) were omitted during *nLS+* model calibration and validation.

Figure 41. Examples of boxplots of log-transformed accumulated nLS+ values, with NED DEMs as input, for Fort Benning, Georgia (left) and Fort Hood, Texas (right) showing outlying values.

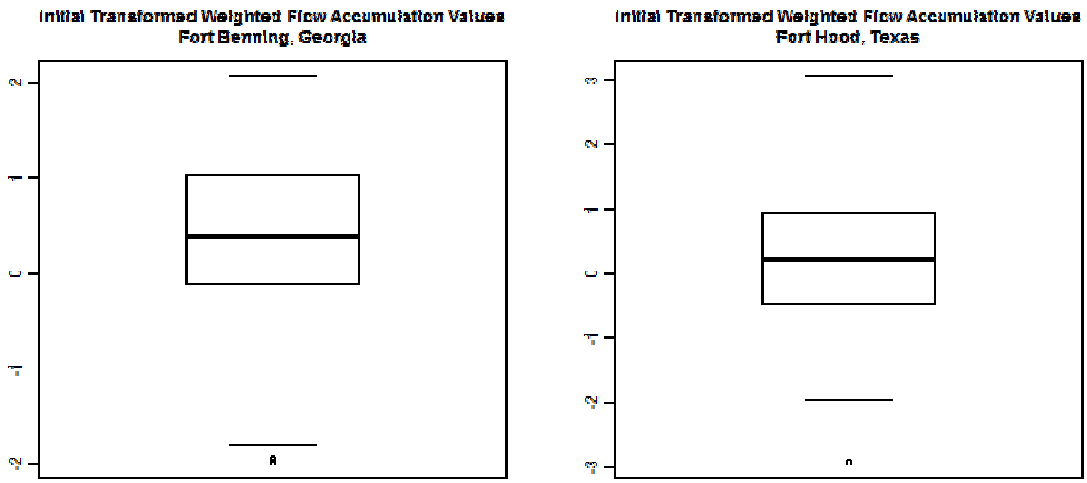

Table 12. Number of gullies excluded from further analysis for each installation (and total) after primary, secondary, and tertiary data pre-processing when using NED DEMs as model input.

Installation	No. of Gullies Excluded from Analysis			Total Gullies Excluded	Original No. of Gullies	No. of Remaining Gullies (%)
	Primary	*Secondary*	*Tertiary*			
Fort Benning	10	5	2	17	65	48 (74%)
Fort Hood	2	23	1	26	192	166 (86%)
Fort Riley	3	5	0	8	49	41 (84%)
Kahuku Range	10	4	0	14	47	33 (70%)
Keamuku Parcel	0	6	0	6	36	30 (83%)
All Installations	25	43	3	71	389	318 (82%)

Table 13. Number of gullies excluded from further analysis for each installation (and total) after primary, secondary, and tertiary data pre-processing when using LIDAR DEMs as model input.

Installation	No. of Gullies Excluded from Analysis			Total Gullies Excluded	Original No. of Gullies	Remaining Gullies (%)
	Primary	*Secondary*	*Tertiary*			
Fort Riley LIDAR	7	7	2	16	49	33 (67%)
Fort Hood (LIDAR)	0	12	1	13	192	179 (93%)
Keamuku Parcel (LIDAR)	5	4	3	12	36	24 (67%)
All Installations	12	23	6	41	277	236 (85%)

6.1.2 Model Calibration

After log-transformation and tertiary data processing, installation means and standard deviations for accumulated *nLS+* values were much better representations of central tendency and dispersion (Table 14). The remaining gullies for each installation were divided into calibration and validation datasets with 30% of the total number of gullies (or a minimum of 10) used for model calibration and the remainder for validation. Installation gullies in the calibration dataset were randomly selected from the complete set by first generating a spatially random point layer in a GIS, whose distribution was constrained by the installation boundary, then choosing gullies closest to each randomly-place point. Installation-level critical thresholds for accumulated *nLS+* values were then calculated as the installation mean plus and minus one-half of the standard deviation (Table 15).

Table 14. Summary statistics for calibration gullies at the installation level.

Installation	No. of Gullies		Log-Transformed Accumulated *nLS*+ Values				
	Calibration	*Validation*	*Mean*	*SD*	*1st Quartile*	*Median*	*3rd Quartile*
Fort Benning	14	34	0.37	0.50	0.22	0.31	0.58
Fort Hood	50	116	0.02	0.87	-0.49	0.00	0.66
Fort Riley	12	29	0.59	0.86	-0.16	0.93	1.16
Kahuku Range	10	23	0.60	0.80	0.18	0.33	1.17
Keamuku Parcel	10	20	0.56	0.81	-0.03	0.39	1.01
Fort Riley (LIDAR)	10	23	1.11	1.38	0.51	0.74	1.48
Fort Hood (LIDAR)	54	125	2.39	1.15	1.48	2.41	3.26
Keamuku Parcel (LIDAR)	10	14	4.14	0.32	3.89	4.12	4.35

Table 15. Critical threshold values from calibration gully datasets for accumulated *nLS*+ values. Threshold values for gully prediction represented by the interval defined by the lower- and upper-bounds.

Installation	Accumulated *nLS*+ Values (Log Transformed)				Contributing Area (m^2)*	
	Mean	*SD*	*Lower Bound#*	*Upper Bound@*	*Minimum*	*Maximum*
Fort Benning	0.37	0.50	0.12	0.62	132	417
Fort Hood	0.02	0.87	-0.42	0.46	38	288
Fort Riley	0.59	0.86	0.16	1.02	145	1,047
Kahuku Range	0.60	0.80	0.20	1.00	158	1,000
Keamuku Parcel	0.56	0.81	0.165	0.97	146	933
Fort Riley – L	1.11	1.38	0.42	1.80	24	568
Fort Hood – L	2.39	1.15	1.24	2.97	156	8,399
Keamuku – L	4.14	0.32	3.98	4.30	85,949	179,574

Lower bound calculated as mean – (0.5 * SD)
@ Upper bound calculated as mean + (0.5 * SD)
* Estimates backcalculated from log-transformed accumulated *nLS*+ values and DEM resolution

The range of expected contributing watershed areas for gullies at each installation was calculated using the DEM resolution and the accumulated nLS+ values. Contributing areas ranged from 38 m^2 (Fort Hood) to 1,047 m^2 (Fort Riley) when using a 10 m DEM and 24 m^2 (Fort Riley) to 179,574 m^2 (Keamuku) when using LIDAR data. Because gully formation is expected to occur

near the transition of overland flow from sheet to concentrated flow, which is expected to occur at or before 100 m of flow (McCuen and Spiess 1995, USDA 1986), these contributing areas are reasonable and suggest that gully formation will occur on upland areas with higher slope and relatively small contributing areas.

6.1.2 Model Validation and Accuracy Assessment

The lower- and upper-bounding values for each installation were then used in a conditional statement to query a log-transformed accumulated *nLS+* grid. The result of the query showed each grid cell that fell between the lower and upper bounding values controlled by the installation mean and standard deviation and, hence, where gullies were predicted to form.

To better visualize the results of the conditional value query that selected the predicted cells, a line density surface was created after converting predicted cells to lines of erosive flow (Figures 42 through 44). Density was calculated using 500 m radius as:

$$\text{Density} = (L_1 + L_2 + \ldots + L_k) / (\pi * r^2)$$

where:
$L_1 \ldots L_k$ = length of line segments falling within the circular search
r = radius of circular search area

Figure 42. Predicted gully locations (left) and gully density surface (right) representing number of predicted gullies per square kilometer for Fort Benning, Georgia based on a natural breaks classification and NED DEM model input. Gully locations used for calibration and validation are shown as blue and yellow dots, respectively, on the left image.

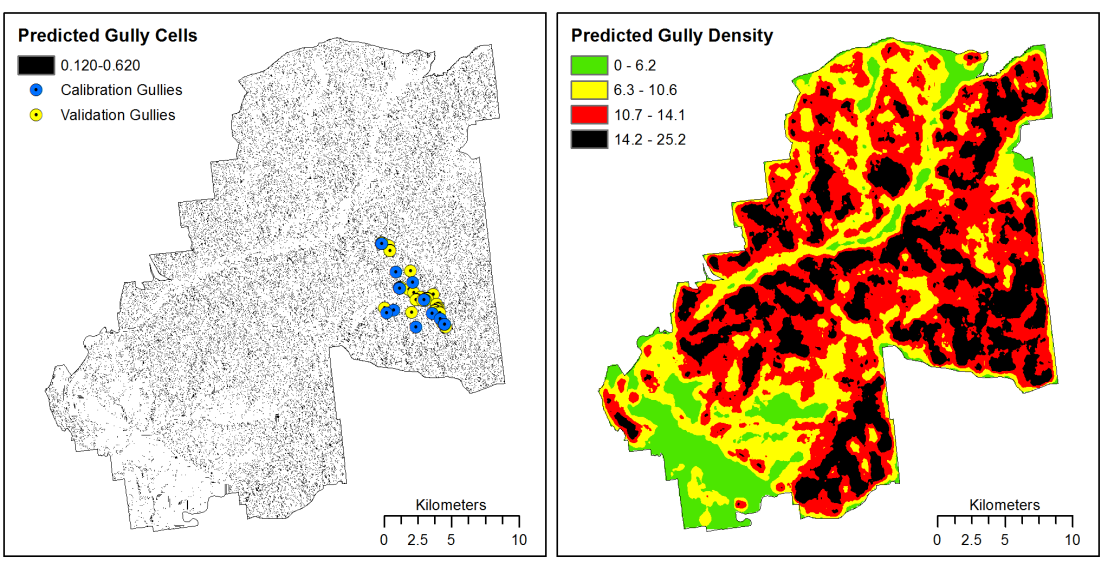

Figure 43. Predicted gully locations (left) and gully density surface (right) representing number of predicted gullies per square kilometer for Fort Hood, Texas based on a natural breaks classification and NED DEM model input. Gully locations used for calibration and validation are shown as blue and yellow dots, respectively, on the left image.

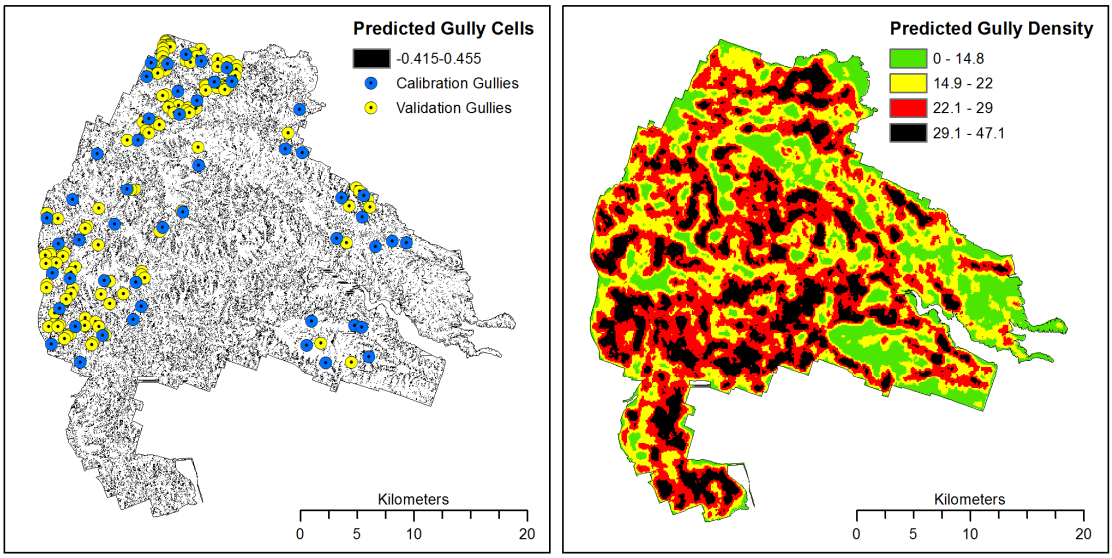

Figure 44. Predicted gully locations (left) and gully density surface (right) representing number of predicted gullies per square kilometer for Fort Hood, Texas based on a natural breaks classification and LIDAR DEM model input. Gully locations used for calibration and validation are shown as blue and yellow dots, respectively, on the left image.

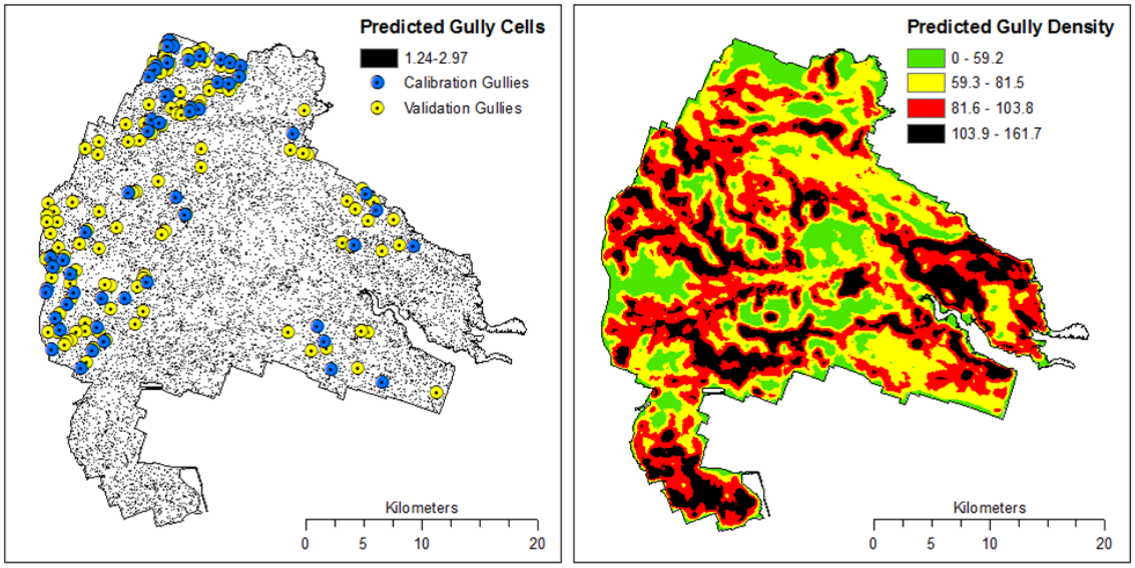

A spatial join between installation validation gully datasets and erosive flow lines generated from the predicted cells was performed and used to determine the distance between each validation gully and the nearest predicted gully location. Predictions were considered correct if they were within a distance equivalent to a maximum of one DEM cell width from the predicted location. In this analysis, the spatial resolution of each installation DEM was 10 and 3 meters, respectively, when using the NED or LIDAR as the elevation source.

When considering all installations and only model runs using NED DEM inputs, 131 of 222 total validation gullies (59%) were predicted within 10 meters of their correct location (Figure 45). This percentage correct value increases to 79% and 89% for distances within 20 and 30 m, respectively. Mean distance to correct location ranged from a low of 4.93 m at Keamuku Parcel to a high of 18.46 m at Fort Hood. Percentage correct predictions (<= 10 m) for individual installations ranged from a high of 85% for Keamuku Parcel and a low of 50% for Fort Benning (Table 16). The total range in distances varied from a low of 20 m at Keamuku Parcel to a high of 95.52 m at Fort Hood. Predictions for only one installation, Keamuku Parcel, met the success criteria of having more than 80% of gully locations correctly identified using installation-specific accumulated *nLS+* thresholds within the required distance precision. If the precision condition is loosened to a distance window of 2 times DEM cell resolution, model success is also achieved at Fort Benning and Kahuku Range. All installations reached the minimum 80% prediction accuracy level at 3 times DEM cell resolution.

Figure 45. Bar plot of distances between predicted and validation gully locations for all installations (n = 222). Predictions within a distance of 10 m or less were considered correct when using 10 m DEMs as model input.

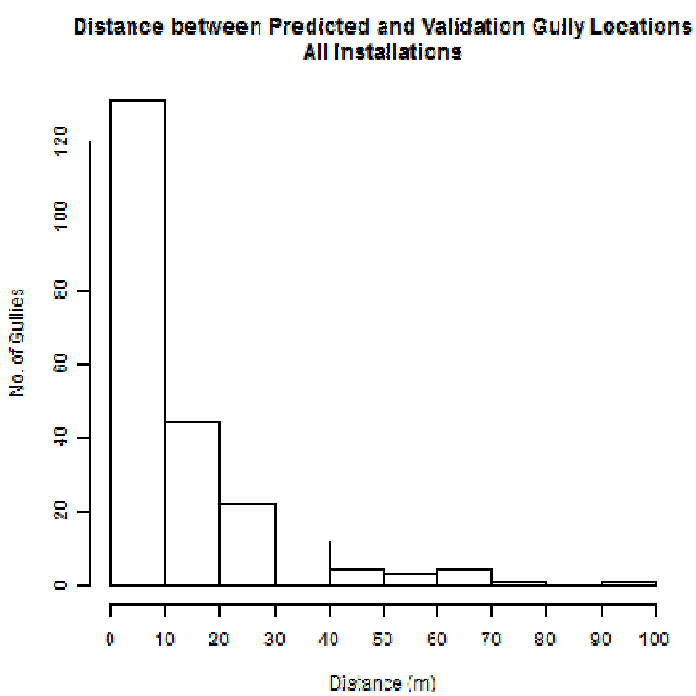

Table 16. Distance (in meters) summary statistics and prediction accuracy for *nLS+* model results at each installation using validation gully datasets and NED DEM inputs.

Installation	**Distance Summary Statistics (m)**					***Correct Predictions – No. (%)**			
	Min	*Mean*	*SD*	*Max*	*Range*	*<=10m*	*<=20m*	*<=30m*	*<=40m*
Fort Benning	0	11.79	10.58	45.89	45.89	17 (50%)	30 (**88%**)	32 (94%)	33 (97%)
Fort Hood	0	14.73	18.46	95.52	95.52	68 (59%)	86 (74%)	99 (**85%**)	106 (91%)
Fort Riley	0	13.25	15.19	51.48	51.48	17 (59%)	19 (66%)	24 (**83%**)	28 (97%)
Kahuku Range	0	10.65	11.46	45.28	45.28	12 (52%)	20 (**86%**)	22 (96%)	23 (100%)
Keamuku Parcel	0	4.93	5.68	20.00	20.00	17 (**85%**)	20 (100%)	20 (100%)	20 (100%)
All Installations						131 (59%)	175 (79%)	197 (**89%**)	210 (95%)
* Numbers and percentages are cumulative by distance.									

The total hectares of land identified as potential gully erosion sites ranged from a low of 496 (Kahuku Range) to a high of 17,051 (Fort Hood), with the total installation area susceptible to predicted gully erosion falling between 2% (Fort Hood) and 21% (Keamuku Parcel) (Table 17). The predicted cell output from the *nLS+* model, along with the related gully density surface, can be used as a tool to focus field surveys for gully monitoring, reducing the need to conduct detailed fieldwork for extensive portions of an installation. This same information may also be used in planning military exercises to limit, where possible, training in gully-prone areas and to promote solider safety by showing where gully hazards are mostly likely to be encountered.

Table 17. Comparison of predicted gully to total installation areas based on model runs using NED DEM inputs.

Installation	Total No. Cells (Ha)	Predicted No. Cells (Ha)	Predicted Gully Area (% of Total Installation)	#Reduction in Monitoring Area (ha)
Fort Benning	7,360,670 (73,608)	715,289 (7,153)	10%	66,455
Fort Hood	8,851,863 (88,519)	1,686,203 (16,862)	19%	71,657
Fort Riley	4,114,075 (41,141)	476,945 (4,769)	12%	36,372
*Kahuku Range	382,803 (3,828)	49,618 (496)	13%	3,332
*Keamuku Parcel	931,294 (9,313)	193,772 (1,938)	21%	7,375
* Values for these sites are a subset of their respective installations. # Area where gully field surveys can be minimized.				

For the three installations with available LIDAR-derived DEMs, 98 of 163 total validation gullies (60%) were predicted within 3 meters of their correct location (Figure 46). This percentage correct value increases to 75% and 82% for distances within 6 and 9 m, respectively. Mean distance to correct location ranged from a low of 1.64 m at Fort Riley to a high of just over 100 m at Keamuku Parcel. Percentage correct predictions (<= 3 m) for individual installations ranged from a high of 75% for Fort Riley and a low of 36% for Keamuku Parcel (Table 18). The total range in distances varied from a low of 10.61 m at Fort Riley to a high of over 300 m at Keamuku Parcel. No installations met the success criteria of having more than 80% of gully locations correctly identified using installation-specific accumulated *nLS+* thresholds within the required distance precision. If the precision condition is loosened to a distance of 3 times DEM cell resolution, model success is achieved at Fort Riley and Fort Hood.

Figure 46. Bar plot of distances between predicted and validation gully locations for Fort Hood, Fort Riley, and Keamuku Parcel (n = 163). Predictions within a distance of 3 m or less were considered correct when using LIDAR DEMs as model input.

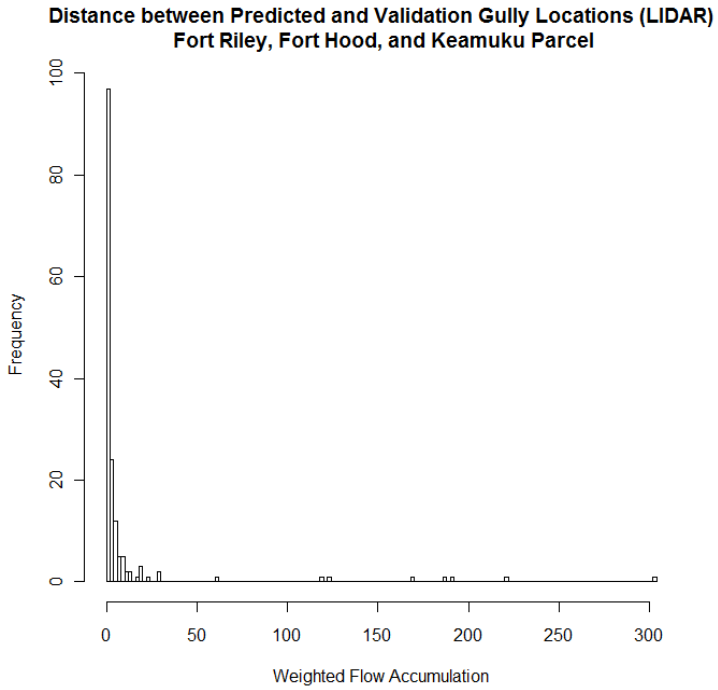

Table 18. Distance (in meters) summary statistics and prediction accuracy for *nLS+* model results at each installation using validation gully datasets and LIDAR-derived DEMs.

Installation	**Distance Summary Statistics (m)**					***Correct Predictions – No. (%)**			
	Min	*Mean*	*SD*	*Max*	*Range*	*<=3m*	*<=6m*	*<=9m*	*<=12m*
Fort Riley	0	1.64	3.13	10.61	10.61	18 (75%)	21 (**88%**)	21 (88%)	23 (100%)
Fort Hood	0	3.19	4.97	29.55	29.55	75 (60%)	97 (78%)	107 (**86%**)	112 (90%)
Keamuku Parcel (Priority 1 Area)	0	100.32	101.66	303.71	303.71	5 (36%)	5 (36%)	5 (36%)	5 (36%)
All Installations						98 (60%)	123 (76%)	133 (**82%**)	140 (86%)
* Numbers and percentages are cumulative by distance.									

The total hectares of land identified as potential gully erosion sites ranged from a low of 1 (Keamuku Parcel) to a high of 1,241 (Fort Hood), with the total installation area susceptible to predicted gully erosion ranging from approximately 1-2% (Table 19). Use of the higher spatial resolution DEMs result in substantially lower areas of predicted gully erosion as compared to similar estimates made using NED data and may prove useful in further limiting the extent of fieldwork needed for ground-based gully surveys.

Table 19. Comparison of predicted gully to total installation areas based on model runs using LIDAR-derived DEM inputs.

Installation	Total No. Cells (Ha)	Predicted No. Cells (Ha)	Predicted Gully Area (% of Total Installation)	#Reduction in Monitoring Area (ha)
Fort Riley	45,712,015 (41,141)	990,763 (892)	2%	40,249
@Fort Hood	219,720,338 (87,888)	3,103,310 (1,241)	1%	86,647
Keamuku Parcel	3,516,359 (3,165)	13,254 (12)	< 1%	3,153

@ The spatial resolution of the Fort Hood DEM was 4 m x 4 m.
* Values for this site is a subset of its respective installation.
\# Area where gully field surveys can be minimized.

Assessment of both *nLS+* model performance was also evaluated by using a contingency table, or classification error matrix (Story and Congalton 1986, Lillesand and Kiefer 1994). Error matrices compare the relationship between known and predicted data and makes explicit the magnitude and relationships between accuracy and related errors of commission and omission (Table 20). Three measures of accuracy are typically used to assess model/classification performance. Producer's accuracy is a "reference-based" accuracy computed by determining the percentage of correct predictions. Consumer, or user, accuracy is a "map-based" accuracy measure determined by comparing reference data (*e.g.*, ground truth) for a class and calculating the percentage of correct predictions. Errors of omission and commission, then, are found by subtracting from the value of 1 the producer and user accuracies, respectively, for a given class. Errors of commission occur when locations are incorrectly identified (*i.e.*, gully locations identified by the model are not actually gully locations in the field). Errors of omission occur when locations are not correctly classified (*i.e.*, gully locations in the field are not predicted by the model). Finally, total model accuracy is determined by assessing the total number of correctly identified points with respect to the total number of points assessed.

Table 20. Example classification error matrix used to further assess nLS+ model performance.

		Model Predictions					
Ground Truth Data		Gully	Non-Gully	Row Total	Producer Accuracy	Omission Error	Total Accuracy
	Gully	A	B	A+B	A/(A+B)	1 – (A/(A+B)	
	Non-Gully	C	D	C+D	D/(C+D)	1 – (D/(C+D)	
	Column Total	A+C	B+D	A+B+C+D			
	User Accuracy	A/(A+C)	D/(B+D)				
	Commission Error	1 – (A/(A+C))	1 – (D/(B+D))				(A+D)/ (A+B+C+D)

A = actual gully locations correctly identified by the model (includes gullies at 4 times the distance criterion)
B = actual gully locations incorrectly identified as non-gully locations by the model or at > 4 times the distance criterion
C = actual non-gully locations incorrectly identified as gully locations by the model
D = actual non-gully locations correctly identified as non-gully locations by the model

In classification error matrices, ground truth data consists of gully locations recorded in the field using GPS receivers or digitized from high resolution digital orthophotography using standard aerial photo interpretation techniques (Arnold 1997). Predicted gully locations are those where the *nLS+* model predicts the presence of a gully. In a GIS, the number of pixels corresponding to locations of predicted, and actual, gully locations are summed and entered into the corresponding column and row in the error matrix. Similarly, the number of cells where no actual or predicted gullies were found is also summed and their values placed in the matrix. Simple calculations are them performed to determine model accuracies and errors.

The classification error matrices for model results using NED and LIDAR DEM inputs are presented in Tables 21 and 22, respectively. For this assessment, actual gullies that were within 4 times the distance criterion established by quantitative performance objective 1 were considered correct predictions. Model accuracies, specifically producer's accuracy for both the gully and non-gully class, as well as overall accuracy for predictions using both DEM types were very high. The principle issue with model results is in the significant overprediction of gully locations, resulting in commission errors for the gully class of 100% (rounding).

Table 21. Classification error matrix consisting of data from all installations and based on results from nLS+ model runs using NED DEM inputs.

	Model Predictions						
Ground Truth Data		Gully	Non-Gully	Row Total	Producer Accuracy	Omission Error	Total Accuracy
	Gully	210	12	222	95%	5%	
	Non-Gully	3,121,617	18,518,866	21,640,483	86%	14%	
	Column Total	3,121,827	18,518,878	21,640,705			
	User Accuracy	0%	100%				
	Commission Error	100%	0%				86%

Table 22. Classification error matrix consisting of data from Fort Riley, Fort Hood, and Keamuku Parcel and based on results from nLS+ model runs using LIDAR DEM inputs.

	Model Predictions						
Ground Truth Data		Gully	Non-Gully	Row Total	Producer Accuracy	Omission Error	Total Accuracy
	Gully	140	22	162	86%	14%	
	Non-Gully	4,107,187	264,841,363	268,948,550	98%	2%	
	Column Total	4,107,327	264,841,385	268,948,712			
	User Accuracy	0%	100%				
	Commission Error	100%	0%				98%

6.2 OBJECTIVE #2: DETERMINE WHETHER A SINGLE CRITICAL THRESHOLD FOR ACCUMULATED *nLS+* VALUES IS ADEQUATE FOR ALL STUDY INSTALLATIONS

The second performance objective seeks to determine whether a single critical threshold for accumulated *nLS+* values is adequate for all study installations. Thresholds for each installation were identified as explained in the previous section and log-transformed values of accumulated *nLS+* values for all gullies, combining the calibration and validation datasets, were used in this statistical analysis.

A one-way analysis of variance (ANOVA) test was used to compare mean differences in log-transformed accumulated *nLS+* values for gullies from each installation. One-way ANOVA tests are appropriate when there is only one independent variable (*i.e.*, the accumulated *nLS+* value) and if three key assumptions are met. First, the gully populations from which the sample locations were obtained should be normally (or near normally) distributed. In this analysis, log-transformation of the raw accumulated *nLS+* values allows the independent variable to better meet this normality requirement. For example, Table 23 lists the skewness and excess kurtosis values for the distribution of accumulated *nLS+* values at installation gully locations before and after transformation and Figure 47 shows the histogram for accumulated *nLS+* values at Kahuku Range, Hawaii before and after transformation. Both Table 23 and Figure 47 are based on data generated from *nLS+* model runs using NED DEM inputs, but results from model output using LIDAR DEM as input were similar.

Table 23. Measures of the shape of the distributions of accumulated nLS+ values at gully locations for study area military installations based on model runs using NED DEM inputs.

Installation	Accumulated *nLS+* Values (Original)		Accumulated *nLS+* Values (Log Transformed)	
	Skewness#	Kurtosis@	Skewness#	Kurtosis@
Fort Benning	1.16	0.38	-0.93	1.08
Fort Hood	2.68	8.41	-0.24	-0.74
Fort Riley	2.29	5.08	-0.13	-0.12
Kahuku Range	2.69	8.90	-0.11	-0.46
Keamuku Parcel	2.49	6.99	0.62	-0.22
FRK_L	4.22	22.96	-0.14	0.60
FHT_L	4.98	32.57	-0.46	-0.41
PTA_L	1.76	3.76	0.42	-0.10

Skewness for a perfectly normal distribution equals 0.
@ The kurtosis value shown here is "excess kurtosis" where, for a perfectly normal distribution, the kurtosis value equals 0 rather than 3.

Figure 47. Histograms showing the distribution of accumulated nLS+ values for gully locations at Kahuku Range, Hawaii before (left) and after (right) log-transformation needed to meet the normality assumption of the one-way ANOVA test. Data are based on model runs using NED DEM inputs.

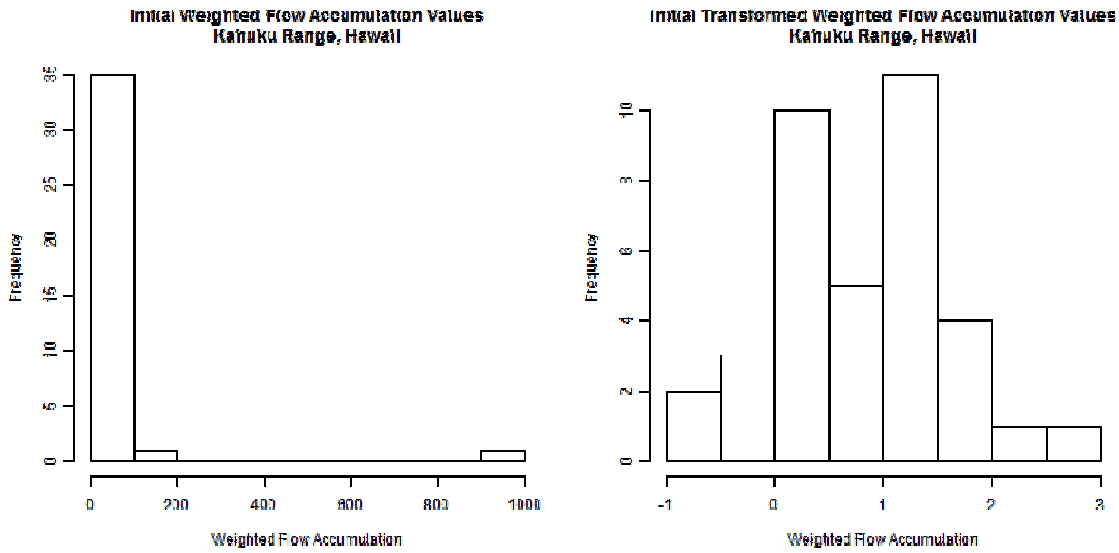

The second consideration is sample independence. This assumption is met because gully sample members from each installation are unrelated to one another. In other words, selection of an actual gully location at one installation, for example Fort Benning, did not result in the selection of another specific gully present at the Keamuku Parcel (Pohakuloa Training Area).

Last, the variance associated with accumulated *nLS+* values for the gully "populations" must equal. Bartlett's test for homogeneity of variance (Snedecor and Cochran 1983) was used to assess this assumption for the log-transformed accumulated *nLS+* values based on data from model runs using both NED and LIDAR DEM inputs. Tested was the null hypothesis that sample variances were equal. For NED-derived output, the computed test statistic, Bartlett's K-squared, was 8.25 (df = 4, p-value = 0.08). If the *p*-value was greater than the chosen significance level, the null hypothesis cannot be rejected. Here, the p-value was greater than α = 0.05. Given this result, the conclusion was that installations have equal variances associated with log-transformed accumulated *nLS+* values. For LIDAR-derived output, the computed Bartlett's K-squared statistic was 33.91 (df = 2, p-value << 0.01). Since the p-value was less than α = 0.05, the null hypothesis that the variance of installation log-transformed accumulated *nLS+* values are equal is rejected.

The Bartlett test, however, is sensitive to departures from normality and, despite transformation, the installation accumulated *nLS+* values derived from both NED and LIDAR DEM data do not have perfectly normal distributions. The Levene test is an alternative to the Bartlett test that is less sensitive to departures from normality. As with the Bartlett test, the null hypothesis being tested was that sample variances were equal. A modified robust Brown-Forsythe Levene-type test (Brown and Forsythe 1974), or Levene test, based on the absolute deviations from median installation *nLS+* values from NED DEM model runs yielded a test statistic of 2.31 (p-value =

0.06). Since the resulting p-value is greater than $\alpha = 0.05$, the Levene test confirmed that the variance associated with installation accumulated *nLS+* values was equal. For *nLS+* values calculated from LIDAR DEM calculations, the Levene test statistic was 13.12 (p-value << 0.01), rejecting the null hypothesis. In this instance, the variance of LIDAR-derived installation accumulated *nLS+* values were not equal.

After confirming that all assumptions had been met for NED-derived accumulated *nLS+* values, a one-way analysis of variance (ANOVA) test was used to compare mean differences in accumulated *nLS+* values from gully locations across each installation. A one-way layout consists of a single factor (log-transformed accumulated *nLS+* values) with several groups (installations) and multiple observations (gullies) at each group. By comparing the within-group variances to the between-group variance, a one-way ANOVA helps to determine whether accumulated *nLS+* values for gullies at each installation were significantly different. The null hypothesis tested was that the mean accumulated *nLS+* value at each installation was the same. The resulting F test statistic equaled 12.85 (numerator df = 4, denominator df = 91.60, *p*-value << 0.001) which allowed rejection of the null hypothesis that installation mean accumulated and log-transformed *nLS+* values were equal.

Since the decision was to reject the null hypothesis, at least one of the installation means was different from the others. However, the ANOVA does not indicate for which installation(s) a significant difference exists. A Tukey's Honestly Significant Difference (HSD) test was performed to examine all possible pairwise differences between installation means to help identify which installation(s) contributed most to the ANOVA result. The Tukey HSD test is based on the studentized range distribution of group (installation) means and assigns each group an upper and lower mean value limit according to a confidence coefficient (Table 24). Based on a 95% confidence level, a total of 4 out of 10 possible pairwise comparisons (40%) show significant differences in the studentized means. The visual comparison in Figure 48 helps illustrate this further where, if intervals for pairwise installation comparisons do not contain the zero value, then a significant difference in means exists.

Table 24. Results from the post-hoc Tukey HSD test based on data from NED DEM model runs. Installations in bold have significant differences in mean accumulated nLS+ values based on a 95% confidence coefficient.

Installation Pairs	Difference in Means	Lower Limit	Upper Limit	p-Value (Adjusted)
FHT-FBG	-0.24250561	-0.62664950	0.1416383	0.4157654
FRK-FBG	0.46071399	-0.03776190	0.9591899	0.0854122
KAH-FBG	0.41199004	-0.11807191	0.9420520	0.2089164
KEA-FBG	**0.75092499**	**0.20538353**	**1.2964665**	**0.0017699**
FRK-FHT	**0.70321960**	**0.29442900**	**0.29442900**	**0.0000350**
KAH-FHT	**0.65449565**	**0.20773261**	**1.1012587**	**0.0006942**
KEA-FHT	**0.99343060**	**0.52840692**	**1.4584543**	**0.0000001**
KAH-FRK	-0.04872396	-0.59691088	0.4994630	0.9992158
KEA-FRK	0.29021100	-0.27295747	0.8533795	0.6191600
KEA-KAH	0.33893496	-0.25237390	0.9302438	0.5160636

FHT = Fort Hood; FBG = Fort Benning; KAH = Kahuku Range (Schofield Barracks); KEA = Keamuku Range (Pohakuloa Training Area); FRK = Fort Riley

Figure 48. Graphical results from the post-hoc Tukey HSD test based on data presented in Table 17. Intervals that do not contain a zero value (dashed vertical line) indicate a significant difference exists between installation mean accumulated nLS+ values.

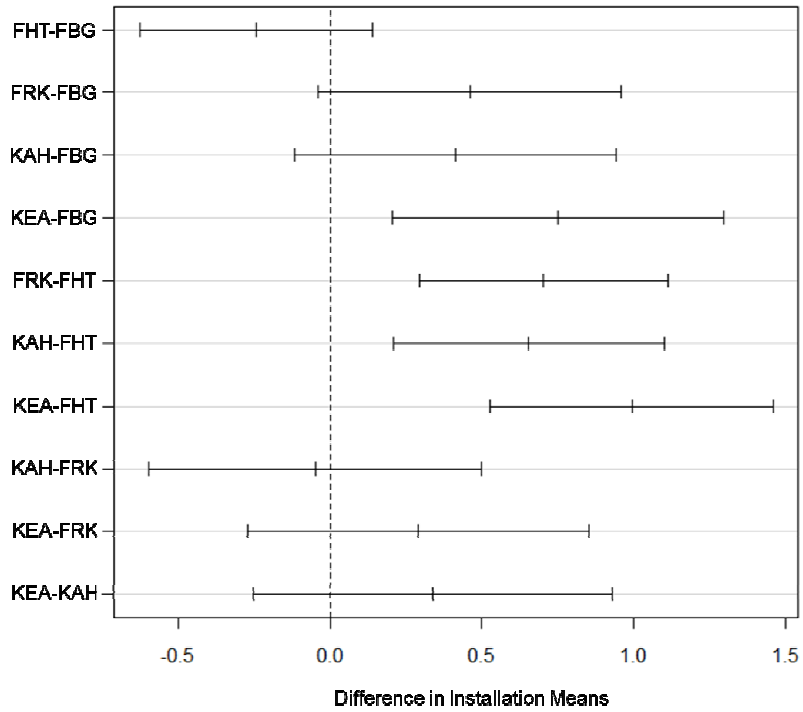

Defining a single critical threshold for log-transformed accumulated *nLS+* values was not appropriate given the installations studied and using NED DEM inputs. Values calculated for two installations – Fort Hood and Keamuku Parcel – contributed most to this difference. While Fort Hood was significantly different in all pairwise comparisons except for Fort Benning, Keamuku Parcel differed from all but Kahuku Range and Fort Riley.

Since previous results from the Levene test for LIDAR-based accumulated *nLS+* values confirmed unequal variances, an ANOVA was not the appropriate test to compare mean difference in accumulated *nLS+* values. The non-parametric Kruskal-Wallis one-way ANOVA test, however, is an alternative to the parametric ANOVA for non-normal distributions or in situations where variance is unequal and tests the equality of median, rather than mean, population values. A one-way ANOVA is then applied to the ranked data rather than the original measures.

A box plot of LIDAR-derived and log-transformed accumulated *nLS+* values (Figure 49) suggested that the installation medians were not similar. This was confirmed by the Kruskal-Wallis chi-squared test statistic = 89.67 (df = 2, p-value << 0.01). The null hypothesis here was that log-transformed accumulated *nLS+* values came from the same data distribution. Since the p-value was much less than 0.01, we rejected the null hypothesis and concluded that installation

values were significantly different (non-identical populations where the same critical threshold would not be accurate). As was the result with NED-derived *nLS+ values, d*efining a single critical threshold for log-transformed accumulated *nLS+* values was not appropriate for the installations studied and using LIDAR DEM inputs.

Figure 49. Box plot of installation median log-transformed accumulated nLS+ values based on data from models runs using LIDAR DEM inputs.

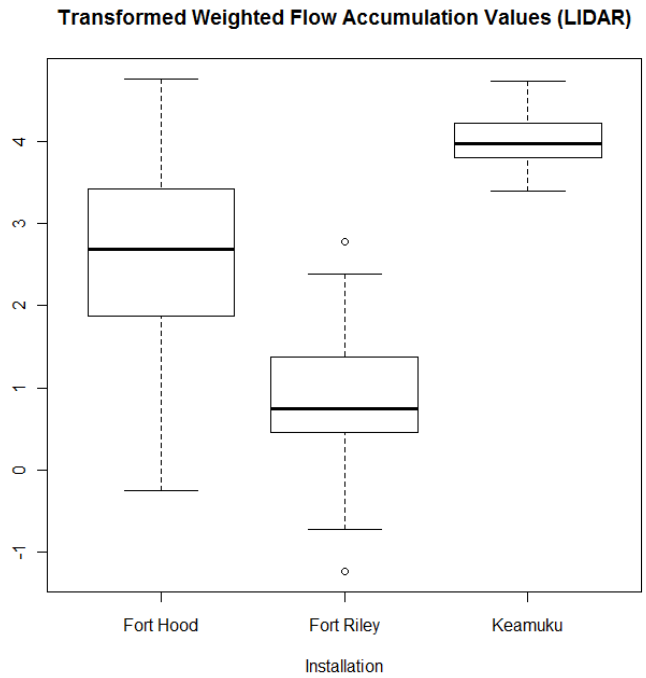

6.3 OBJECTIVE #3: FORECAST AREAS WHERE GULLIES ARE LIKELY TO FORM IN RESPONSE TO FUTURE MILITARY TRAINING EVENTS AT FORT RILEY AND POHAKULOA TRAINING AREA (KEAMUKU PARCEL)

Data analysis in support of the third performance objective is broken down into information concerning rut depth and impact severity scores, GIS processing, and modeling results.

6.3.1 Computing Rut Depth and Impact Severity Scores

The third, and final, quantitative performance objective used the *nLS+* model to predict where gullies were likely to form in response to a military training event. For this objective, the location of vehicle tracks was used to modify the original installation DEM and LULC layers (and associated Manning's *n* coefficient) based on information regarding the velocity of a traveling military vehicle, the radius of track curves, and estimated soil moisture conditions (*e.g.*, wet vs. dry). Past research by investigators from the University of Tennessee and the

Engineering Research and Development Laboratory – Construction Engineering Research Laboratory (ERDC-CERL) that quantified vehicle track impacts in terms of rut depth and vegetation damage was used to modify the original DEM and LULC datasets. Though actual vehicle track widths will almost always be less than the spatial resolution of DEM and LULC datasets used as model input, vehicle-induced changes to the landscape were applied to any pixel through which a track passed, regardless of that pixel's dimension. Because the erosion potential model, and its resulting gully predictions, are based on a raster, or grid, format, it is not necessary to account for sub-pixel impacts or processes. All that is necessary to know is (1) that a vehicle passed through a cell and (2) the estimated reduction in elevation (*i.e.*, rut depth) and change in surface roughness *(i.e.*, vegetation removal) caused by that passage.

Three Stryker vehicles from a reconnaissance platoon of the 2nd Brigade of the 25th Infantry Divison were tracked during an off-road proofing mission on the Keamuku parcel using GPS-based tracking systems to determine vehicle movement patterns and estimate soil loss impacts (Howard *et al.* 2011). Track data recorded by GPS units onboard the three Stryker vehicles were obtain from Dr. Paul Ayers (pers. comm.). The data was received as a text file with geographic coordinate information acquired at approximately one second intervals. Each GPS record also included key attributes such as vehicle velocity (VEL) and course over ground (COG) along with a detailed date/time stamp identifying when the position record was acquired.

Rut depth was calculated as a function of vehicle turning radius. Liu *et al.*, (2009) described the relationship between the inside and outside tracks for a Light Armored Vehicle (LAV) operating in a spiral test pattern at two speed (4 and 8 meters per second) during experimental maneuvers at Fort Lewis, Washington in 2002 (Figure 50).

Figure 50. Relationship between rut depth and LAV turning radius (from Liu et al., 2009).

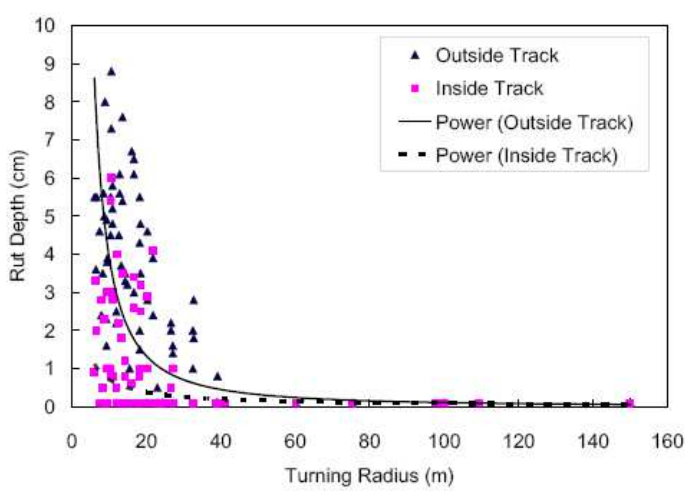

Based on these findings, a generic power function was defined to estimate vehicle rut depth using the curve for the outside track that generates the deeper rut:

$RD = 67.571 * TR^{-1.278}$

where:
RD = rutting depth (cm) for wet soil conditions
TR = vehicle turning radius (m)

To obtain rut depth predictions, estimates of vehicle turning radius at each location were calculated from five consecutive position fixes using the five-point method outlined in ERDC/CERL Technical Report 00-43 (Ayers et al., 2000) (Figure 51). All calculations related to the five-point method were executed with the use of a Python script with results appended to the original vehicle track file along with the derived rut depth values for both wet and dry conditions.

Figure 51. Turning radius measurement points following the five-point method (adapted from Ayers et al., 2000).

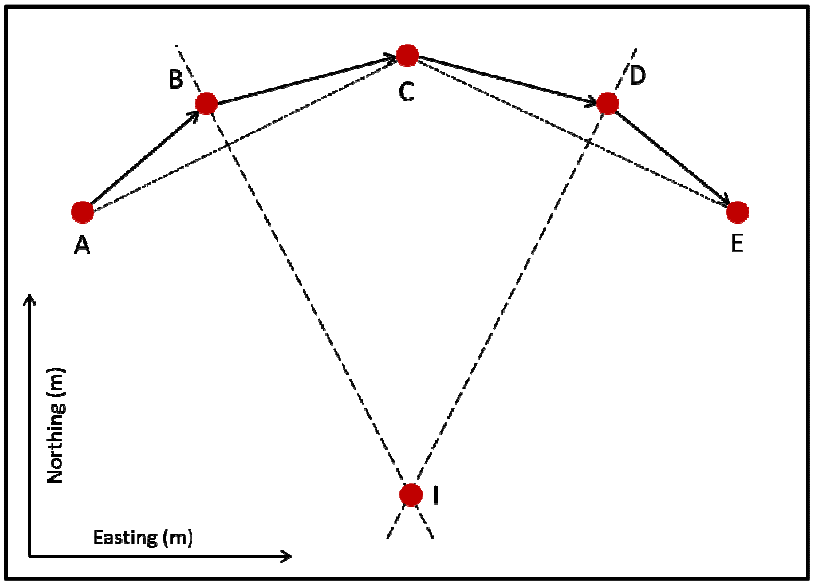

First, the slope of lines from the first (A) to third (C) and third (C) to fifth (E) locations were calculated from their respective coordinate points:

$m_{A\text{-}C} = (C_N - A_N) / (C_E - A_E)$
$m_{C\text{-}E} = (E_N - C_N) / (E_E - C_E)$

where:
X_N = value of northing coordinate (latitude) for point X
X_E = value of easting coordinate (longitude) for point X

Next, the slope of the perpendicular bisects to line A-C at position B and line C-E at position D were computed:

$m_{B\text{-}I} = -1 / m_{A\text{-}C}$
$m_{D\text{-}I} = -1 / m_{C\text{-}E}$

where:
$m_{A\text{-}C}$ = slope of line from first (A) to third (C) vehicle positions
$m_{C\text{-}E}$ = slope of line from third (C) to fifth (E) vehicle positions

From this, the intercepts of these perpendicular bisects were found by:

$b_{B\text{-}I} = B_N - m_{B\text{-}I} * B_E$
$b_{D\text{-}I} = D_N - m_{D\text{-}I} * D_E$

where:
X_N = value of northing coordinate (latitude) for point X
X_E = value of easting coordinate (longitude) for point X
$m_{B\text{-}I}$ = slope of the perpendicular bisect to line A-C
$m_{D\text{-}I}$ = slope of the perpendicular bisect to line C-E

Next, the intersection of these perpendicular bisects were found by solving two equations with two unknowns:

$I_N = \mathrm{m_{B\text{-}I}} * \mathrm{I_E} + \mathrm{b_{B\text{-}I}}$
$I_N = \mathrm{m_{D\text{-}I}} * \mathrm{I_E} + \mathrm{b_{D\text{-}I}}$

where:
$m_{B\text{-}I}$ = slope of the perpendicular bisect to line A-C
$m_{D\text{-}I}$ = slope of the perpendicular bisect to line C-E
$b_{B\text{-}I}$ = intercept of the perpendicular bisect to line A-C
$b_{D\text{-}I}$ = intercept of the perpendicular bisect to line C-E

Last, the distance from point C to intersection I was calculated. This distance was equivalent to the vehicle turning radius at point C:

$$TR = ((I_N - C_N)^2 + (I_E - C_E)^2)^{0.5}$$

where:
TR = vehicle turning radius (m)
I_N = value of the northing coordinate (latitude) for the intersection of the perpendicular bisects to lines A-C and C-E
I_E = value of the easting coordinate (longitude) for the intersection of the perpendicular bisects to lines A-C and C-E

To account for possible vegetation removal after the passage of a military vehicle, an impact severity (IS) score was generated to reflect the percentage of soil and vegetation damaged (or removed) (Ayers *et al.*, *2*000):

$$IS = 261(TR^{-0.75}) * VEL^{0.62}$$

where:
IS = impact severity (%)
TR = vehicle turning radius
VEL = vehicle velocity (m/s)

The range of impact severity scores and their meaning relative to soil and vegetation disturbance are summarized in Table 25. These computed impact severity scores were used to scale the original Manning's *n* surface roughness values associated with the LULC types traversed by a military vehicle by subtracting from 100% the product of values for impact severity original surface roughness. For example, a calculated turning radius value of 100 m yielded an impact severity score of 8.8 which would then be used to reduce the Manning's *n* surface roughness coefficient at that location by only 8.8%. Similarly, a turning radius of approximately 8.5 m (or less) resulted in an IS score of 100 and a transformed Manning's n value of 0. In this study, however, the minimum surface roughness condition used was 0.05, equivalent to that of "barren land". Computed IS scores were also appended to the original vehicle track file.

Table 25. Summary of impact severity scores and their corresponding meanings (Source: Li et al., 2007)

Impact Severity (%)	Description
0	No visible disturbance as compared to surrounding vegetation/area
10	Laying down of vegetation; few, if any, broken stems; no evidence of vegetation shearing
20	Some broken stalks/plants; visible soil disturbance, possibly exposing bare soil
30	Obvious depressed soil and vegetation with significant vegetative damage and slight removal; piling on track edge evident; movement of plants/soils towards the edge of vehicle track without completely shearing plant at roots; some bare soil exposed
40	About 1/3 of vegetation still present and intact on the track; significant amount of bare soil exposed; larger piling of vegetation on edge of track due to shearing motion of the vehicle, fully removing species from the track; some of the pile has overturned, exposing roots
60	Few vegetative species still intact on vehicle path; piling of vegetation and soil on the edge of the path; pile is completely overturned, exposing roots
80	Few vegetative species still intact on vehicle path; piling of vegetation and soil on the edge of the path; pile is completely overturned, exposing roots
100	Complete removal of vegetation and soil; shearing action of vehicle has left vehicle track bare; sheared vegetation and soil is piled on edge of track

6.3.2 GIS Processing

Following the impact severity, turning radius, and rut depth calculations, vehicle track files were imported into a GIS and combined into a single file of all GPS position records. These points, and their corresponding attributes were then converted into two gridded track files representing the calculated values for impact severity (IS) and rut depth (RD), respectively, at the same spatial resolution of the DEM used to describe installation terrain. During this point to raster conversion, the maximum value for IS and RD were retained if more than one GPS point would be located within the same grid cell. The IS and RD grids were then used to modify the original Manning's *n* and DEM layers for the installation using conditional statements embedded within a raster calculation to create new inputs for the *nLS+* model.

6.3.3 Modeling and Results

As reported by Howard *et al.*, (2011), most of the vehicle movement during proofing maneuvers occurred on roads (Table 26). A total of over 27 km of off-road travel was recorded with a vehicle average of 9.1 km at an average speed of 3.69 m/sec. For all of the vehicles, 1,251 m^2 of vegetation was removed per vehicle during the proofing maneuver.

Table 26. Summary data from the Stryker proofing maneuver conducted at Keamuku Parcel (Pohakuloa Training Area), Hawaii (from Howard et al., 2011).

Vehicle	**Total**		**Off-Road**		**Vegetation Removed**
	Distance (km)	*Avg Speed (m/s)*	*Distance (km)*	*Avg Speed (m/sec)*	*Area (m^2)*
PTA 08	65.27	4.86	5.90	3.33	722
PTA 17	118.30	5.00	11.85	4.00	1,642
PTA 19	117.32	5.15	9.65	3.75	1,388

A summary of the computed data for IS and RD used to modify the *nLS+* model inputs in shown in Table 27. Figure 52 illustrates the resulting IS and RD values for Stryker vehicle PTA19 for a portion of its off-road track.

Table 27. Summary of computed data for impact severity and rut depth used to modify nLS+ model inputs and predict new gully erosion areas after the Stryker proofing maneuver conducted at Keamuku Parcel (Pohakuloa Training Area), Hawaii.

Vehicle	**No. GPS Points**	**Impact Severity (IS) Score (%)**			**Rut Depth (cm)**		
		1st Quart	*Median*	*3rd Quart*	*1st Quart*	*Median*	*3rd Quart*
PTA 08	1672	10.15	22.46	53.32	0.03	0.17	0.93
PTA 17	2972	13.62	42.37	52.44	0.07	0.24	0.85
PTA 19	2518	11.42	39.86	54.22	0.04	0.17	0.70

Figure 52. Estimated impact severity (IS) and rut depth (RD) values for Stryker vehicle PTA19 for a portion of its off-road track during proofing maneuvers conducted at Keamuku Parcel (Pohakuloa Training Area), Hawaii.

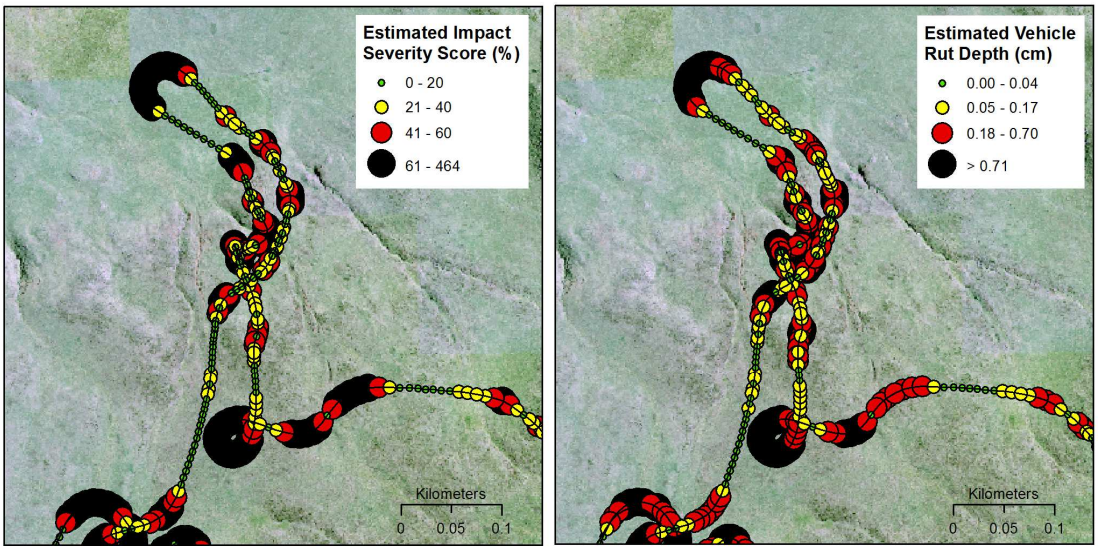

The *nLS+* model was re-run for Keamuku Parcel using the modified DEM and Manning's *n* grids to reflect post-maneuver landscape conditions. The previously computed accumulated *nLS+* threshold value for Keamuku Parcel, 0.155 to 0.965, was used again to determine if new areas of erosive potential would be generated and visible after applying estimated landscape impacts from GPS-derived vehicle tracks. This "re-analysis" of model results showed an additional 326 cells that were candidate sites for gully erosion (Figure 53). Given the 10 m spatial resolution of the Keamuku DEM used, this translates into an additional 3.26 ha of new land area that may be subject to active erosion or approximately 0.12 ha per off-road kilometer travelled by the maneuvering Strykers.

Figure 53. Predicted future gully erosion sites (left) from Stryker proofing maneuvers conducted on the Keamuku Parcel (Pohakuloa Training Area), Hawaii (right).

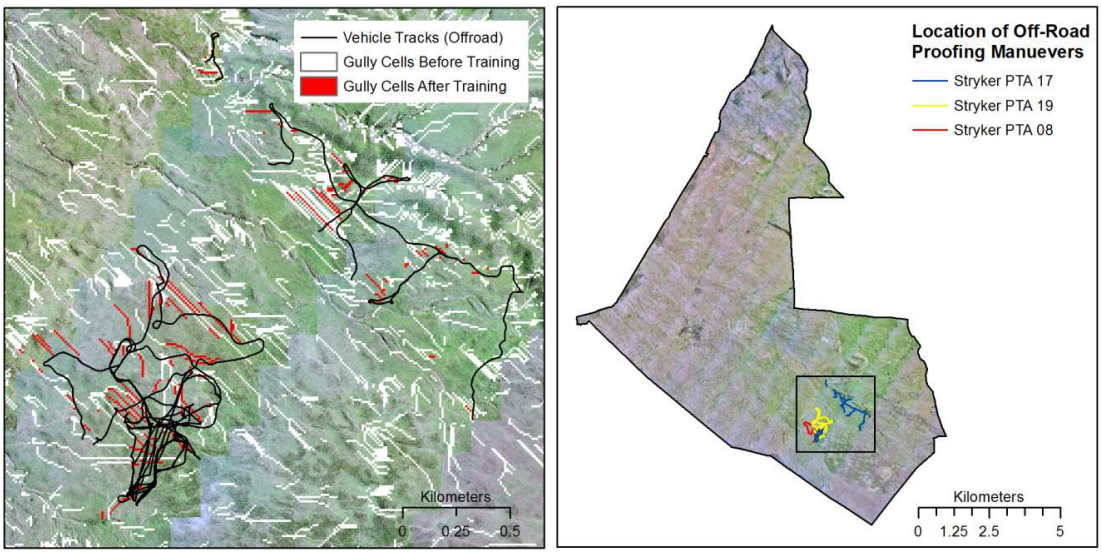

As of this report, predicted new erosion sites had not been re-visited in the field to assess erosion status. However, Howard *et al.*, (2011) noted that significant vegetation recovery and regrowth took place one month after the proofing maneuver and that over 90% of the damaged vegetation had recovered after 15 months of the initial impact. This rapid vegetation recovery rate will help limit post-maneuver erosion unless precipitation events take place soon after maneuvers.

6.4 OBJECTIVE #4: PROPOSE GEOGRAPHIC REGIONS WITHIN WHICH INSTALLATION-SPECIFIC CRITICAL THRESHOLDS FOR ACCUMULATED *nLS*+ VALUES ARE VALID

Results from Performance Objective #2 showed that a single critical threshold for accumulated *nLS*+ values was not valid for all study installations. Instead, the critical thresholds calculated in this study have location-specific significance. Because of this, the fourth performance objective sought to use of ecoregion boundaries (*e.g.*, EPA Level II/III) as a framework to make installation-specific critical thresholds more applicable off-site.

As an initial check on the feasibility of using ecoregion boundaries as a means to translate individual installation results into a spatially continuous estimate of critical *nLS*+ thresholds, general environmental conditions at each site were assessed using the Jaccard distance (J_δ), or dissimilarity index (Jaccard 1902, Jaccard 1912). The Jaccard index is commonly used to analyze ecological data recorded in binary format, often in the form of "presence/absence" data, and is defined as the quotient between the intersection and the union of the pairwise compared variables among two objects. Values range between 0-1, with large values indicating more dissimilarity and low values less dissimilarity (more similar).

Variables selected for Jaccard analysis included soil hydrologic groups, landcover types, and slope > 10% for each installation (refer to Section 4.2 Site Characteristics). These qualitative and quantitative data were recorded in a binary matrix such that a value of "1" indicated a particular soil condition, landcover type, or slope criteria was present and/or dominant and "0" if it was absent or not dominant (Table 28). Typically, soil hydrologic groups or landuse/landcover types accounting for less than 15% of the installation study area were not recorded. For this analysis, the "mixed forest", "developed", and "other" landcover classes were omitted as none were dominant for any installation.

Table 28. Binary matrix of installation soil and landuse/landcover types used to computer the Jaccard dissimilarity index.

Installation	**Soil Hydrologic Groups**				**Landuse/Landcover Types**					**Slope < 10%**
	A	*B*	*C*	*D*	*Grass*	*Deciduous Forest*	*Coniferous Forest*	*Shrub/Scrub*	*Wetland*	
Fort Hood	0	0	1	1	1	0	1	1	0	0
Fort Benning	1	0	1	0	0	1	1	0	0	0
Fort Riley	0	0	1	1	1	0	0	0	0	0
Fort Irwin	1	0	0	10	0	0	0	1	0	1
Camp Lejeune	1	0	0	0	0	0	1	0	1	0
Kahuku Range	0	1	0	1	0	0	1	1	0	1
Keamuku Parcel	1	1	0	0	1	0	0	1	0	1

Most pairwise $J_\delta$values (15 of 21) were large, indicating important differences existed in the soil, landcover/landuse, and slope conditions analyzed (Table 29). Only three installation pairs had distance values less than 0.5, including Fort Hood-Fort Riley (0.333), Fort Irwin-Kahuku Range (0.429), and Fort Irwin-Keamuku Parcel (0.429). Another three pairs had index values equal to 0.500: Fort Hood-Kahuku Range, Fort Benning-Camp Lejeune, and Kahuku Range-Keamuku Parcel.

Table 29. Values for Jaccard's distance (Jδ) for all study installations, including Fort Irwin and Camp Lejeune. Values range between 0-1, with higher values indicating more differences between sites.

	Fort Hood	Fort Benning	Fort Riley	Fort Irwin	Camp Lejeune	Kahuku Range
Fort Benning	0.625					
Fort Riley	0.333	0.714				
Fort Irwin	0.625	0.750	0.714			
Camp Lejeune	0.750	0.500	0.857	0.714		
Kahuku Range	0.500	0.778	0.750	0.429	0.750	
Keamuku Parcel	0.667	0.778	0.750	0.429	0.750	0.500

The large distance values reported by the Jaccard's test suggested that using common biogeophysical properties (*e.g.*, ecoregions) as the means to make installation critical *nLS+* values, as computed here, more spatially explicit would not be successful. As an example, environmental conditions at Fort Hood and Fort Riley were relatively similar (J_δ = 0.333), yet the means of for their respective critical *nLS+* thresholds were significantly different (see Table 14) and the mean accumulated *nLS+* values for each were significantly different (see Figure 45). However, two installations that were very dissimilar in terms of environment, such as Fort Benning and Kahuku Range (J_δ = 0.778), had more similar critical *nLS+* thresholds and mean accumulated *nLS+* values. Interestingly, Fort Benning had the same Jaccard's distance value (J_δ = 0.778) with Keamuku Parcel as Kahuku Range, but their mean accumulated *nLS+* values were dissimilar.

Given that ecoregionalization of critical *nLS+* threshold values do not hold promise at this time, two different techniques were applied to help visualize how these thresholds might be applied in a more spatially continuous manner. First, a Euclidean allocation calculation was run in a GIS that identified for each location in the lower 48 United States the nearest "source" or installation (note that EPA Ecoregions are not available for Hawaii). The allocation function generates a gridded output with unique values corresponding to a specific source that was summarized using zonal statistics with EPA Level III ecoregion boundaries (USEPA 2013) as the unique zones. Each Level III ecoregion was then assigned to an installation based on the majority value present within each boundary (Figure 54).

Figure 54. Ecoregion assignment of installation critical nLS+ thresholds based on Euclidean allocation criteria. Majority values from the initial allocation grid (left) are used to assign each ecoregion to a unique installation (right).

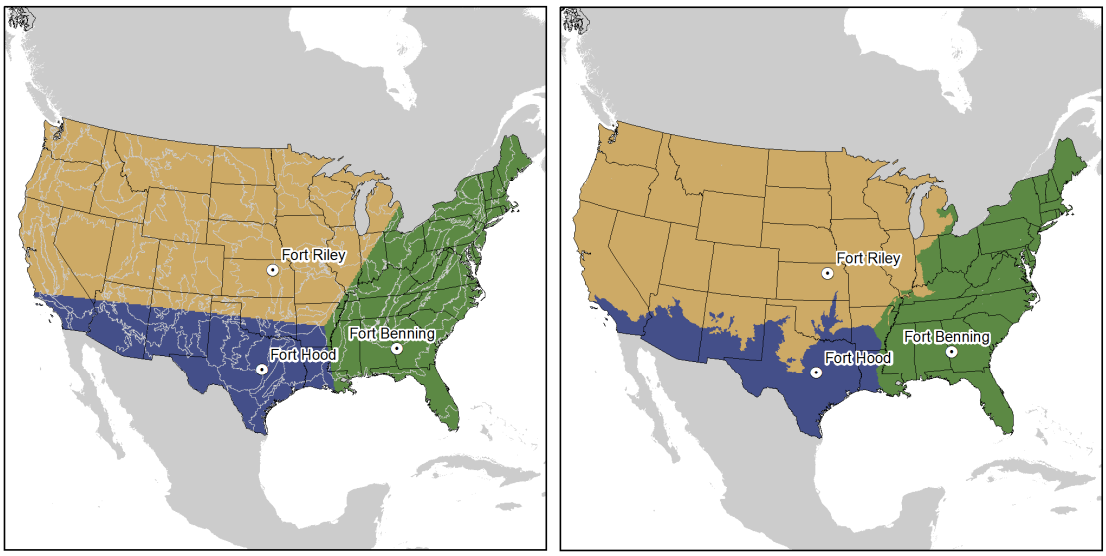

The second approach used to create a more spatially continuous view of the installation critical *nLS+* thresholds involved spatial interpolation. A thin-plate spline radial basis functions (RBF) was selected as the interpolation method (Figure 55). Though an exact interpolator, RBF's will predict values above, and below, the measured maximum and minimum values in the dataset. Though mean prediction error for this interpolation was low (0.006), the root-mean-square error was high (0.621) given the paucity of data points used in the interpolation.

Figure 55. Preliminary spatially distributed estimate of critical nLS+ threshold values based on the interpolation of installation results using a thin-plate spline radial basis function technique.

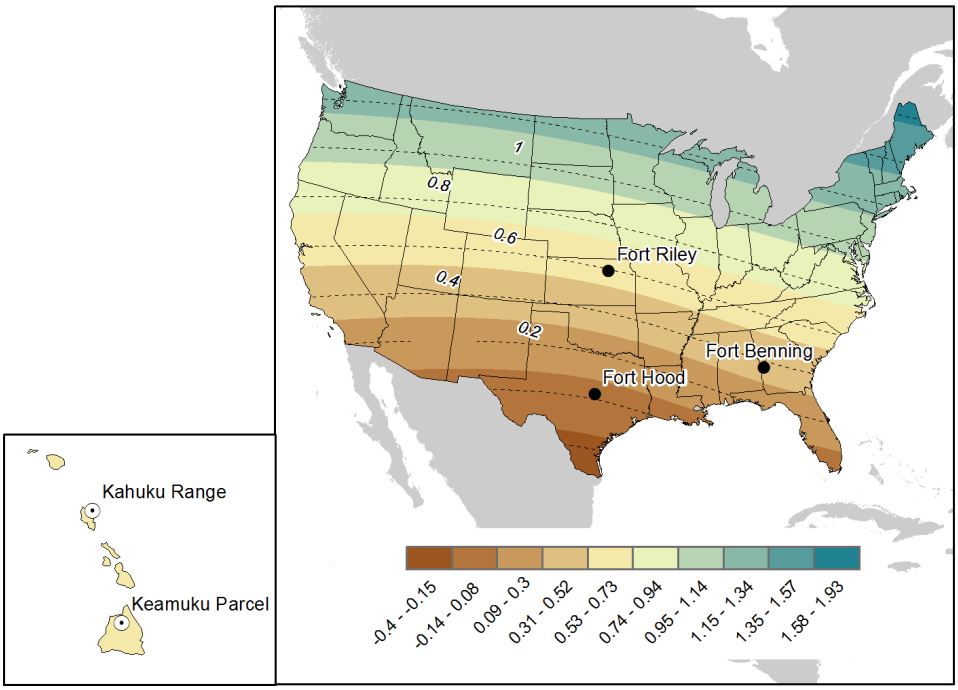

6.5 OBJECTIVE #5: DEVELOP AND DISSEMINATE A DOWNLOADABLE AND EASY-TO-USE GIS-BASED MODELING TOOL WITH DOCUMENTATION

Data analysis in support of the fifth performance objective is broken down into information concerning model design, model performance, and the web application.

6.5.1 Model Design

The *nLS+* model was developed with the ArcGIS 10.0 (Esri, Redlands, CA) suite of GIS software applications that are routinely utilized across DoD agencies and installations. Because of this, the model itself can be delivered in a variety of forms, including as an ArcToolbox "tool", a Python script, or as a ModelBuilder graphic model. For this project, the model was packaged as "toolbox" with multiple sequenced tools than can be downloaded and used on a local computer workstation running ArcGIS version 10.0 or above (Figure 56). The toolbox and associated modeling tools also included an integrated help system to explain the underlying processes, data requirements, and recommendations for default settings or values as they apply to execution of the model.

Figure 56. Screen capture image of the model toolbox and component sub-models in the ArcToolbox application of Esri's ArcGIS 10.0 GIS program.

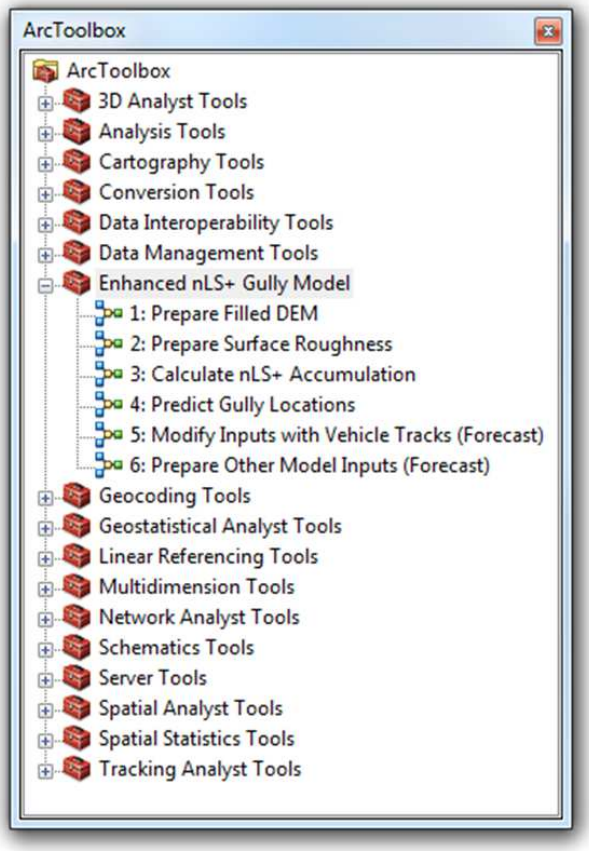

The final model – Rapid Soil Erosion Assessment Toolbox – is comprised of 6 total sub-models labeled within the toolbox by number and title. Users run the model and arrive at final results by executing each sub-model in numeric sequence from #1 (Prepare Filled DEM) to #4 (Predict Gully Locations). Sub-models #5-6 can be used to forecast future gully locations by modifying the installation DEM and Manning's *n* grid with GPS-derived vehicle tracks. The inputs, outputs, and overall function of each submodel are summarized in Table 30 and a graphic example of Sub-Model #1 is provided in Figure 57. Complete model diagrams can be found in Appendix G.

Table 30. Summary of sub-model inputs, outputs, and overall function.

Sub-Model No.	Function	User Inputs	Final Outputs
1: Prepare Filled DEM	Prepare DEM and DEM-derived grids for Sub-Model 3.	DEM; Installation Boundary File	Flow Accumulation Grid; Flow Direction Grid; Slope (%) Grid; Profile Curvature Grid
2: Prepare Surface Roughness	Generate Manning's n grid from NLCD 2006 LULC data layer.	DEM (Sets Analysis Cell Size); Installation Boundary File; NLCD Landcover Grid; Lookup Table of Manning's *n* Surface Roughness Coefficients	Manning's *n* Surface Roughness Grid
3: Calculate *nLS*+ Accumulation	Compute cell-based *nLS*+ values and perform a weighted flow accumulation.	Slope (%) Grid; Flow Direction Grid; Profile Curvature Grid; Manning's *n* Grid Installation Boundary File;	Accumulated *nLS*+ Value Grid; Log-transformed Accumulated *nLS*+ Value Grid
4: Predict Gully Locations	Uses installation critical thresholds for accumulated *nLS*+ values to identify areas of gully erosion.	Log-transformed Accumulated *nLS*+ Value Grid; *nLS*+ Threshold Values; Flow Direction Grid; Installation Boundary File	Gully Erosion Lines; Gully Density Grid
5: Modify Inputs with Vehicle Tracks (Forecast)	Generate modified DEM and Manning's n grid based on vehicle tracks.	Input Vehicle Track GPS Points; Original Filled DEM; Original Manning's n Grid Snap Grid	Modified DEM; Modified Manning's n Grid
6: Prepared Other Model Inputs (Forecast)	Calculate new inputs for Sub-Model #3 with the track-modified DEM.	Modified DEM; Installation Boundary	Flow Accumulation Grid; Flow Direction Grid; Slope (%) Grid; Profile Curvature Grid

Figure 57. Diagram of Sub-Model #1: Prepare Filled DEM. Model inputs are shown in blue and final outputs in green with the superscripts "P".

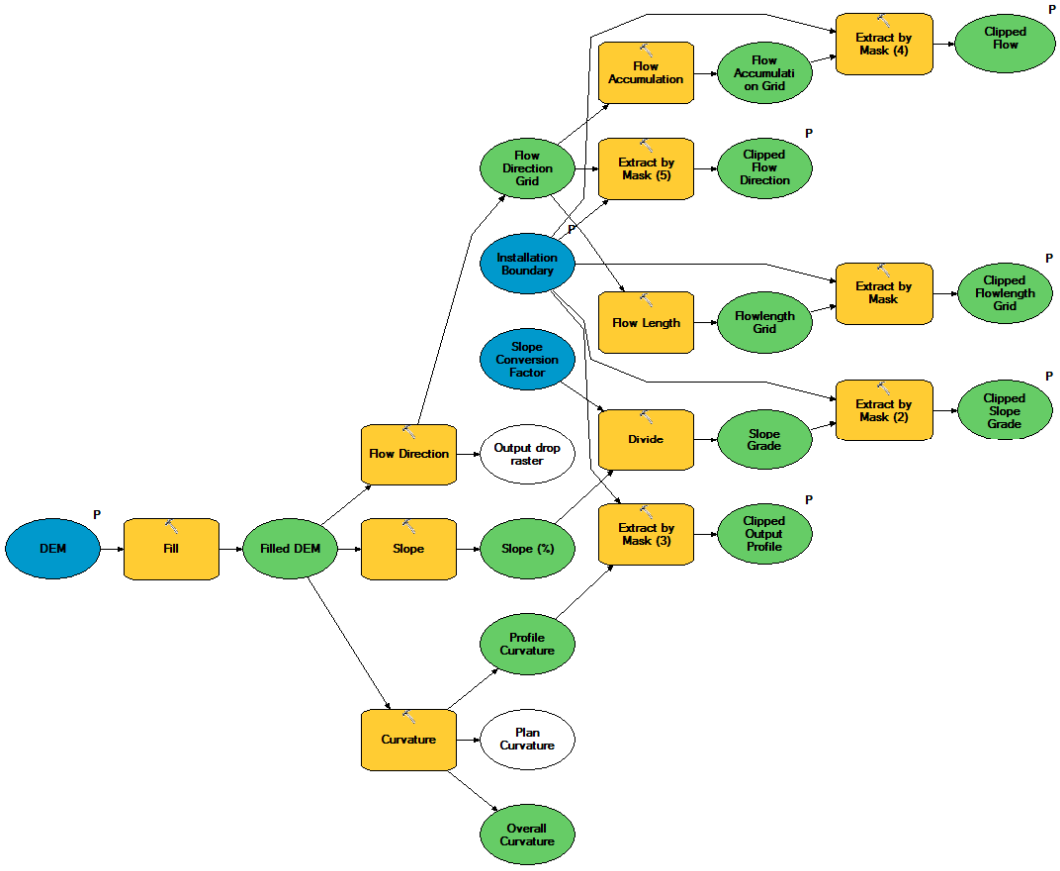

Feedback from installation ITAM GIS technicians helped shape the final form of the modeling tool as a sequence of smaller and quicker performing sub-models rather than one large model. Comments and questions generated during site visits were also invaluable in creating of the integrated help system to guide users through the geoprocessing procedures.

6.5.1 Model Performance

Model performance testing was conducted using an Alienware Area 51 M15X desktop workstation computer based on an Intel® Core™ 2 Quad Core CPU running at 2.66 GHz with 4 GB of RAM and using the Windows 7 Profession (64-bit) operating system.

Run time for the model, including all sub-models and assuming a non-LIDAR DEM and satellite resolution landuse/landcover grid for the installation was already on hand, averaged 8.3 minutes, with a high of 22.4 minutes for Fort Hood (largest installation by area) and a low of 1.1 minutes for Kahuku Range (smallest by area) (Figure 58).

Figure 58. Cumulative model execution time based on complete model runs for all study installations.

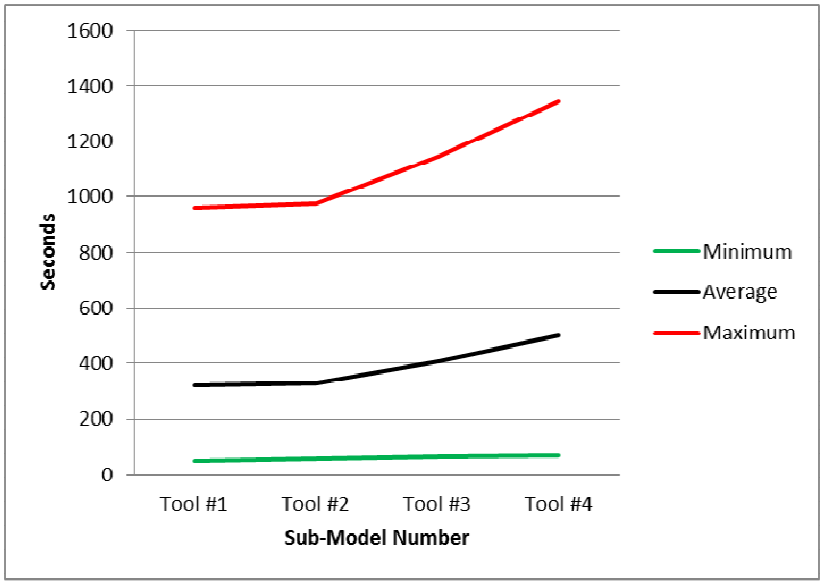

The first sub-model (Tool #1 Prepare Filled DEM) took the longest time to complete with an average execution time of 5.3 minutes and was the only sub-model to require in excess of 2 minutes to complete processing (Figure 59). On a per unit area basis, complete model execution required approximately 0.0005 sec/ha of land using gridded data at a 10 m spatial resolution.

Figure 59. Average sub-model execution times with standard deviation bars.

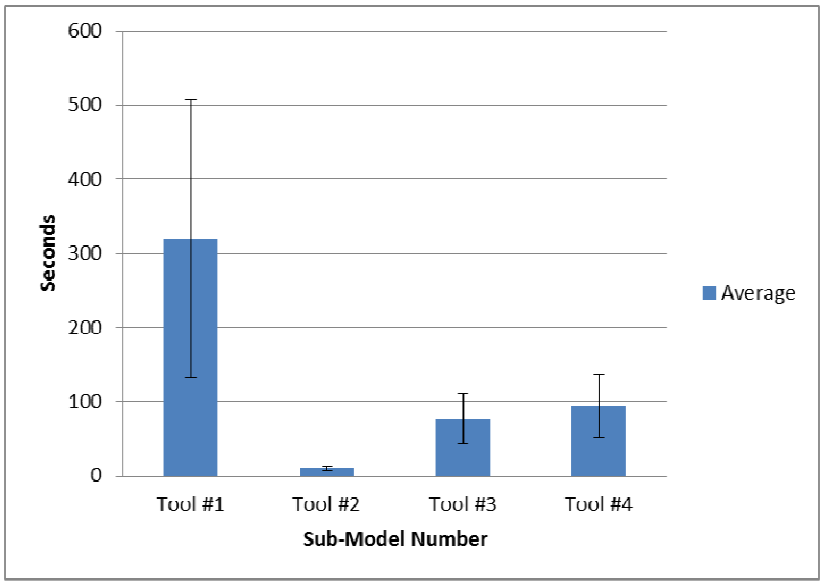

6.5.2 Model Geoprocessing Web Application

Current Esri and open-source GIS technology supports development and deployment of GIS web services and GIS server applications that minimizes and, in some cases eliminates, the need for users/installations to operate proprietary software as long as Internet access is available. Central management of modeling tools benefits end users by rendering much of the analytical complexity transparent while ensuring they adhere to best practices and techniques defined by GIS professionals. To demonstrate some of these benefits, a limited ArcGIS Server application was developed that delivers *nLS+* geoprocessing for a single installation (Fort Riley) to users over a network via the following URL: http://services.geog.ksu.edu/ESCTP. This application will be maintained at this URL for approximately one year following the conclusion of this project.

This prototype delivery method facilitates the technology transfer process by simplifying model use, facilitating access to required input datasets, and eliminating the need to physically distribute executable files and updates. This approach also offers the potential for greater efficiency as models and data developed once can be used by the entire organization. Alternatively, end users can utilize Web services based on ArcGIS Server on their own desktop systems and infuse their own data or supplement new applications with existing models and data. By delivering an effective and user friendly GIS server application in this project, the potential for using server applications as an integrative analysis platform with other biological, hydrological, and engineering models within the DoD enterprise is demonstrated.

7.0 COST ASSESSMENT

This section provides cost information for implementation of the model at a site.

7.1 COST MODEL

No significant cost element is introduced with implementation and operation of the *nLS+* model (Table 31). The requisite software is already available to all DoD agencies through a separate software site license agreement. The model will also operate with nationally-available, and free, input data. However, model results may be superior if using higher spatial resolution DEM and LULC inputs. Time to operate the model is minimal, though installation ITAM personnel should dedicate some time to field assessment and refinement of critical threshold values. Finally, the GIS model tool, itself, may require revision to operate within future updates to the current GIS software version.

Table 31. Cost model for Enhance nLS+ model.

Cost Element	Data Tracked during Demonstration	Estimated Costs
GIS Software Acqusition	No unique data tracked	Covered by DoD License Agreement with Esri
Model Data Acquisition	No unique data tracked	Nothing – nationally available and free datasets
Operation Costs	• Time to operate model • Computer specifications	< 2 man-hours
Model Operation	• Refine model critical thresholds to improve site performance.	160 man-hours dedicated to field assessment and model updates.
Model Maintenance	• Update/Revise model to reflect new GIS software versions	10 man-hours

7.2 COST DRIVERS

The U.S. Army Integrated Training Area Management (ITAM) program is charged with managing its training lands to achieve the objectives outlined in Army Regulations 250-4 and 350-19. ITAM, itself, is composed of four sub-programs, including Range and Training Land Assessment (RTLA), Land Rehabilitation and Maintenance (LRAM), Sustainable Range Awareness (SRA), and Training Requirements Integration (TRI). Each of these sub-programs fills specific roles in ensuring military commanders have suitable training lands at their disposal. A key term used in these guiding regulations is “sustainable use” which helps installation ITAM offices develop an overall philosophy for training land management, as well as identifying specific methods and approaches for conduct of the RTLA, LRAM, SRA, and TRI elements.

Over the last several years the DoD has significantly reduced funding for the ITAM program and is considering eliminating the RTLA program, responsible for monitoring natural resources within training lands and identifying when, and where, problems might prevent their use by

military units, due to a perceived lack of value. This is largely due to the lack of guidance on how to balance the often conflicting demands of current training needs and land management for a sustainable future as well as the limited automated and/or low-cost monitoring tools in place to support training land assessments that facilitate proactive land rehabilitation efforts. Current monitoring practices in place to assist military commanders with maximizing the availability and use of training lands are essentially done on an "ad hoc" basis without the benefit of a consistent set of landscape metrics being examined or uniform methods for interpreting and reporting the results of environmental assessments. Such a decentralized approach prevents (1) consistent descriptions of the condition of military training lands at the installation and national scales and (2) the ability to implement early and proactive land rehabilitation efforts and to fund those rehabilitation and maintenance efforts in an effective and efficient manner.

By developing land assessment and management tools, such as the rapid erosion assessment tool, that can take advantage of automated data acquisition and analysis using scripts and geographic information system (GIS) models, installations can shift available land management funds toward rehabilitation and mitigation of training lands.

7.3 COST ANALYSIS AND COMPARISON

It is difficult to compare the cost of implementing the rapid erosion assessment tool with current military land management practices for identifying gully sites because the amount currently spent is typically dictated by the funding available rather than installation need. Prior to this project, all installations located gullies using extensive, on-the-ground land surveys. For installations with significant vegetation, such as the tallgrass prairie on Fort Riley, gully locations were often difficult to see requiring personnel to traverse the entire landscape at close intervals to locate gully/erosion problems. A complete survey of Fort Riley would take 4 to 6 months and require 600-1000 hours of labor. Because of the dynamic nature of training area damage and erosion potential, these surveys were needed on a relatively continuous basis. Using the rapid erosion assessment tool to identify locations susceptible to extensive erosion and gully formation, the area requiring detailed ground surveys is reduced on average by more than 15% when using the nationally available data sets (10 m DEM) and 1% when using high resolution LIDAR data. This significantly reduces the amount of time required in locating gullies and allows installations to become more proactive in preventing future gully formation. Additionally by reducing the cost of locating gullies, installations can invest more funds into fixing current gullies, and more importantly, preventing new gullies.

8.0 IMPLEMENTATION ISSUES

This section provides information to aid in the future implementation of the technology at new installations.

8.1 MODEL PERFORMANCE, INTEGRATION, AND TECHNOLOGY TRANSFER

Military commanders and Department of Defense (DoD) resource managers face the difficult challenge of maximizing accessibility to ranges and training lands to meet mission requirements while ensuring their sustainable use for future operational demands. Little guidance exists on how to balance these often conflicting demands and few automated and/or low-cost monitoring tools are in place to support training land assessments that facilitate the prioritization of rehabilitation work.

Current monitoring practices that might be in place to assist military commanders with maximizing the availability and use of training lands are essentially done on an "ad hoc" basis without the benefit of a consistent set of landscape metrics being examined or uniform methods for interpreting and reporting the results of environmental assessments. Such a decentralized approach prevents (1) consistent descriptions of the condition of military training lands at the installation and national scales and (2) the ability to implement early and proactive land rehabilitation projects and to efficiently budget for future work needs.

The results of this project were largely positive, despite not meeting the success criteria for each performance objective. Future users should be aware that the operational definition of a "gully" and the positional accuracy of mapped gully locations greatly influences the threshold accumulated *nLS+* values, and other basic measures such as flow accumulation and contributing area, used to characterize and predict gully locations. Assuming future users at the installations studied here target gully locations consistent with the definition presented in this report, no evidence was found that would dictate the need re-calibrate the model prior to implementation. However, users at other installations would be wise to invest some time in model calibration and validation prior to using the *nLS+* model on an operational basis. Another issue that remains with interpreting model results is the large rate of false positive gully predictions. Despite the strong tendency for the *nLS+* model to overpredict gullies, the area identified as being a potential gully site is significantly lower than the total installation area. This benefits the planning and execution of field monitoring activities by focusing time and attention on the limited geographic extent likely to pose a gully hazard.

Use of the *nLS+* model in "forecasting" mode illustrated how data from recent activities can be used to predict where gullies might develop in the future. Though vehicle tracking data is neither routinely collected by installations nor often made available to natural resources staffs for use, the technology and procedures for geolocating each military vehicle at fine spatial and temporal scales exists and will likely become "standard operating procedure" in the future. However, use of vehicle tracking data to modify *nLS+* model inputs illustrates how installations might approach simulating the impact of other landuse changes on training lands, such as road construction, addition of hardened vehicle pads supporting firing exercises, and the placement of

agricultural leases. Any planned development that would change installation topography or landcover, and its resulting impact on gully erosion, can be assessed with the model.

Although this project included a comparison of *nLS+* model results using DEMs of varying spatial resolutions, the impact of spatial (or temporal) scale on the generation of model inputs was not assessed. Direct comparison of model output with different resolution DEMs show comparable results with respect to the spatial precision of gully predictions and modest improvements in classification accuracy. Perhaps more important than resolution is the "currentness" of model inputs and how well digital representations of topography and LULC reflect actual ground conditions.

Methods for using LIDAR data to generate estimates of Manning's *n* have been published (*e.g.*, Smith *et al.*, 2004). The scientific consensus is that LIDAR holds promise in this effort, but additional research is needed to document appropriate data procedures, scales of analysis, and improvements over traditional and field-derived estimates. Much of the work accomplished to date focuses on extracting the Chow's theoretical roughness in feet (*k*) from data derived from the difference of LIDAR-derived digital terrain (DTM) and digital surface models (DSM) (Chow 1973, Smith et a., 2004). While an interesting approach, this resulting measure of vegetation canopy depth and architecture may be a better estimator of rainfall interception than true surface roughness. It should also be noted, that each of the three installations in this study with LIDAR DEMs purchased only "bare earth" DEM products from contractors. Including multiple return data may be useful – for a variety of applications – but would result in greater acquisition and data handling costs.

Should the *nLS+* model find widespread use across installations, it is important that an organization be identified to maintain the model and make any updates and/or revisions necessitated by future GIS software versions. As with any GIS-based model for which installation use is expected, the *nLS+* model is an ideal candidate to be delivered to end-users as a Web-based geoprocessing service made available, and maintained, by a central environmental organization.

Results from Performance Objective 4 showed that using ecoregion boundaries to recommend operational critical thresholds for accumulated *nLS+* values at other installations would not be appropriate. Instead, two approaches – Euclidean distance allocation and interpolation – were used to provide rough estimates of thresholds as an alternative to the ecoregion framework. It is important to note that these values have not been validated for other installations and that they should only be used with caution and in cases where installations are unable to perform their own nLS+ model calibration and validation. Should the model itself be maintained by a central organization, this organization could also assume responsibility for model calibration and validation if provided with a spatially and temporally accurate dataset of gully locations for partnering installations.

Along with providing for online geoprocessing capabilities, all data products required by the nLS+ model, and other environmental/sustainability indicators, could be stored in a geospatially-enabled relational database to facilitate access to current data by both installations and centralized management/support organizations. Storing data in the geospatially enabled

relational database supports distributed viewing and editing by land managers and their staffs, as well as distribution via mapping and geoprocessing web services. An example of this capability is the "Military Training Lands Map Viewer" Web application, and its underlying SQL Server geodatabase, hosted by Kansas State University (http://services.geog.ksu.edu/frk_rtla) that provides a shared and real-time decision support tool for Fort Riley land managers.

The *nLS+* model represents one tool that is now available to military land managers to promote sustainability by demonstrating the data types, analytical methods, visualization tools, and information delivery mechanisms that could become routine across installations for assessing training land condition and trends. One installation – Fort Riley – already takes advantage of the model to assess erosion potential and help planning for field surveys. For maximum benefit, this single tool needs to be complemented with others that form a coordinated suite of environmental/sustainability indicators for key monitoring themes that can be collected, assessed, and synthesized to help identify when, and where, sustainable use of training lands is not being achieved.

8.2 DEFINITIONS AND DATA HANDLING

During the course of this project, it was clear that among ITAM personnel there was no consensus definition for the term "gully." When asked to visit gullies during initial site visits, ITAM staff drove to erosional features varying in size from ephemeral rills to large ravines. Contributing to this inconsistency might be the varying definitions for, and meanings behind, the terms "gully" and "gap" presented in military literature.

Related to this definition concern, is the varied ways in which installation land managers and GIS technicians measure and record gully information. Datasets ranged in quality from gullies represented digitally as line features spanning all, or most, of the length of the gully and including complete descriptive attributes such as depth, width, and date surveyed to completely undocumented point datasets. In no case did digital gully datasets also include FGDC-compliant metadata

The by-product of this inconsistent definition and lack of required practices and procedures for recording gullies are datasets that they varied significantly in spatial, temporal, and attribute quality. Clearly these characteristics can greatly influence the corresponding accumulated *nLS+* values calculated for an individual gully. Despite care in data processing, some of the variation in model results reported in this study could be attributed to a lack of common definitions and procedures across installations. The gully definition presented in this report, informed both the agricultural sciences and military mobility restrictions, might be considered for official adoption. So, too, should a set of required minimum attributes to be recorded for each gully instance including depth, width, and date of survey.

8.3 INSTALLATION ITAM STAFFING

Most of this project was conducted during an extremely volatile period for installation ITAM staffs. Frequent changes in ITAM personnel, including ITAM directors, and significant reductions in the number of GIS staff members was a near universal issue at each installation

participating in this effort. While certainly a factor in the execution of this project, continued staffing issues for any installation office interested in better understanding the spatial and temporal dynamics of gully formation will discourage widespread adoption and use of model-based natural resource management tools. Prerequisites for successful implementation include technical staffs with training in GIS as well as administrative leaders who see value in the approach and can effectively use model output to improve land rehabilitation efforts.

9.0 REFERENCES

Abrahams, A.D. and J.F. Atkinson. 1993. Relation between grain velocity and sediment concentration in overland flow. *Water Resources Research* 29(9):3020-3028.

Abrahams, A.D., L. Gary, C. Krishnan, and J.F. Atkinson. 1999. Predicting sediment transport by interrill overland flow on rough surfaces. *Earth Surface Processes and Landforms* 23(12):1087-1099

Anderson, J., E. Hardy, J Roach, and R. Witmer. 1976. A land use and land cover classification system for use with remote sensor data. Geological Survey Professional Paper 964, U.S. Geological Survey. Washington, D.C.: U.S. Government Printing Office.

Arcement, Jr, G.J. and V.R. Schneider. 1984. Guide for Selecting Manning's Roughness Coefficients for Natural Channels and Flood Plains United States Geological Survey Water-Supply Paper 2339

Arnold, R.H. 1997. Interpretation of Airphotos and Remotely Sensed Imagery. Upper Saddle River, NJ: Prentice-Hall.

Ayers, P., M. Vance, L. Haugen, and A. Anderson. 2000. An evaluation of DGPS-based continuously operating vehicle monitoring systems to determine site-specific event severity factors. ERDC/CERL TR-00-43.

Ayers, P. D., A. B. Anderson, and C. Wu. 2005a. Analysis of vehicle use patterns during field training exercises. *Journal of Terramechanics* 42(3-4) 321-338.

Ayers, P. C. Butler, A. Fiscor, C. Wu, Q. Li, and A. Anderson. 2005b. Vehicle Impact Study, Fort Riley, Kansas, October 2004. Submitted to ITAM, Fort Riley Military Installation, Kansas (March 2005).

Bennett, S.J., C.V. Alonso, S.N. Prasad, M.J.M. Romkens. 2000. Experiments on headcut growth and migration in concentrated flows typical of upland areas. *Water Resources Research* 36(7):1911–1922.

Brown, M. B. and A.B. Forsythe. 1974. Journal of the American Statistical Association, 69, pp. 364-367.

Burrough, P. A. and R.A. McDonnell. 1998. Principles of Geographical Information Systems. New York: Oxford University Press.

Chow, V. T. 1959. Open-channel Hydraulics. New York, NY, McGraw-Hill Book Co., p. 680.

Chow, V. T. 1973. Open-channel Hydraulics. New York, NY, McGraw-Hill Book Co.

Department of the Army. 1988. Army Regulation 200-2: Environmental Effects of Army Actions. Headquarter, Department of the Army, Washington, D.C.

Department of Defense. 1985. Field Manual (FM) 5-101: Mobility. Headquarters, Department of the Army: Washington, D.C.

Doe, William W., D. Jones and S.Warren. 1999. Soil Erosion Model Guide for Military Lands: Analysis of Erosion Models for Natural and Cultural Resources Applications, Contract Report/Technical Report CADD-99-XX, Tri-Service CADD/GIS Technology Center, U.S. Army Waterways Experiment Station, Vicksburg, MS, 146 pp

Engman, E.T. 1986. Roughness coefficients for routing surface runoff. *Journal of irrigation and Drainage Engineering* 112(1):39-53.

Foster, G.R., R. A. Young, and W.H. Neibling. 1985. Sediment composition for nonpoint source pollution analysis. *Transactions of the ASAE* 28(1):133-139.

Frazier, B.E., D. K. Mc Cool, and C. F. Engle. 1983. Soil erosion in the Palouse: An aerial perspective. *Journal of Soil and Water Conservation* 38:70-74.

Howard, H., P. Ayers, D. Koch, A. Anderson, J. Kane, G. Bozdech, and N. Svensdsen. 2011. Predicting Soil Erosion Potential from Military Vehicle Tracking and Terrain Impacts. ESTCP poster presentation.

Jaccard P. 1902. Lois de distribution florale. Bulletin de la Socíeté Vaudoise des Sciences Naturelles 38:67-130.

Jaccard P. 1912. The distribution of the flora in the alpine zone. New Phytologist 11(2):37-50.

Laguna, A. and J.V. Giraldez. 1993. The description of soil erosion through a kinematic wave model. *Journal of Hydrology* 145:65-82.

Li, Q., P.D. Ayers, and A.B. Anderson. 2007. Modeling of terrain impact caused by tracked vehicles. *Journal of Terramechanics* 44(6):395-410.

Liu, K., P. Ayers, H. Howard, and A. Anderson. 2009. Influence of turning radius on wheeled military vehicle induced rut formation. *Journal of Terramechanics* 46:49-55.

McCuen, R.H. and J.M. Spiess. 1995. Assessment of kinematic wave time of concentration. *Journal of Hydrologic Engineering* 121(3):256-266.

Meyer, L.D., S.M. Dabney, C.E. Murphree, W.C. Harmon, and E.H. Grissinger. 1999. Crop production systems to control erosion and reduce runoff from upland silty soils. *Transactions of the ASAE* 42(6):1645-1652.

Moore, I. D., R. B. Grayson, and A. R. Landson. 1991. Digital Terrain Modelling: A Review of Hydrological, Geomorphological, and Biological Applications. *Hydrological Processes* 5: 3–30.

O'Callaghan, J.F. and D.M. Mark. 1984. The extraction of drainage networks from digital elevation data. *Computer Vision, Graphics, and Image Processing* 28(3):323-344.

Omernik, J. M. 1987. Ecoregions of the continuous United States. Map (scale 1:7,500,000). *Annals of the Association of American Geographers* 77(1): 118-125.

Overholt, J. 2001. U.S. Army TACOM-TARDEC Intelligent Mobility Program. http: www.dtic.mil/ndia/2001technology/overholt.pdf. Last accessed on April 27, 2010.

Rice, M., P. Ayers, A. Anderson, and L. Randolph. 2006. Assessment of ecological impacts of military maneuvers in training areas. Paper No. 067013 presented at the 2006 ASABE Annual International Meeting. ASABE, 2950 Niles Rd., St. Joseph, MI 49085-9659.

Rice, M. K., and P. D. Ayers. 2005. Evaluation of Tracking Study for Maneuvers performed at Fort Riley, Kansas Military Installation in May of 2005. Research Report Submitted to Fort Riley Military Installation.

Singh, V. P. 2001. Kinematic wave modelling in water resources: a historical perspective. *Hydrological Processes.* 15(4):671-706.

Smith, M.J., F.F.F. Asal, and G. Preistnall. 2004. The use of photogrammetry and LIDAR for landscape roughness estimation in hydrodynamic studies, in Altan Orhan, M., ed., International Society for Photogrammetry and Remote Sensing, Volume 35. http://www.isprs.org/proceedings/XXXV/congress/comm3/papers/361.pdf (last accessed November 14, 2013).

Snedecor, G.W. and W.G. Cochran. 1989. Statistical Methods (8th Ed). Iowa State University Press.

Steichen, J.M., S.L. Hutchinson, N. Zhang, J.M. Shawn Hutchinson, C. Oviatt, A. Anderson, T. Keane, P.L. Barnes. 2009. Assessing the Impact of Maneuver Training on NPS Pollution and Water Quality - Project SI-1339 Final Report. Arlington, VA: Strategic Environmental Research and Development Program.

USDA. 1986. Urban Hydrology for Small Watersheds. United States Department of Agriculture, Natural Resources Conservation Service, Conservation Engineering Division. Technical Release 55, June 1986.

U.S. Department of Agriculture, Natural Resources Conservation Service. National Soil Survey Handbook, title 430-VI. Available online at: http://soils.usda.gov/technical/handbook/ accessed [012/15/2009].

USEPA. 2000. National Water Quality Inventory. Available at: http://www.epa.gov/305b/2000report. Last accessed May 16, 2007.

USEPA, Western Ecology Division. 2013. Ecoregion Maps and GIS Resources. http://www.epa.gov/wed/pages/ecoregions.htm (last accessed August 16, 2013).

Wong, T.S.W. and C.N. Chen 1999. Time of Concentration Formula for Sheet Flow of Varying Flow Regime. *Journal of Hydrologic Engineering* 2(3):136-139.

Zeverbergen, L. W., and C. R. Thorne. 1987. Quantitative Analysis of Land Surface Topography. *Earth Surface Processes and Landforms* 12: 47–56.

APPENDICES

Appendix A: Initial Project Points of Contact

POINT OF CONTACT Name	ORGANIZATION Name Address	Phone Fax E-mail	Role in Project
Hutchinson, Stacy	Kansas State University Bio. and Agric. Engr. 129 Seaton Hall Manhattan, KS 66506	Tel: 785-532-5580 Fax: 785-532-5825 sllhutch@k-state.edu	Co-PI
Hutchinson, J.M. Shawn	Kansas State University Dept of Geography 118 Seaton Hall Manhattan, KS 66506	Tel: 785-532-3414 Fax: 785-532-7310 shutch@k-state.edu	Co-PI
Anderson, Alan	2902 Newmark Drive Champaign, IL 61822-1076	Tel: 217-373-7233 Fax: 217-373-7266 alan.b.anderson@usace.army.mil	US military liaison
Howland, Mark	Bldg 1150 Beaver Road DPTM Schofield Barracks, HI 96857	Tel: 808-655-1597 mark.howland@us.army.mil	HI installation (Schofield and PTA) ITAM coordinator
Faucette, David	Pohakuloa Training Area 36 Mile Marker Saddle Rd Hilo, HI 96720	Tel: 808-935-0424 dave.faucette1@us.army.mil	PTA LRAM coordinator
Hoffman, Dennis	Blackland Research and Extension Center 720 E. Blackland Rd Temple, TX 76502	Tel: 254-774-6040 Fax: 254-774-6001	Fort Hood Senior Research Scientist
Sparks, Ruth	AFZJ-PT ITAM Office PO Box 105100 Bldg 6109 Southloop Rd Fort Irwin, CA 92310	Tel: 760-380-3169 Fax: 760-380-3180 ruth.sparks@us.army.mil	Fort Irwin ITAM coordinator
Westbury, Hugh	Building 6, Room 307 Fort Benning, GA 31905	Tel: 706-545-4208 hugh.westbury@us.army.mil	Fort Benning Environmental Compliance
Cohen, Susan	Camp Lejeune Marine Corps Base Jacksonville, NC	Tel: 910-451-7900 susan.cohen@usmc.mil	Defense Coastal/Estuary Research

			Program
Woodford, Phil	Bldg 77709 Victory Road Fort Riley, KS 66442	Tel: 785-239-8733 Fax: 785-239-9373 philip.b.woodford@us.army.mil	Fort Riley ITAM coordinator

Appendix B: Histograms of Accumulated *nLS+* Values after Initial Processing

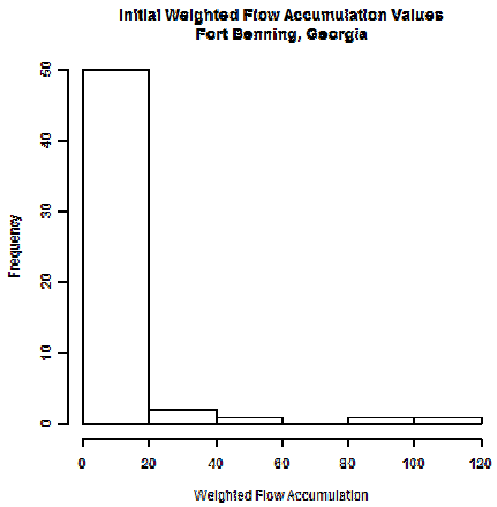

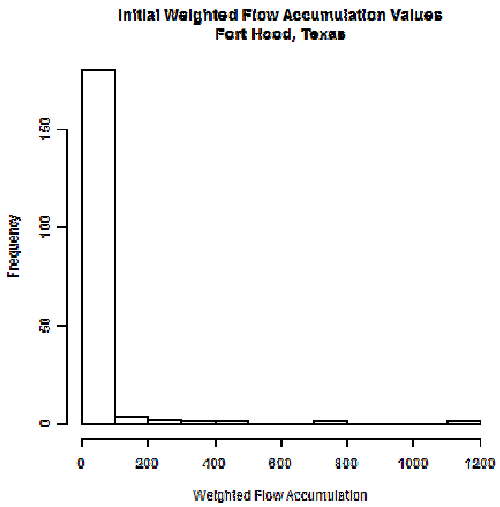

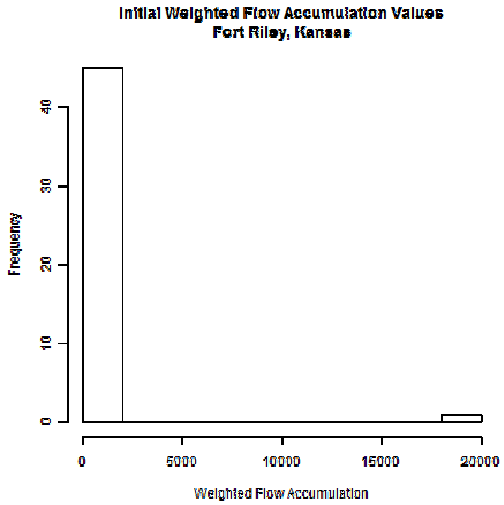

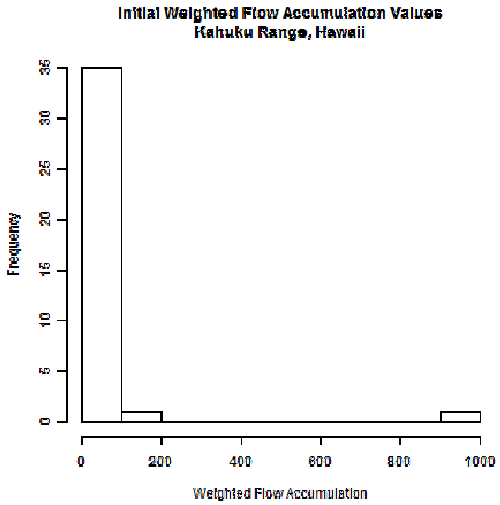

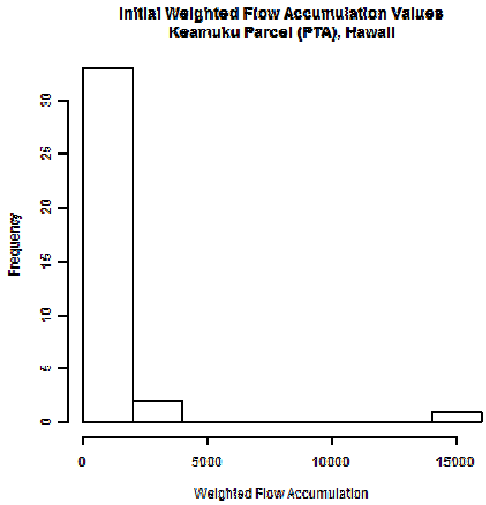

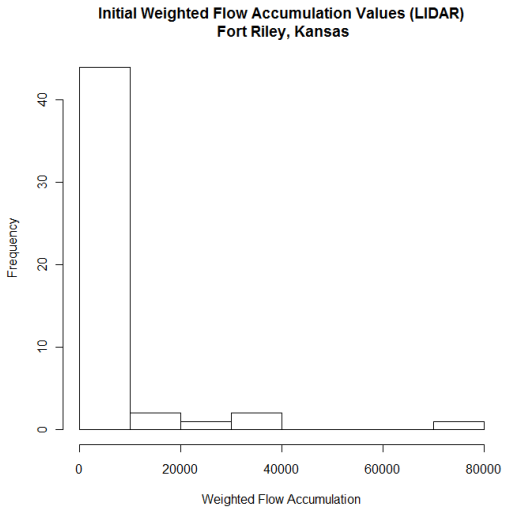

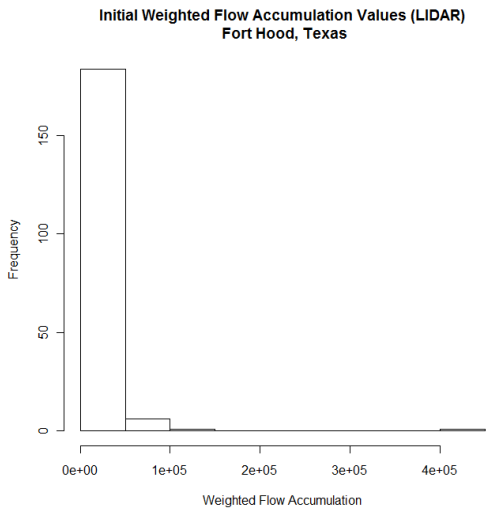
Initial Weighted Flow Accumulation Values (LIDAR)
Fort Hood, Texas
Frequency
0
50
100
150
0e+00
1e+05
2e+05
3e+05
4e+05
Weighted Flow Accumulation

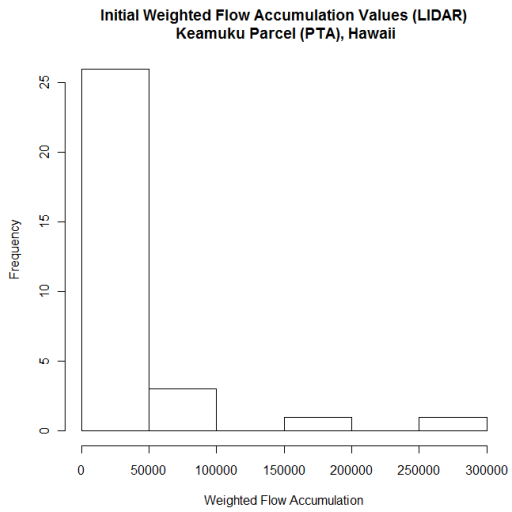
Initial Weighted Flow Accumulation Values (LIDAR)
Keamuku Parcel (PTA), Hawaii
Frequency
0
5
10
15
20
25
0
50000
100000
150000
200000
250000
300000
Weighted Flow Accumulation

Appendix C: Histograms of Accumulated *nLS+* Values after Secondary Processing

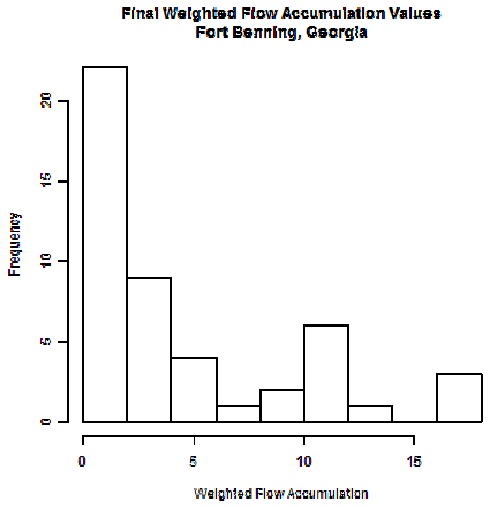

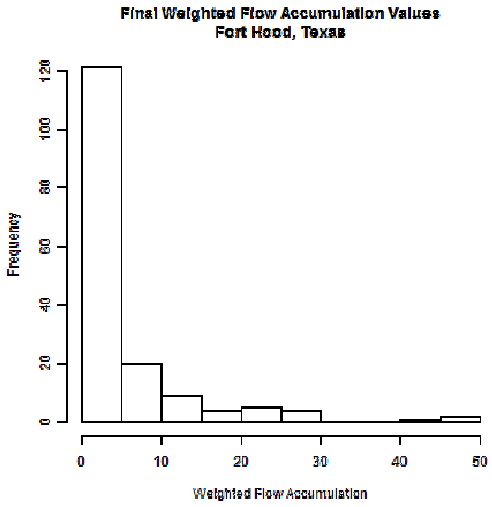

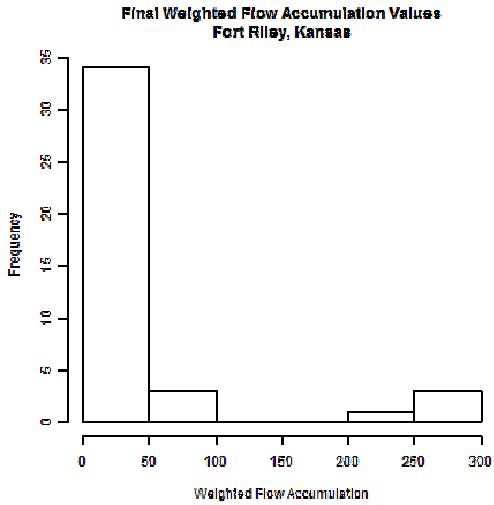

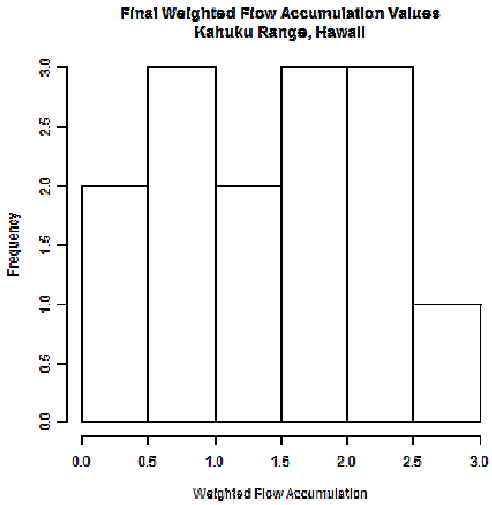

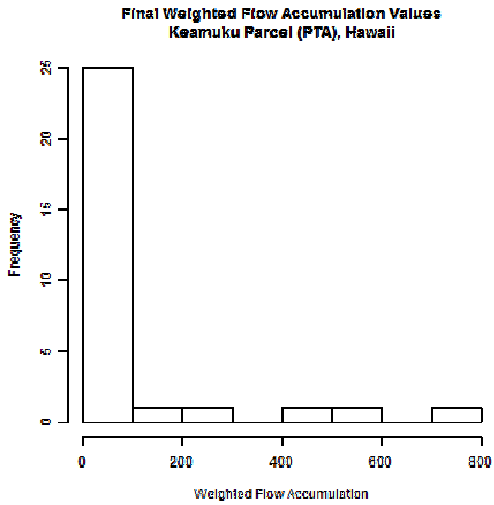

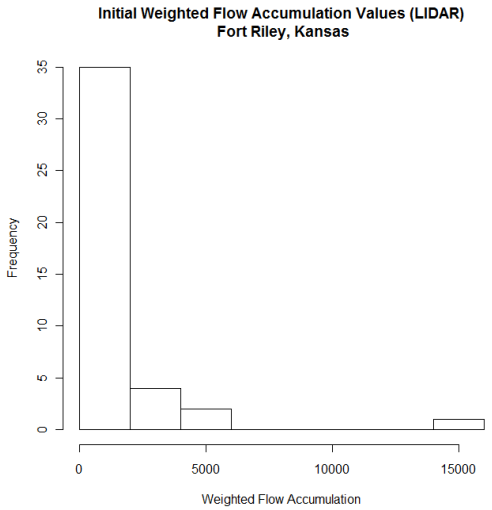

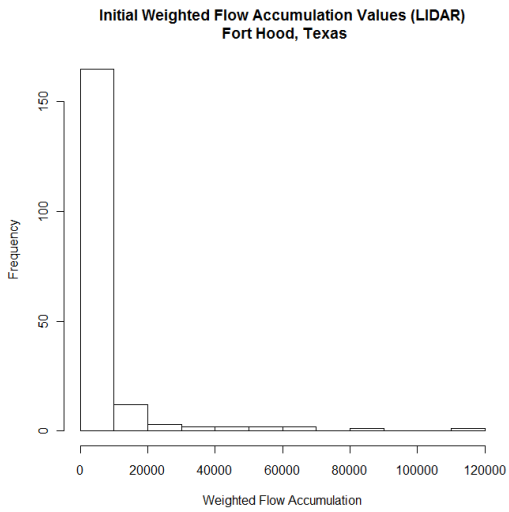
Initial Weighted Flow Accumulation Values (LIDAR)
Fort Hood, Texas
Frequency
0
50
100
150
0
20000
40000
60000
80000
100000
120000
Weighted Flow Accumulation

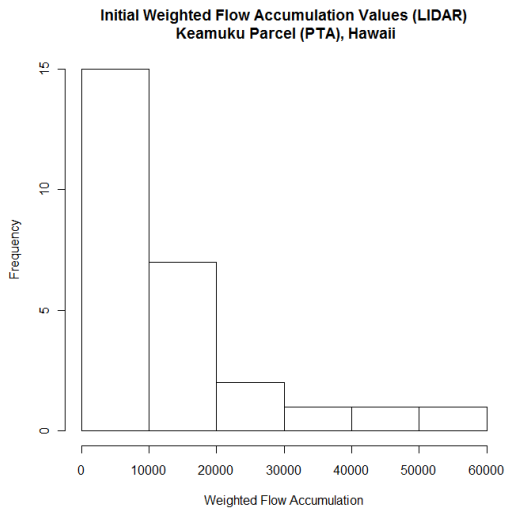
Initial Weighted Flow Accumulation Values (LIDAR)
Keamuku Parcel (PTA), Hawaii
Frequency
0
5
10
15
0
10000
20000
30000
40000
50000
60000
Weighted Flow Accumulation

Appendix D: Histograms of Final Log-Transformed Accumulated *nLS+* Values

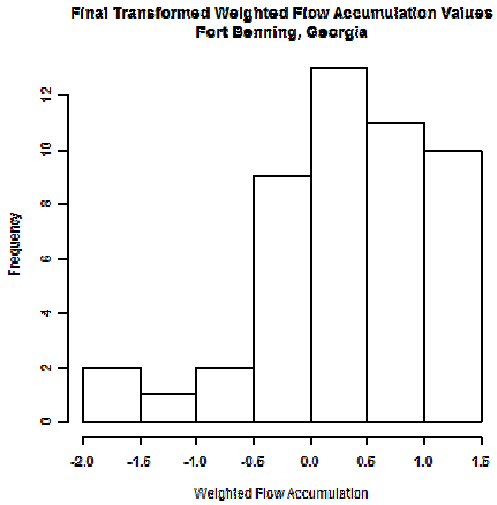

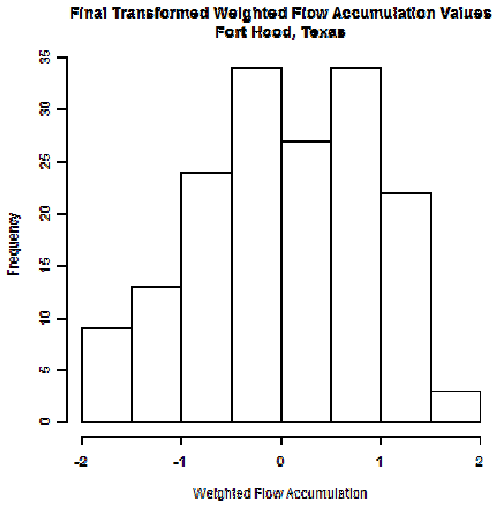

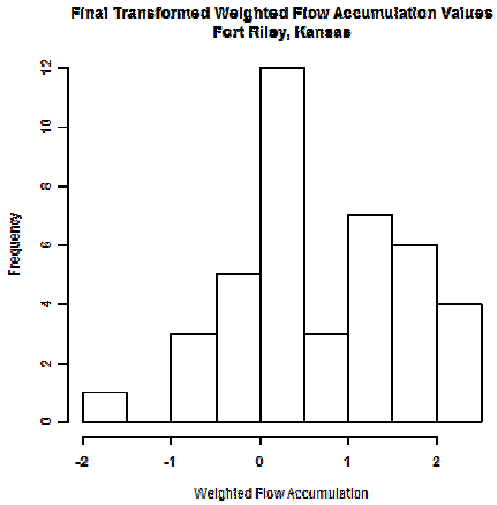

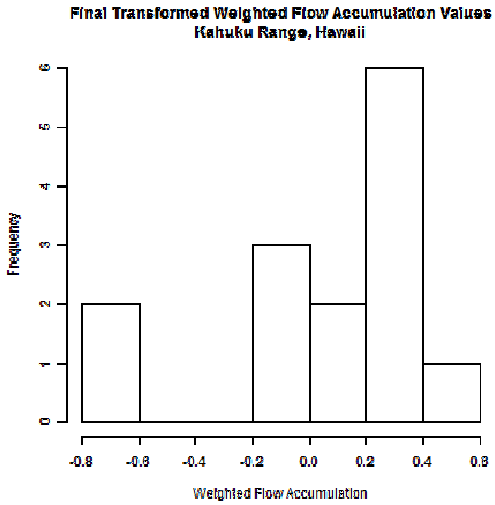

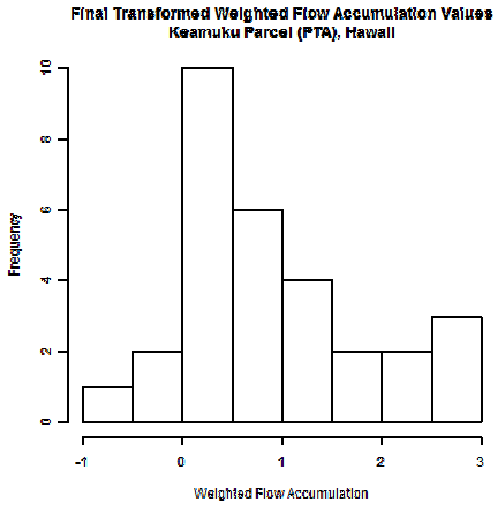

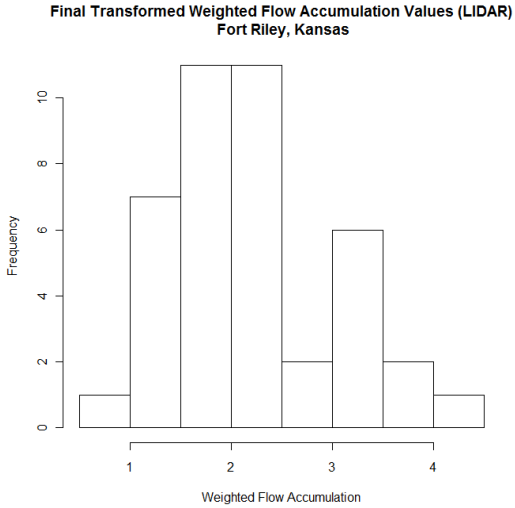

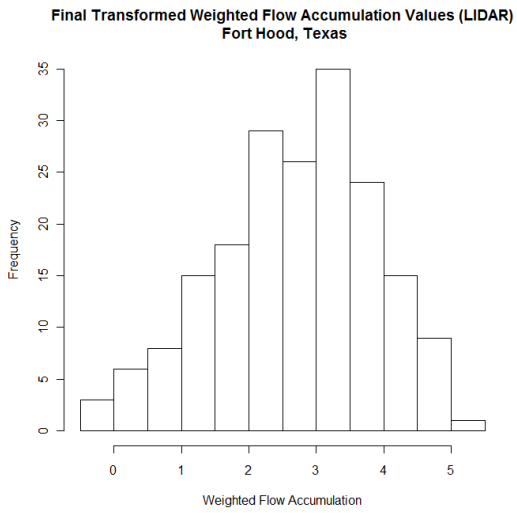
Final Transformed Weighted Flow Accumulation Values (LIDAR)
Fort Hood, Texas
Frequency
0
5
10
15
20
25
30
35
0
1
2
3
4
5
Weighted Flow Accumulation

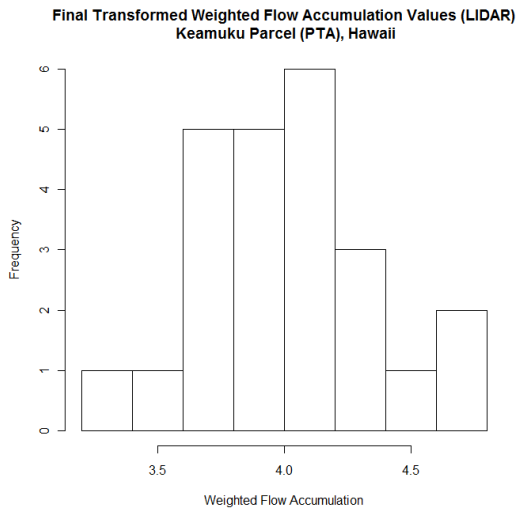
Final Transformed Weighted Flow Accumulation Values (LIDAR)
Keamuku Parcel (PTA), Hawaii
Frequency
0
1
2
3
4
5
6
3.5
4.0
4.5
Weighted Flow Accumulation

Appendix E: Installation Maps of Predicted Cells and Gully Density Surface

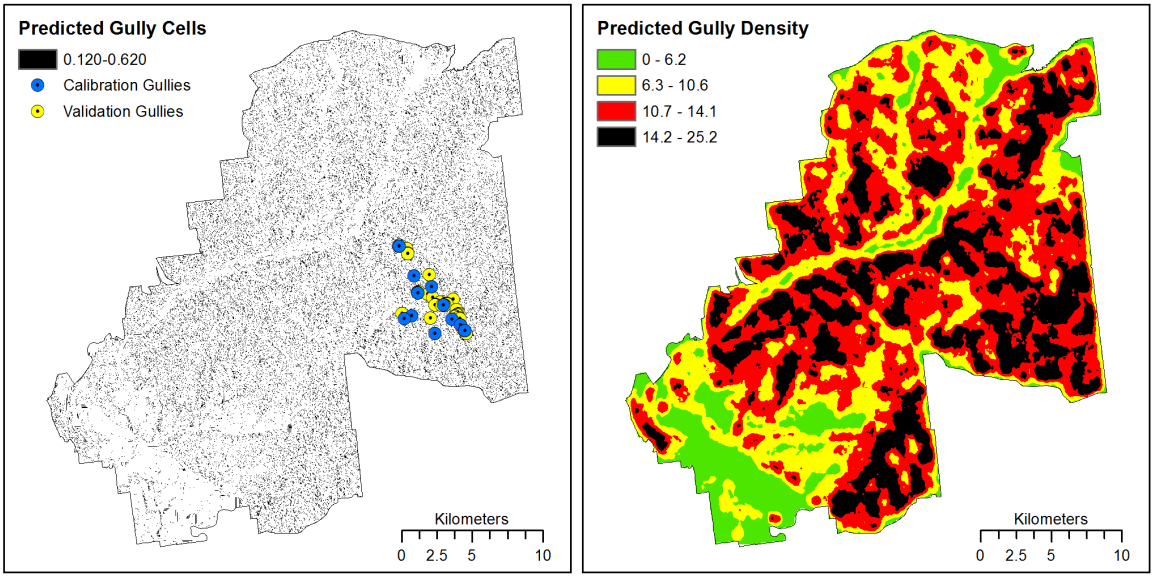

Fort Benning, Georgia
NED DEM Input

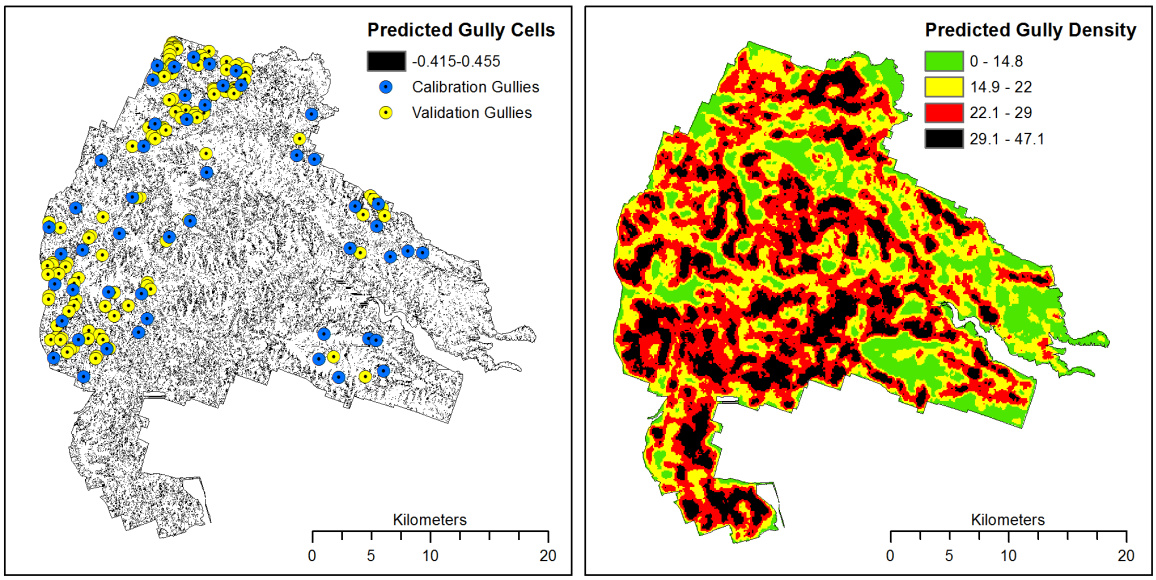

Fort Hood, Texas
NED DEM Input

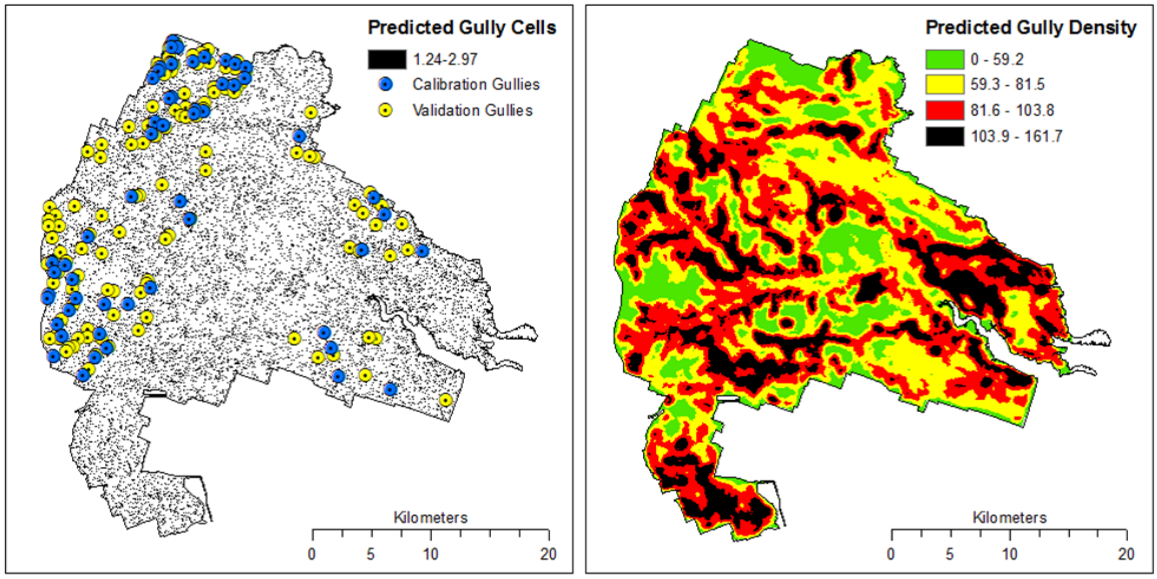

Fort Hood, Texas
LIDAR DEM Input

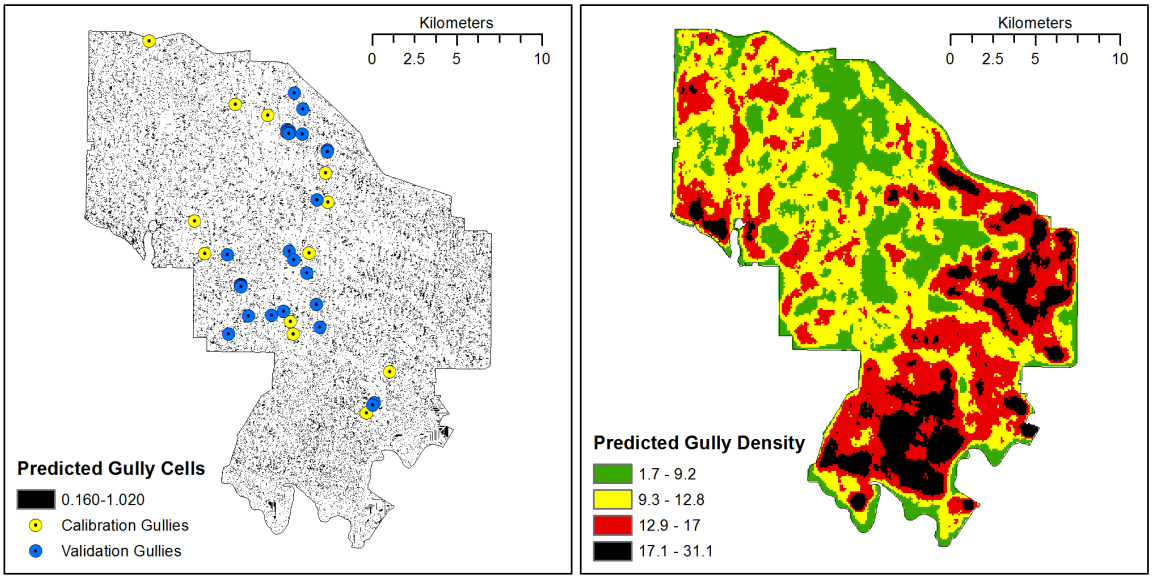

Fort Riley, Kansas
NED DEM Input

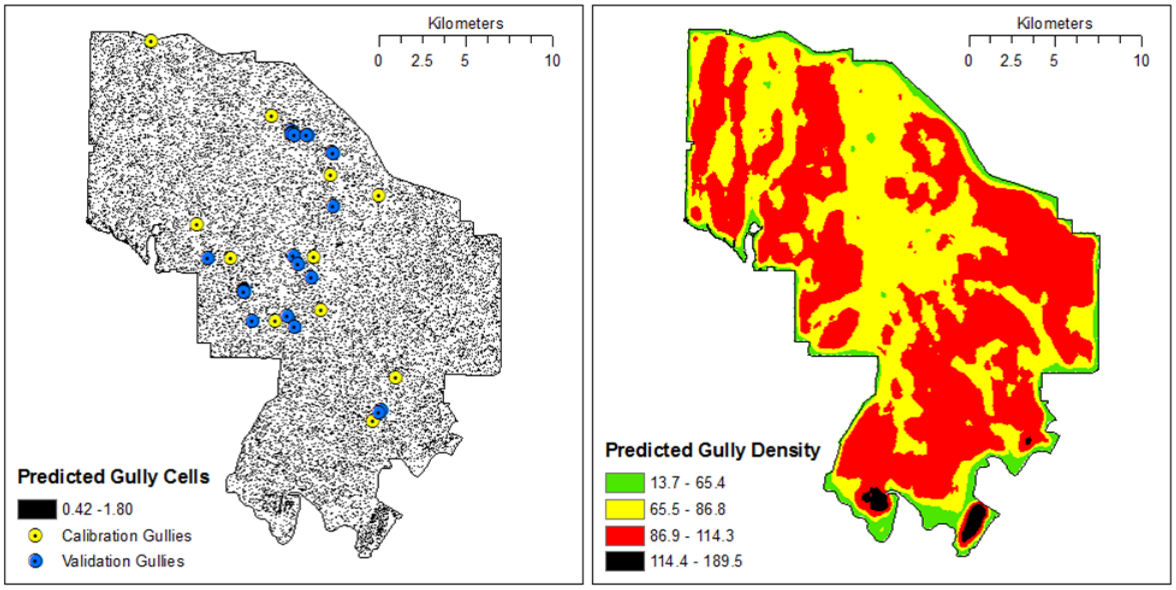

Fort Riley, Kansas
LIDAR DEM Input

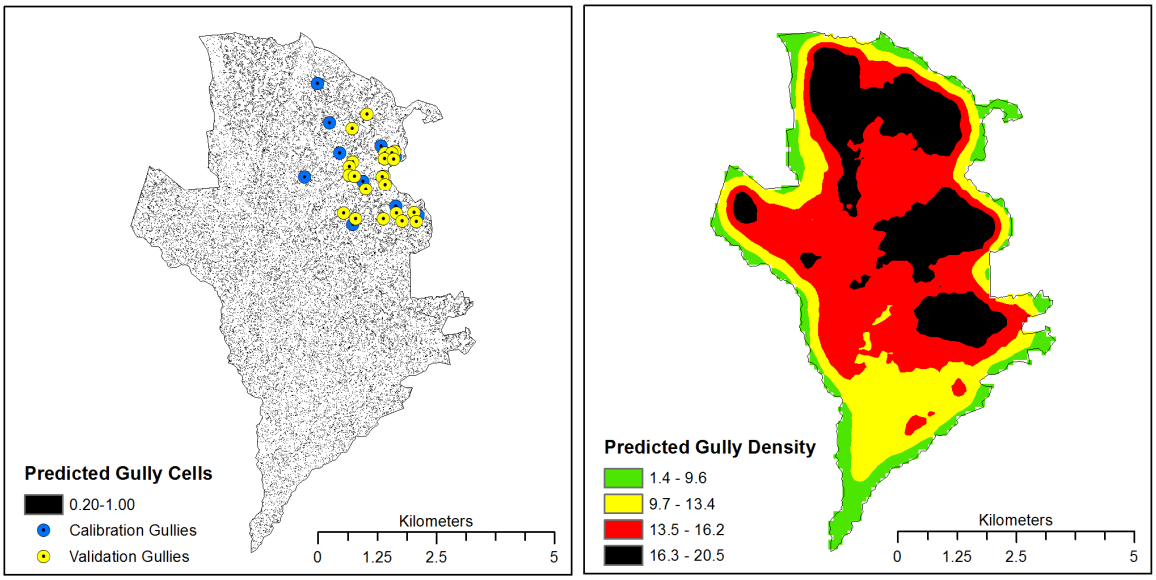

Kahuku Range (Schofield Barracks), Hawaii
NED DEM Input

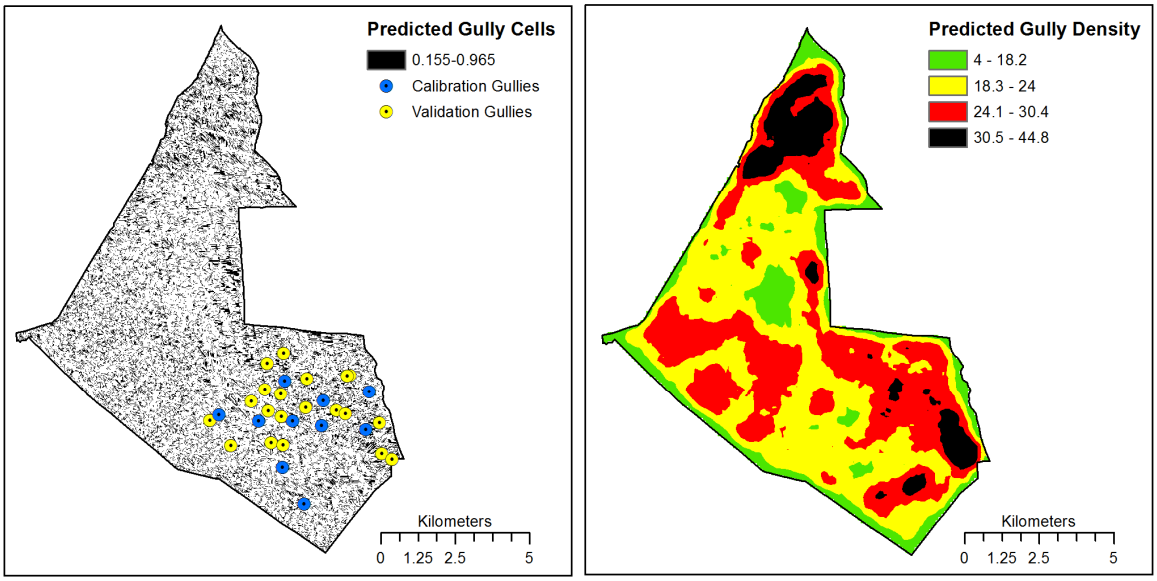

Keamuku Parcel (Pohakuloa Training Area), Hawaii
NED DEM Input

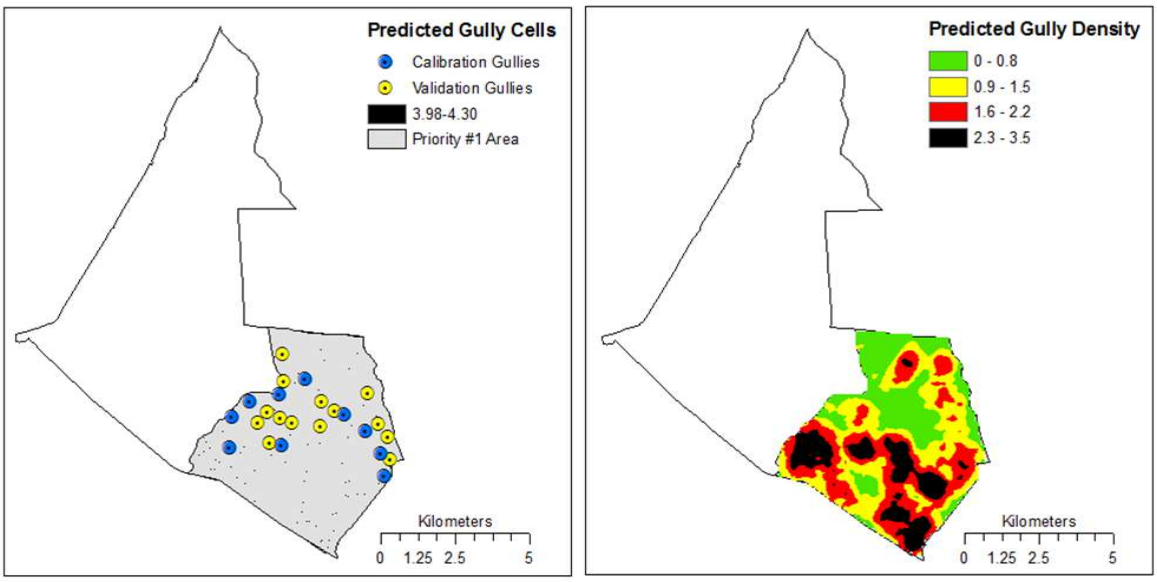

Keamuku Parcel (Pohakuloa Training Area), Hawaii – Priority #1 Area Only
LIDAR DEM Input

Appendix F: Bar Charts of Gully Prediction Accuracy Distances

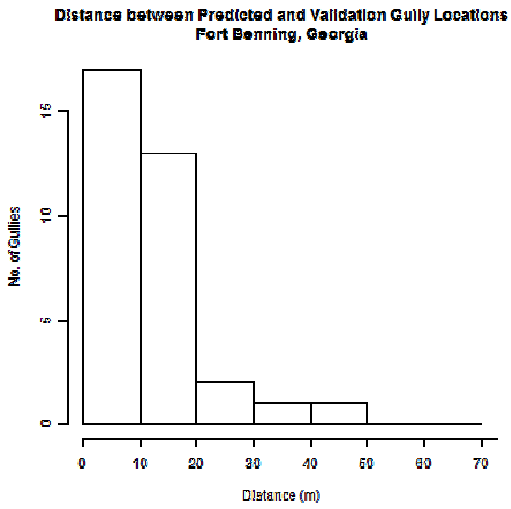

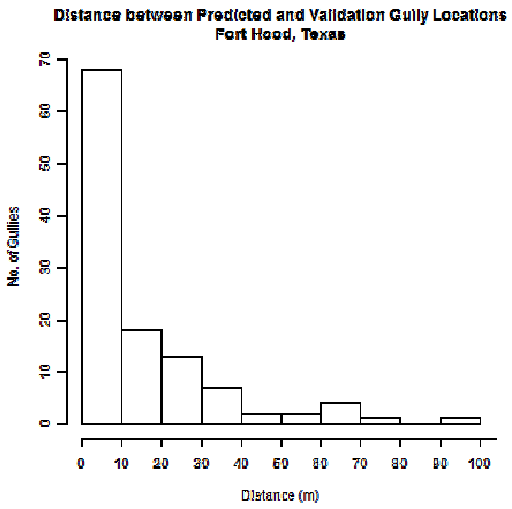

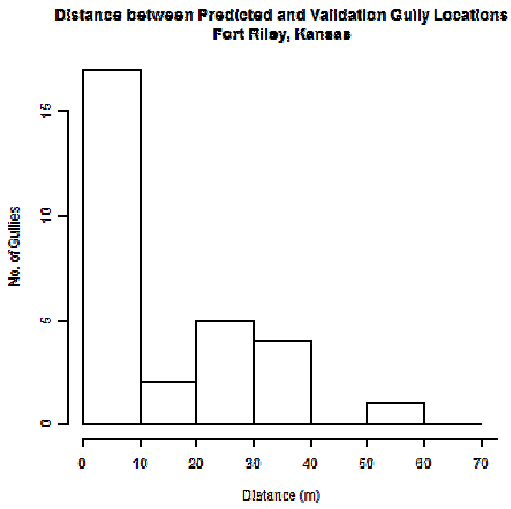

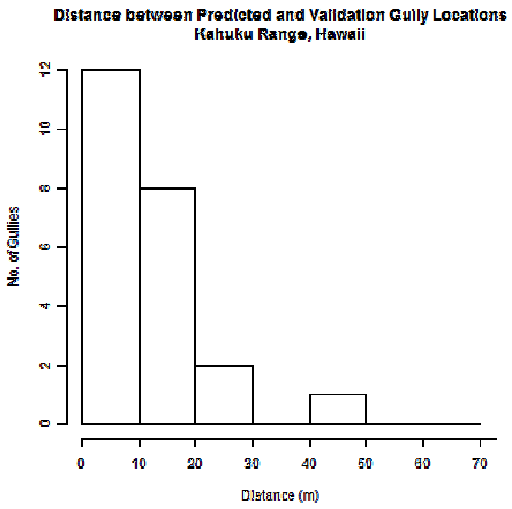

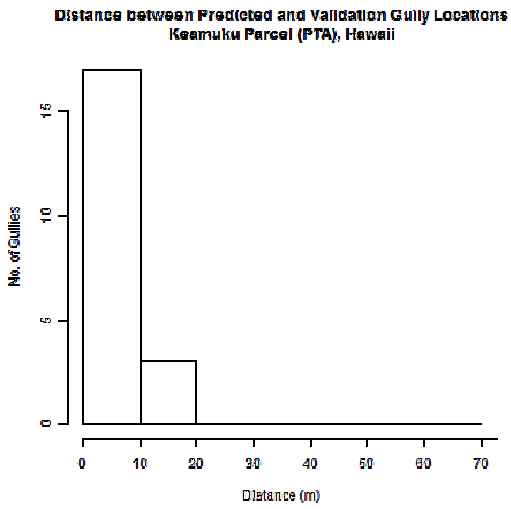

Appendix G: Sub-Models of the Enhanced *nLS+* Gully Model

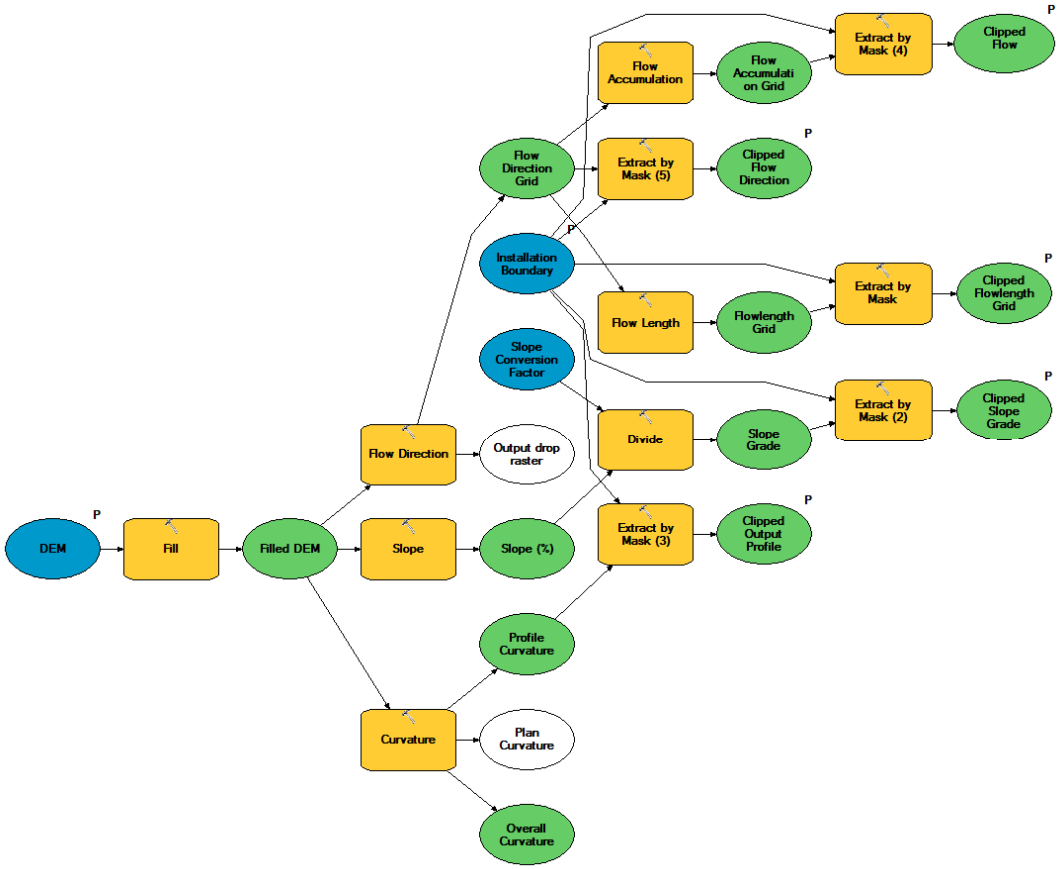

Sub-Model #1: Prepare Filled DEM

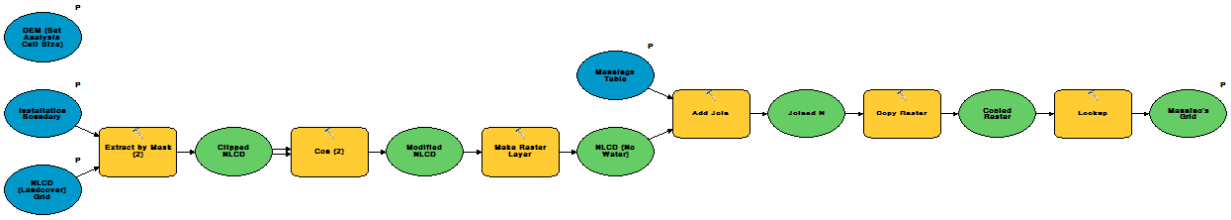

Sub-Model #2: Prepare Surface Roughness

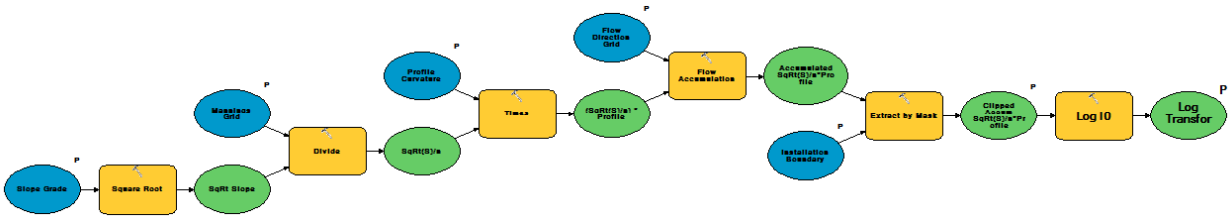

Sub-Model #3: Calculate *nLS*+ Accumulation

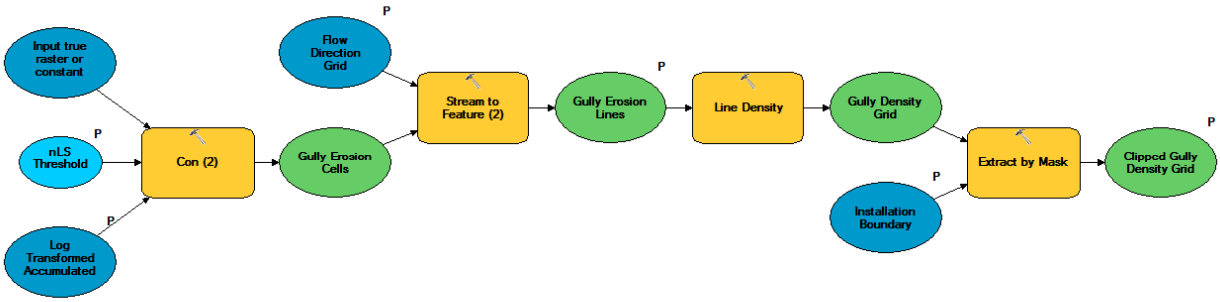

Sub-Model #4: Predict Gully Locations

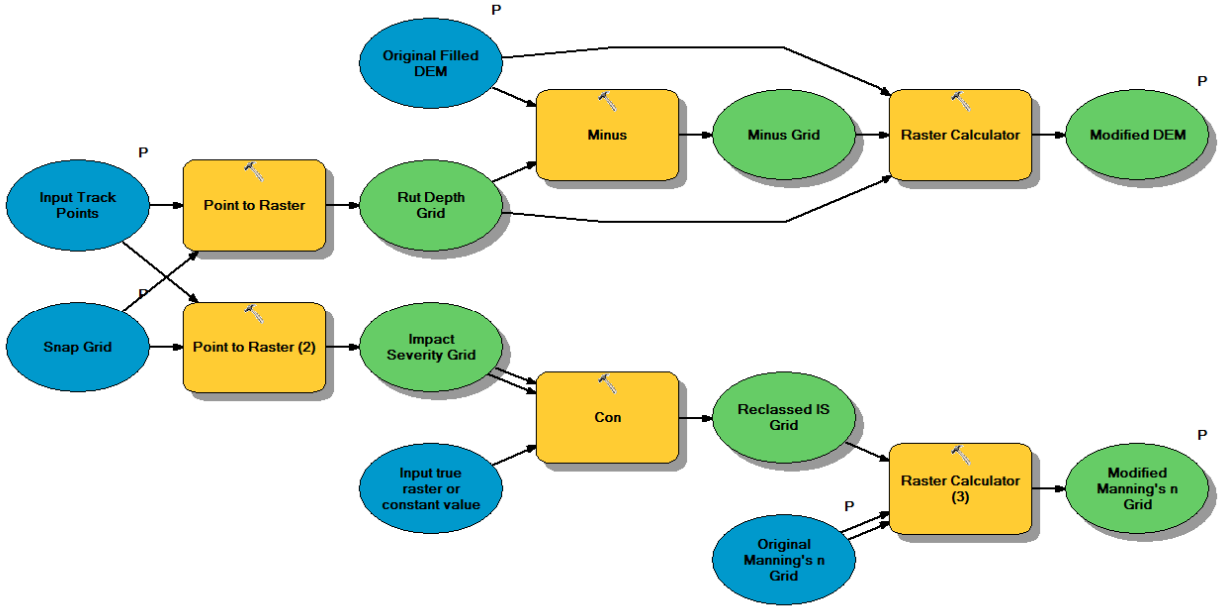

Sub-Model #5: Modify Inputs with Vehicle Tracks (Forecast)

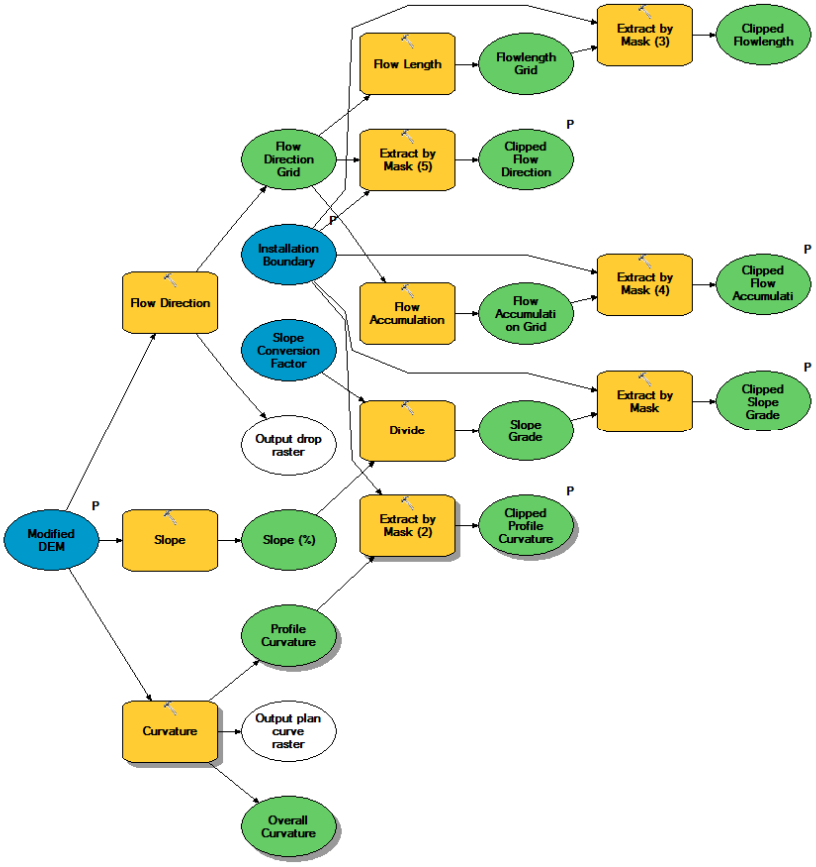

Sub-Model #6: Prepare Other Model Inputs (Forecast)